

51027

0-315-03131-X



National Library of Canada

Bibliothèque nationale du Canada

CANADIAN THESES ON MICROFICHE

THÈSES CANADIENNES SUR MICROFICHE

NAME OF AUTHOR/NOM DE L'AUTEUR Sean François Johnston

TITLE OF THESIS/TITRE DE LA THÈSE "The Far Infrared Reflectivity of Liquid

Gallium-Tellurium Alloys"

UNIVERSITY/UNIVERSITÉ Simon Fraser University

DEGREE FOR WHICH THESIS WAS PRESENTED/
GRADE POUR LEQUEL CETTE THÈSE FUT PRÉSENTÉE Master of Science - Physics

YEAR THIS DEGREE CONFERRED/ANNÉE D'OBTENTION DE CE GRADE 1980

NAME OF SUPERVISOR/NOM DU DIRECTEUR DE THÈSE Dr. B.P. Clayman

Permission is hereby granted to the NATIONAL LIBRARY OF CANADA to microfilm this thesis and to lend or sell copies of the film.

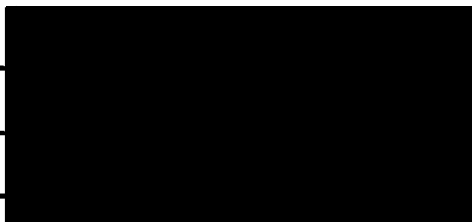
L'autorisation est, par la présente, accordée à la BIBLIOTHÈQUE NATIONALE DU CANADA de microfilmer cette thèse et de prêter ou de vendre des exemplaires du film.

The author reserves other publication rights, and neither the thesis nor extensive extracts from it may be printed or otherwise reproduced without the author's written permission.

L'auteur se réserve les autres droits de publication; ni la thèse ni de longs extraits de celle-ci ne doivent être imprimés ou autrement reproduits sans l'autorisation écrite de l'auteur.

DATED/DATE 18 June 1980 SIGNED/SIGNÉ _____

PERMANENT ADDRESS/RÉSIDENCE FIXÉ _____





NOTICE

The quality of this microfiche is heavily dependent upon the quality of the original thesis submitted for microfilming. Every effort has been made to ensure the highest quality of reproduction possible.

If pages are missing, contact the university which granted the degree.

Some pages may have indistinct print especially if the original pages were typed with a poor typewriter ribbon or if the university sent us a poor photocopy.

Previously copyrighted materials (journal articles, published tests, etc.) are not filmed.

Reproduction in full or in part of this film is governed by the Canadian Copyright Act, R.S.C. 1970, c. C-30. Please read the authorization forms which accompany this thesis.

THIS DISSERTATION
HAS BEEN MICROFILMED
EXACTLY AS RECEIVED

AVIS

La qualité de cette microfiche dépend grandement de la qualité de la thèse soumise au microfilmage. Nous avons tout fait pour assurer une qualité supérieure de reproduction.

S'il manque des pages, veuillez communiquer avec l'université qui a conféré le grade.

La qualité d'impression de certaines pages peut laisser à désirer, surtout si les pages originales ont été dactylographiées à l'aide d'un ruban usé ou si l'université nous a fait parvenir une photocopie de mauvaise qualité.

Les documents qui font déjà l'objet d'un droit d'auteur (articles de revue, examens publiés, etc.) ne sont pas microfilmés.

La reproduction, même partielle, de ce microfilm est soumise à la Loi canadienne sur le droit d'auteur, SRC 1970, c. C-30. Veuillez prendre connaissance des formules d'autorisation qui accompagnent cette thèse.

LA THÈSE A ÉTÉ
MICROFILMÉE TELLE QUE
NOUS L'AVONS REÇUE

THE FAR INFRARED REFLECTIVITY
OF
LIQUID GALLIUM-TELLURIUM ALLOYS

by

Sean François Johnston
B.Sc., Simon Fraser University, 1978

A THESIS SUBMITTED IN PARTIAL FULFILLMENT OF
THE REQUIREMENTS FOR THE DEGREE OF
MASTER OF SCIENCE
in the Department
of
Physics

© Sean François Johnston 1980

SIMON FRASER UNIVERSITY

May 1980

All rights reserved. This thesis may not be
reproduced in whole or in part, by photocopy
or other means, without permission of the author.

APPROVAL

Name: Sean François Johnston

Degree: Master of Science

Title of Thesis: The Far Infrared Reflectivity of
Liquid Gallium-Tellurium Alloys.

Examining Committee:

Chairman: Dr. K. Colbow

Dr. B.P. Clayman
Senior Supervisor

Dr. E.D. Crozier

Dr. M. Plischke

Dr. K.E. Rieckhoff
External Examiner
Professor
Department of Physics
Simon Fraser University

Date Approved: 14 MAY 1980

PARTIAL COPYRIGHT LICENSE

I hereby grant to Simon Fraser University the right to lend my thesis, project or extended essay (the title of which is shown below) to users of the Simon Fraser University Library, and to make partial or single copies only for such users or in response to a request from the library of any other university, or other educational institution, on its own behalf or for one of its users. I further agree that permission for multiple copying of this work for scholarly purposes may be granted by me or the Dean of Graduate Studies. It is understood that copying or publication of this work for financial gain shall not be allowed without my written permission.

Title of Thesis/Project/Extended Essay

"The Far Infrared Reflectivity of

Liquid Gallium-Tellurium Alloys"

Author: _____

(signature)

Sean Francois Johnston

(name)

18 June 1980

(date)

ABSTRACT

The reflectivities of liquid $\text{Ga}_{1-x}\text{Te}_x$ alloys have been measured as a function of composition, temperature, and frequency in the far infrared, using an optically pumped far infrared laser and Fourier-transform spectroscopy (FTS).

Three laser wavelengths were used to investigate alloy compositions with $0.34 < x < 0.85$. At 119μ , dramatic increases in reflectivity and its temperature dependence were observed between the compositions $0.5 < x < 0.6$, corresponding to the stoichiometric alloys GaTe and Ga_2Te_3 . Measurements at 571μ and 1217μ however, were found to contain systematic errors resulting from diffraction and interference of the laser radiation. The composition-dependence of the reflectivity results deviates strongly from that predicted from published resistivity data using the Drude model.

Broad-band spectra of the two intermetallic melts, measured using FTS, show smooth frequency dependence, free of modes attributable to suspected molecular clusters. Liquid Ga_2Te_3 has a Drude-like far infrared spectrum, but GaTe has nearly constant reflectivity below 100 cm^{-1} .

The far infrared properties are similar to those of the

liquid Mg-Bi system, the only previously investigated binary liquid semiconductor, and to several amorphous solids, suggesting that the properties may be intrinsic to disordered systems in general.

Results are discussed in terms of current theories.

Friends, escape the dark enclosure
Where they tear the light apart
And in wretched bleak exposure
Twist, and cripple Nature's heart

Goethe

ACKNOWLEDGEMENTS

I would like to thank Dr. Bruce P. Clayman for suggesting this study, and acknowledge the always pertinent advice offered by him and Dr. E. D. Crozier. This work would not have been possible without the availability of their excellent equipment.

For specific information about the interferometer and laser systems, thanks are also due to Dr. Robert Buckley, Bernd Simson, and David Karecki.

I am grateful to Dr. M. Plischke for serving on my supervisory committee, to Dr. J. M. D'Auria for performing composition analyses, and to Dr. J. F. Cochran for generously supplying the Gallium used in the initial measurements.

The financial support provided by the Natural Sciences and Engineering Research Council and the Physics Department of Simon Fraser University is also gratefully acknowledged.

TABLE OF CONTENTS

	page
APPROVAL.....	ii
ABSTRACT.....	iii
QUOTATION.....	v
ACKNOWLEDGEMENTS.....	vi
LIST OF TABLES.....	x
LIST OF FIGURES.....	xi
I. INTRODUCTION.....	1
A. Liquid Semiconductors.....	2
B. Models.....	3
C. GaTe Alloys.....	6
1. Previous Work.....	6
2. Far Infrared Studies.....	10
II. INSTRUMENTATION AND PROCEDURE.....	13
A. Laser Reflectivity Measurements.....	14
1. Laser System and Optics.....	14
2. Optical Furnace.....	17
3. Detection.....	21
4. Measurement Procedure.....	24
B. Broad-Band Spectrum Measurement.....	27
1. Introduction.....	27
2. Apparatus.....	28
3. Computer and Programming.....	30

4. Procedure.....	33
C. Sample Preparation	36
1. Requirements.....	36
2. Sample Reactivity.....	37
3. Methods.....	38
D. In-Situ Melting.....	42
III. INITIAL TESTS AND EXPERIMENTAL PROGRAMME.....	44
A. Far Infrared Laser.....	44
1. Mode Differences.....	44
2. Laser Stability.....	45
3. Cavity Pressure.....	47
4. Interference Effects.....	47
B. Procedural Tests.....	51
1. Solder Metal.....	51
2. Ga-Te Observations.....	53
C. Composition Analysis.....	56
IV. RESULTS.....	59
A. Laser Reflectivity.....	59
1. Frequency.....	59
2. Composition.....	64
3. Temperature.....	65
B. Interferometer Reflectivity.....	71
V. MODELS.....	76
A. Activated Conductivity.....	76
B. Fits to Broad-Band Spectra.....	80
1. Drude Reflectivity.....	80

2. Quantum Oscillator.....	85
3. Mechanical Oscillator.....	86
C. Dissociation Model for Enthalpy.....	87
VI. DISCUSSION.....	92
A. Characterization.....	92
1. Temperature Dependence.....	93
2. Frequency Dependence.....	94
B. Comparison with the Mg-Bi System.....	95
C. Explanations for Ga-Te.....	97
1. Pseudogap.....	97
2. Molecular Clusters.....	100
3. Conventional Semiconductor.....	105
D. Long Wavelength Laser Data.....	108
E. Summary and Conclusions.....	114
F. Suggestions for Further Work.....	115
APPENDIX A: EXPERIMENT-RUNNING PROGRAM.....	116
APPENDIX B: CALCULATION OF VIBRATIONAL-ROTATIONAL MODES OF THE GaTe MOLECULE.....	127
REFERENCES.....	129

LIST OF TABLES

Table	page
II-1 Interferometer High Frequency Cut-Off Combinations..	31
III-1 X-Ray Fluorescence Composition Analysis.....	58
VI-1 Effect of Light Pipe Misalignment on Measured Signal.....	112

LIST OF FIGURES

Figure	Page
1-1 Liquid Ga-Te Properties Vs. Alloy Composition: (a) Resistivity; (b) Thermopower; (c) Magnetic Susceptibility.....	7
1-2 Liquid Ga-Te Properties Vs. Alloy Composition: (a) Viscosity; (b) Molar Enthalpy of Mixing.....	8
2-1 Block Diagram of Laser Spectroscopy Experiment.....	15
2-2 Cut-Away View of Optical Furnace.....	18
2-3 Optical Furnace Sample Area Detail.....	20
2-4 Block Diagram of Fourier-Transform Spectroscopy Experiment.....	29
2-5 Phase Diagram of the Ga-Te Alloy System.....	41
3-1 Laser Power as a Function of FIR Cavity Length.....	46
3-2 Laser Power Vs. FIR Cavity Pressure.....	48

3-3 Laser Power Leaving the Optical Furnace as a
Function of Sample Height: (a) 119 μ ; (b) 1217 μ50

3-4 Solder Metal Reflectivity Vs. Temperature.....52

4-1 571 μ Reflectivity Vs. Liquid Alloy Composition:
(a) 1200 deg.K; (b) liquidus.....61

4-2 1217 μ Reflectivity Vs. Liquid Alloy Composition:
(a) 1200 deg.K; (b) liquidus.....62

4-3 119 μ Reflectivity Vs. Liquid Alloy Composition:
(a) 1200 deg.K; (b) liquidus.....63

4-4 119 μ Reflectivity Vs. Liquid Alloy Composition at
Three Temperatures.....66

4-5 119 μ Reflectivity Vs. Temperature for Three Alloys....67

4-6 119 μ Differential Reflectivity Vs. Liquid Alloy
Composition.....69

4-7 Long-Wavelength Differential Reflectivity:
(a) 571 μ ; (b) 1217 μ70

4-8	Far Infrared Reflectivity of Ga_2Te_3 at 900 deg.C.....	72
4-9	Far Infrared Reflectivity of GaTe at 900 deg.C.....	73
4-10	Low Frequency Reflectivity of GaTe.....	75
5-1	Static Conductivity Vs. Liquid Ga-Te Alloy Composition.	79
5-2	FIR Conductivity Vs. $1/T$ for Liquid Ga-Te Alloys.....	81
5-3	Activation Energy Vs. Composition.....	82
5-4	Enthalpy of Mixing of Ga-Te: (a) Data of Castanet & Bergman; (b) Deviations of Model from Experimental Data.....	91
6-2	Interference Path Through Light Pipes for Long Wavelengths.....	110
A-1	Flowchart of Experiment-Running Program.....	116a

I. INTRODUCTION

Gallium-Tellurium is a binary alloy system which, when in the liquid state, exhibits anomalous physical and chemical properties, including semiconducting behaviour. Such materials are presently little understood, despite several attempts at semi-quantitative models. A general explanation of their properties would clarify the broad field of disordered-matter physics, the largest unexplained area of condensed-matter studies. Far infrared measurements can provide important information on structural and electronic transport properties, providing input which is essential to proposed models.

•Terminology

In the following sections, abbreviations will usually be used for certain terms:

FIR far infrared

R reflectivity at a particular wavelength

x atomic Tellurium fraction, from the notation $Ga_{1-x}Te_x$.

Compositions will always be quoted in terms of atomic, and not weight or volume, fractions.

Gallium and Tellurium will usually be denoted by their chemical symbols, Ga and Te.

Radiation units will be variously wavelength in microns or frequency (inverse wavelength) in cm^{-1} . The latter term is more correctly called wavenumber; it is proportional to frequency measured in units of 1/time.

Phase changes from liquid to solid are characterized by two temperatures. The upper temperature limit of a two-phase system in which liquid and solid coexist is known as the LIQUIDUS; the lower limit, as the SOLIDUS.

A. LIQUID SEMICONDUCTORS

Liquids characterized by a low-to-moderate (below a few thousand $\text{ohm}^{-1}\text{cm}^{-1}$) electrical conductivity that rises with temperature are known as liquid semiconductors. Elemental Tellurium and Selenium are single-component examples. Most liquid semiconductors are two- or higher-component alloys (such as the group III-VI alloys Ga-Te, In-S, and Tl-Se). All melt at fairly high temperatures (typically above 300 deg.C), and are semiconductors in the solid state. Many, like Ga-Te, exhibit anomalies at particular compositions, suggestive of molecular associations or clustering.

Liquid semiconductors are also considered a subclass of amorphous semiconductors.¹ Chalcogenide-doped glasses are

solid-state examples. This class of material exhibits only short-range atomic ordering. The liquids may change the number and quality of their local bonds with temperature, leading to additional complexity over crystalline semiconductors.

The diversity of alloy combinations provides a wide variation in properties, and a corresponding difficulty in classification. Differences in electronic transport properties are the usual bases of the various classification schemes. Allgaier² suggests a 3-region scheme based on DC conductivity; Cutler,³ a metal/semiconductor dichotomy determined by temperature dependence; and Enderby et al.,⁴ a separation according to 'regular' and 'irregular' composition-dependence of electrical properties.

B. MODELS

Several paradigms have been used to explain particular liquid alloy systems. Liquid semiconductors are usually described in terms of perturbations of better-understood systems, such as crystalline materials or free molecules.

The successful Ziman theory of liquid metals serves as a foundation of the Mott pseudogap model for amorphous semiconductors.⁵ The absence of long range order is shown to

cause a minimum in the density of states (the pseudogap).

Based on several theoretical analyses, disorder is believed to localize the electron states which have energies in the pseudogap, preventing them from contributing to conduction except by phonon-assisted 'hopping'. Mott asserts that the characteristics of the pseudogap itself are related to the unique electrical properties of liquid semiconductors. Between such 'localized state' behaviour and true liquid metal conductivity, Allgaier² cites evidence for an intermediate 'Brownian motion' regime. In this transport scheme, the electrons move by rapidly jumping between neighbouring lattice sites without the necessity of phonon intervention, because the states are non-localized (such 'extended' states permit electrons to be found at infinite distances from their starting points after infinite time).

In contrast to Mott's model, more conventional explanations of certain binary alloys are proposed in the work of Cutler et al.³ Assuming liquid semiconductors to have the band structure and energy gaps common to solid semiconductors, Cutler interprets the transport properties in the standard sense of p or n type conduction, etc. For example, increase in conductivity away from the stoichiometric composition may amount to adding electrons or holes to the valence band of the semiconductor, converting it from an intrinsic to an extrinsic material. The gap width may vary with composition and

temperature-dependent structure. This increased variability causes liquid semiconductors to have a broader range of properties than their crystalline counterparts.

The Pseudobinary Alloy model⁶ seems appropriate to some systems. According to Enderby, an alloy A-B may associate as a molecular state A_aB_b (where a and b are the stoichiometric coefficients) plus the excess element, especially when near the stoichiometric composition. Sudden changes in properties at this intermetallic composition are seen as resulting from depletion of the excess constituent. Elaborations of the model include the possibility of partial dissociation of the molecules into their component elements, even at the stoichiometric composition. This scheme has been used to calculate the associated fraction of molecules by fitting the model to thermodynamic data.⁷

C. Ga-Te ALLOYS

1. Previous Work

A number of properties of the liquid $\text{Ga}_{1-x}\text{Te}_x$ alloy system have been investigated: electrical conductivity, thermoelectric power, magnetic susceptibility, viscosity, density, compressibility,⁸ enthalpy of formation, and NMR studies. The only optical measurements have been visible/near-IR reflectivity.⁹

DC conductivity¹⁰ experiences a sharp reduction (to below $100 \text{ ohm}^{-1}\text{cm}^{-1}$) at $x=0.60$ and, to a lesser extent, at $x=0.50$. (x denotes the atomic fraction of Tellurium). This minimum conductivity is small enough for localization of states, according to Mott's model. Similar, but less striking, anomalies exist in the viscosity¹¹ (positive deviations), enthalpy of formation¹² and magnetic susceptibility¹³. Thermoelectric power is positive for most compositions, and reaches a maximum near 0.6. These five quantities are each plotted versus concentration in figures 1-1 and 1-2.

For all these properties, the anomalies become less dramatic with increasing temperature, particularly for the $x=0.5$ composition. The conductivity shows an exponential

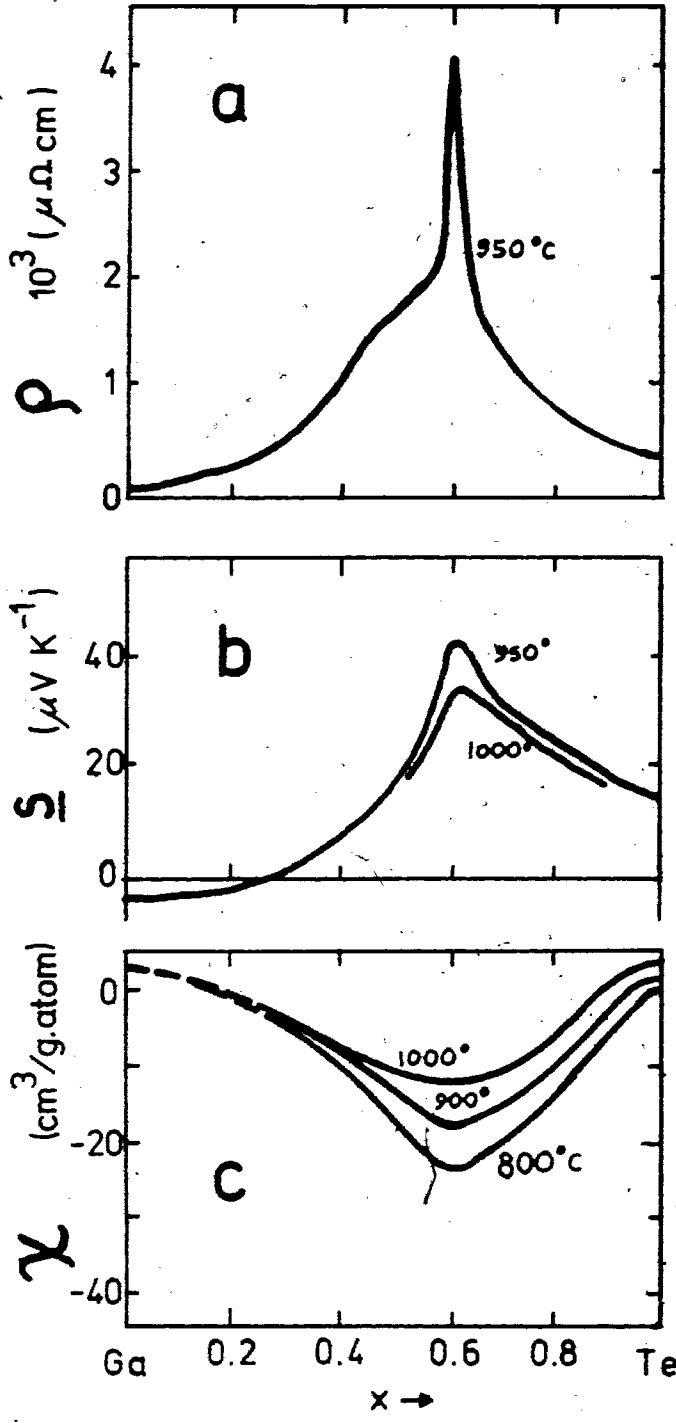


Figure 1-1 Liquid Ga-Te Properties Vs. Alloy Composition:
(a) Resistivity¹⁸; (b) Thermopower¹⁸;
(c) Magnetic Susceptibility¹³.

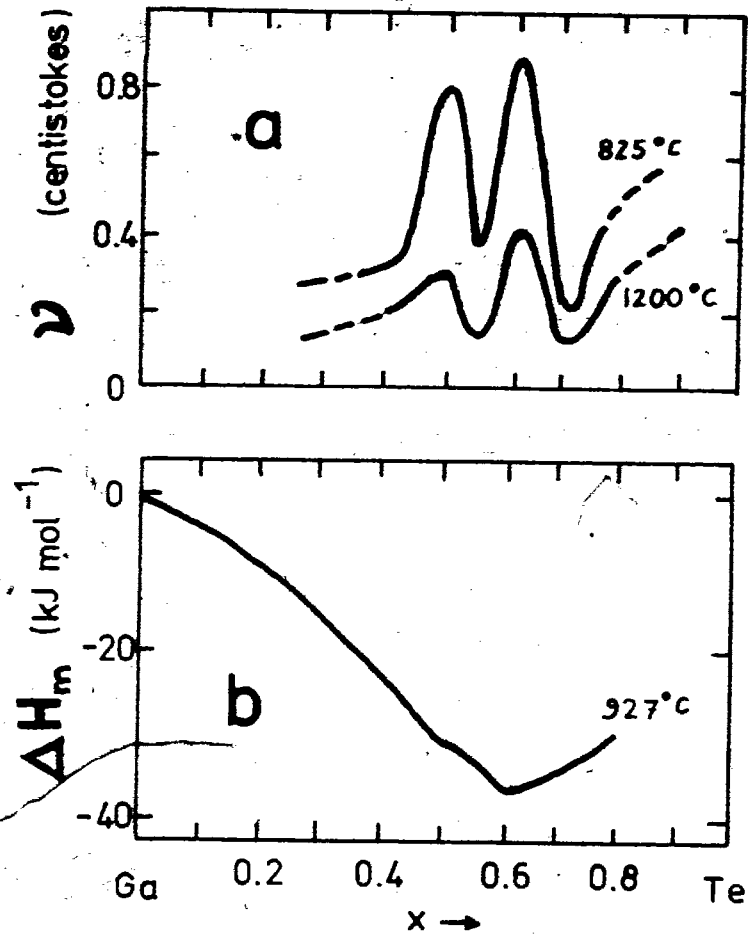


Figure 1-2 Liquid Ga-Te Properties Vs. Alloy Composition:
 (a) Viscosity¹¹;
 (b) Molar Enthalpy of Mixing¹².

temperature dependence:

$$(I-1) \quad \sigma(T) = \sigma_c \exp(-E_0/2kT)$$

The activation energy E_0 has a bell-shaped concentration dependence,¹⁰ peaking at $x=0.6$. By interpreting E_0 as a band gap energy, the investigators implicitly chose Cutler's model of alloy structure.

In combination, these data have been interpreted as indicating the existence of at least two species of atomic cluster, at $x=0.5$ and 0.6 respectively. Because of its greater temperature dependence, the $x=0.5$ compound (a suspected GaTe molecular association) is generally thought to be more weakly bound than the $x=0.6$ (Ga_2Te_3) compound.

The most conclusive evidence for such cluster formation is the NMR work of Warren.¹⁴ The Knight shifts of Ga and Te were measured, along with the quadrupolar relaxation rates for Ga-Te alloys. The shifts show deep minima for low temperature melts with $x=0.6$ and smaller shifts for $x=0.5$ alloys. Warren interpreted this as clustering of GaTe and Ga_2Te_3 near these compositions, in the presence of excess Te or Ga (i.e. a pseudobinary alloy). From the quadrupolar relaxation rate, a Ga_2Te_3 molecular lifetime of about 10^{-11} second was inferred.

Reflectivity at wavelengths between 0.4 and 1.9 microns has been measured for the Ga-Te alloy system.⁹ The results, being typically smooth, nearly featureless spectra, were interpreted in terms of models involving 3 or 14 parameters. For example, the parameters of an oscillator were chosen to represent free carriers, while other oscillators were modelled to have band gaps of various sizes. The investigators cited the reasonable fit of the model to reflectivity data as indicating energy bands and band gap structure for liquid Ga-Te alloys.

Some measurements have been reported only for the solid alloys or for a narrow range of liquid compositions. These are too restricted to elucidate the liquid state structure.

2. Far Infrared Studies

Far infrared frequencies provide valuable electronic transport information and can indicate molecular structure.

Metallic materials usually exhibit featureless FIR spectra, in accord with the Drude free-electron theory of conductivity. In this model, reflectivity is related simply to conductivity, and so should yield extrapolated conductivities in agreement with measured D.C. values.

On the other hand, strongly frequency-dependent reflectivity can often be ascribed to structure-related transitions. Vibrational-rotational modes of many molecules have energies that lie in the FIR frequency range. The optically active modes usually appear as maxima in reflectivity at the resonant frequencies of the molecules. The FIR spectrum can often reveal the masses and bond strengths which characterize the molecule or its component parts.

The far infrared properties of liquid metals have been largely neglected, despite the existence of a very useful tool - the FIR laser. The laser permits fairly precise absolute measurements of reflectivity to be made as a function of sample temperature. In contrast, the standard FIR tool - the Fourier-transform spectrometer - is more suited to constant-temperature, broad-band observations. Both devices have been used in the experiments described here to study the temperature-, frequency-, and composition-dependence of Ga-Te alloy reflectivity. The use of these two systems is described in detail in sections II-A and II-B, respectively.

The only previously published FIR study of this subject is for the Mg-Bi alloy system, using Fourier-transform instrumentation.¹⁵ Other measurements of this system had

suggested the existence of an Mg_3Bi_2 molecule near the stoichiometric composition. An anomaly was indeed found at this composition; reflectivity increased, over a concentration range of $\pm 3\%$ from the intermetallic composition, to nearly unity. This is in contrast to the predictions of the simplistic Drude or nearly-free electron models which predicted a drop in reflectivity in accord with an observed dip in DC conductivity at the critical composition.

This thesis describes FIR reflectivity experiments performed on Ga-Te alloys to determine whether the Mg-Bi results are unique to that system, and, if not, how such unexpected behavior can be understood in terms of a general liquid semiconductor model.

Initial tests, detailed in chapter III, were extended to systematic measurements which yielded the results described in chapter IV. In the light of theories mentioned above, the data are fitted to various models in chapter V. Discussion of the data and conclusions are presented in chapter VI.

II. INSTRUMENTATION AND PROCEDURE

Far infrared reflectivity observations, varying temperature, alloy composition, and optical frequency, were made with the aid of (A) a laser system and (B) interferometer apparatus.

Submillimetre lasers have been available since the early 1960's.^{16,17} During the first decade, laser design and properties occupied the attention of experimenters; it is only in the last ten years that applications of the devices have been much investigated. To date, laser spectroscopy has mostly involved measuring parameter-dependent absorption, e.g. cyclotron resonant absorption as a function of applied magnetic field.¹⁸ Some studies of liquids have been reported,^{19,20} but to the author's knowledge, few if any reflectivity experiments have been performed.

The laser permitted relatively fast measurements to be made as a function of sample temperature. The interferometer was used to obtain reflectivity data at a fixed temperature over a wide range of frequencies.

A. LASER REFLECTIVITY MEASUREMENTS

Reflectivity of the prepared alloys was determined at discrete wavelengths by using a far infrared (FIR) laser as light source. The experimental configuration is shown in fig. 2-1. Measurement of reflectivity consisted essentially of channeling radiation from the laser to the surface of the melted sample. This light was reflected once and channeled to a detector. The intensity measurement was then divided by a similar measurement of a reference material to obtain true reflectivity of the Ga-Te sample. The principal components in the experiment were: (1) a far infrared laser system; (2) a sample melting furnace with optical access; and (3) detection apparatus.

1. Laser System and Optics

The laser is similar to systems described in the literature,^{21,22} and so will be only briefly mentioned. The FIR laser cavity consists of a cylindrical gold-coated waveguide with adjustable end mirrors. The lasing medium is optically pumped by a 25 watt Coherent Radiation Model 42 CO₂ laser. The pump beam is focused through a quartz window and 2 mm hole at one end of the cavity. Methyl alcohol was used as the laser gas because of its large number of strong transitions in the FIR. Three of the strongest lines, 119,

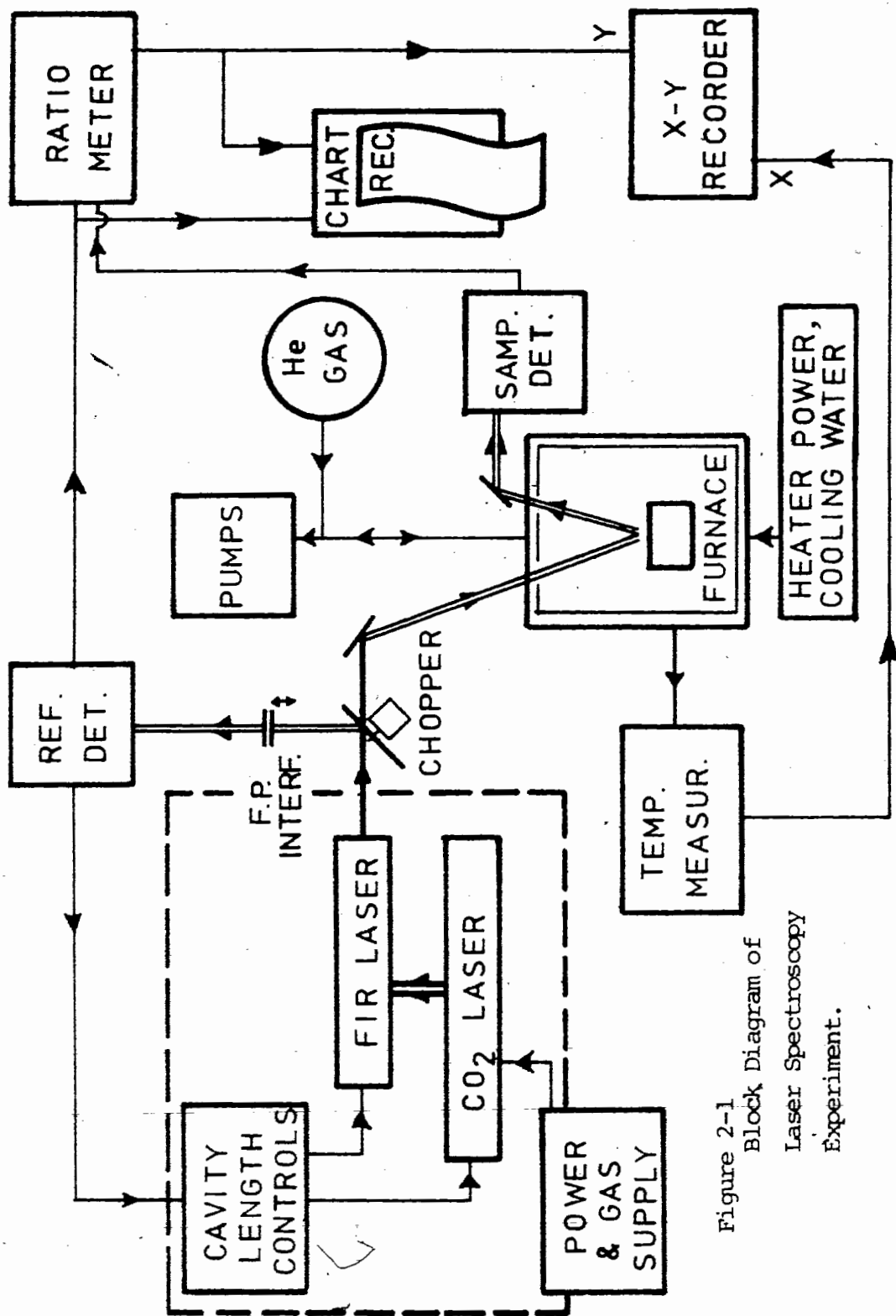


Figure 2-1
 Block Diagram of
 Laser Spectroscopy
 Experiment.

571, and 1217 microns, which span the FIR region, were used for the reflectivity experiments. Their relative intensities (of the order of milliwatts) were roughly 4, 1, and 3, respectively. The FIR output wavelength is selected by first tuning the CO₂ laser to the near-IR wavelength appropriate to excite the methyl alcohol molecules. This is accomplished by selecting the line with an internal diffraction grating, and then adjusting the cavity (henceforth called the IR cavity) length with a piezoelectrically positioned end-mirror. Next, a stepping motor is used to vary the FIR cavity length until it is approximately an integral number of half wavelengths of the FIR transition of methyl alcohol. Fine adjustment is then made with piezoelectric end-mirror positioning. The IR cavity and FIR cavity piezoelectric positioners can both be automatically adjusted by feedback loops to maintain maximum output power.

Radiation is channeled from laser to detectors via light pipes. In these experiments, a mechanical chopper directed light alternately to the reference detector and the optical furnace. The detectors were Molelectron Corp. P4-43 pyroelectric detectors, with average sensitivity of about 100 V/W in the FIR. One detector was used to detect intensity modulations (introduced by vibrating the piezoelectric positioners with an AC voltage) introduced for the feedback loops, and also to act as the 'reference' detector: even with

automatic compensation of cavity length variations, 'raw' output power was not sufficiently constant to serve as a reference in an absolute measurement. The detector signal passed to three lock-in amplifiers, for IR and FIR control and signal amplification, respectively. The amplified signals of the reference detector and a 'sample' detector - monitoring furnace output - were divided by a digital ratiometer to yield an output proportional to the intensity of light leaving the furnace, but corrected for power fluctuations of the laser:

$$I_{\text{compensated}} = I_{\text{sample det.}} / I_{\text{reference det.}}$$

The reference arm of the light path also contained a Fabry Perot interferometer (with mylar mirrors) with which wavelength could be determined to within 2%. This was adequate because FIR methanol lines are widely spaced in wavelength, and because their precisely measured values have been published. The alternate (sample) path directed radiation from the brass light pipes through the furnace windows and ultimately to the sample detector.

2. Optical Furnace

The furnace itself was a double-walled welded stainless steel cylinder with removable lid. A cut-away drawing is given in fig. 2-2. All walls and lid surfaces were cooled by flowing water. The lid contained light pipe and vacuum

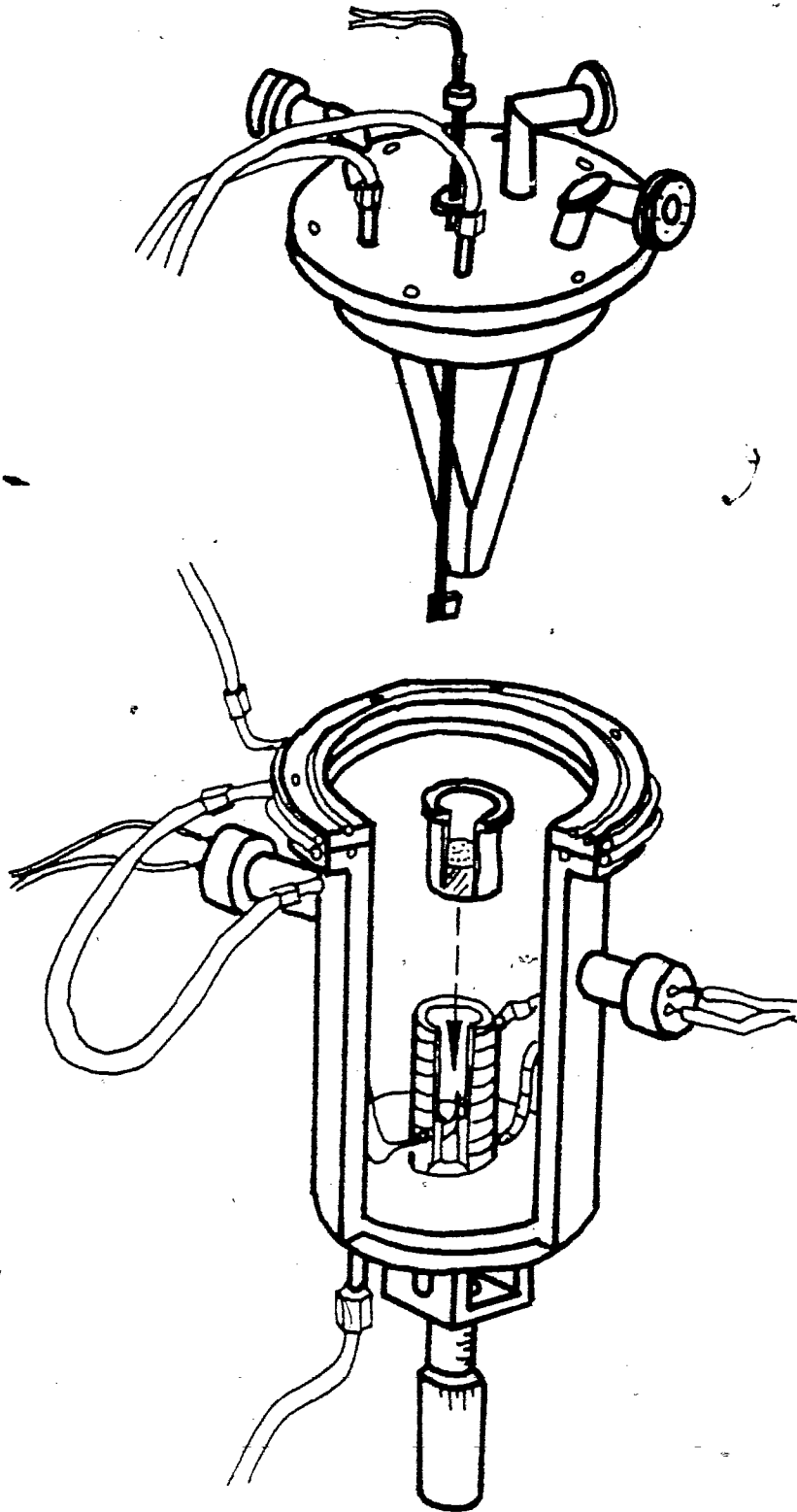


Figure 2-2
Cut-Away View of Optical Furnace

connections, and was rigidly bolted to a metal frame to maintain constant optical alignment with the laser. Radiation passing through 1.5 mm thick polyethylene furnace windows reflected down a stainless steel light pipe, impinged on the sample at 16 degree incidence, and reflected back out to the sample detector. The light pipes delivered and collected radiation from an area about one cm in diameter on the sample surface. The silica crucibles themselves had inner diameters of approximately 2 cm. Sample-area details are illustrated in fig. 2-3. A stirring rod/thermocouple probe could be lowered at any time into the sample crucible. The stirring rod was constructed of silica, one of the few materials which does not react with the alloys. To the crucible holder, which could be moved vertically by an external micrometer to optimize specular reflection, was affixed a second thermocouple. Both thermocouples were Chromel-Alumel. The remainder of the furnace, containing the crucible holder, its heater, electrical and water connections, could be raised with the aid of a jack to facilitate attachment to the lid. The crucible holder was resistance heated, and could reach a maximum temperature of about 940 deg.C. Heater power was controlled by a 3.5 kVA variac.


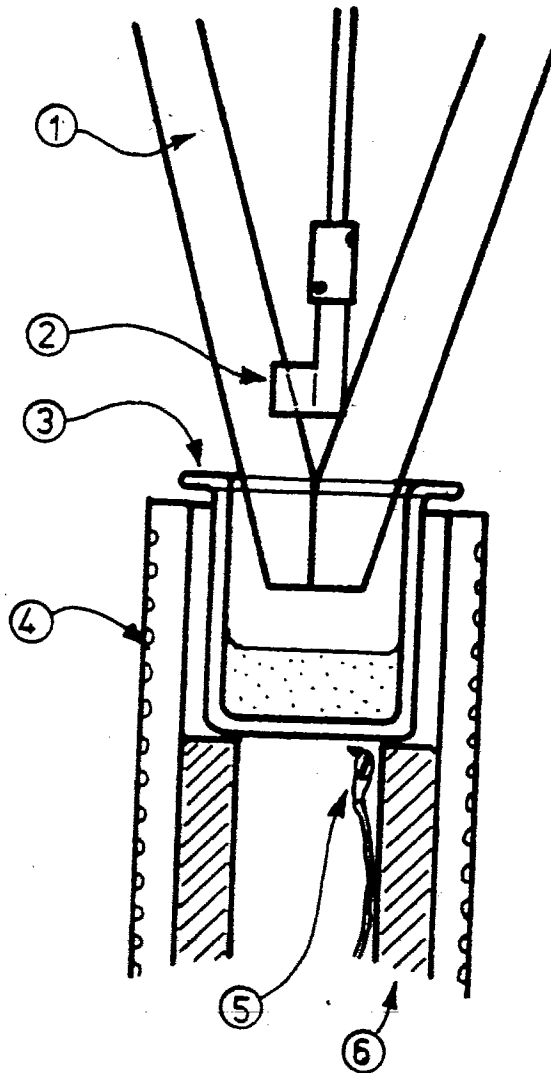


Figure 2-3 Optical Furnace Sample Area Detail:
(1) light pipes; (2) silica stirring rod;
(3) silica crucible; (4) heater wire wound on boron nitride cylinder;
(5) thermocouple; (6) micrometer-adjustable support.



3. Detection

The FIR laser, with its relatively high output power (a few milliwatts), permitted the use of pyroelectric detectors. These have responsivities (signal change per FIR power change) about 10 X worse than He³-cooled detectors, and are about four orders of magnitude noisier. Pyroelectrics, though, have the advantage of operating at room temperature with good reliability. The accuracy of signal detection is limited mainly by mismatch of the response characteristics of the two detectors. For example, the estimated error due to temperature drift in the detector is 0.3%/deg.C.²³ Amplifier noise contributes a comparable random uncertainty. Any differences in spectral sensitivity of the two detectors were compensated for by the scheme of dividing independent reference and sample observations.

Detection of radiation becomes less efficient with smaller wavenumber. Light cones immediately before the pyroelectric detector-element channel the light from the light-pipe diameter to the diameter of the sensing element. Such a decrease in beam area brings a corresponding increase in the angle of the light rays with respect to the cone axis, as described by Williamson.²⁴ The initial maximum angle of radiation leaving the laser exit-mirror is determined by the

wavelength and the coupling hole diameter d by

$$(II-1) \quad \theta = \sin^{-1}(1.22\lambda/d)$$

Thus, smaller-wavenumber radiation is increasingly diverged by diffraction. The ability of a light cone to collect radiation is related to its entrance and exit diameters, D_{in} and D_{out} , and taper. In the limit of infinite cone length, there exists a maximum angle which can be channeled through the cone, given by

$$(II-2) \quad \sin \theta = D_{out}/D_{in}$$

so
$$\lambda_{channelled} < dD_{out}/1.22D_{in}$$

Because of this, orientation of the detectors becomes more critical for long wavelengths, for which the non-paraxial portion of the radiation is not collected. This is also the case for higher transverse laser modes, where the output power is distributed through relatively large angles with respect to the light pipe axis. The effect was also important in the optical furnace, where cones directed the light from 12 mm brass pipes to 9 mm steel furnace pipes.

The effect of blackbody radiation must also be examined.

For sample temperatures of 900 deg.C, Stefan's radiation law predicts power radiation of nearly ten watts per square centimeter, with peak emission at a wavelength of about 2.4

microns. The samples glow bright red at this temperature. Much of this emitted light is scattered by the diffuse furnace window or is too divergent for light-pipe channeling. Black polyethylene and quartz filters in the detectors proper also absorb most non-FIR radiation.

While the remaining blackbody radiation is comparable to the laser output power, it is unmodulated: the mechanical light chopper precedes the furnace. Accordingly, the constant blackbody component of the detected radiation is ignored by the frequency-selective lock-in amplifier. It is still possible, though, for this light to overload the pyroelectric detector. To test for an offset or overload, the furnace light pipes were blocked before and after the hot furnace: in both cases, the modulated signal fell exactly to zero, indicating that no offset had been introduced. Additionally, the light pipe was blocked with mylar when the furnace was first hot and then cold; no difference in transmissivity was noted, implying linear detector response at high temperatures. As a second test, the reflectivity of a copper mirror was observed as the furnace was heated to 900 deg.C. Warming caused a very reproducible 18% decrease in signal strength. This is ascribed entirely to thermal expansion, which caused deviation from specular reflection by shifting the sample's height. A similar result was obtained by cooling a mirror from 900 deg.C, provided that its height had been initially

optimized for reflection. Hence, sample emission had no effect on measurements. The lack of any observable change in the reflectivity of the stainless steel light pipes with temperature implies that room temperature copper reflectivity measurements were valid references.

4. Measurement Procedure

Experimental procedure was as follows. The laser system was adjusted to the desired wavelength and allowed to stabilize. The signal from the furnace detector was measured, at room temperature, with a reference material in the furnace. A flat aluminum disk in a steel crucible was used as the reference. Later, the aluminum disk reflectivity was found to be less than that of some liquid samples, implying less-than-100% R. The low reflectivity is ascribed to roughness of the surface rather than intrinsic aluminum properties or surface contamination. To correct this error, the aluminum reflectivity was compared to that of a gold-coated glass disc, which was known to have near-100% reflectivity in the far infrared. The gold reference had a reflectivity larger than any alloy.

After the reference measurement, the furnace was opened carefully. The reference crucible was replaced by the sample ingot in its silica crucible. The system was pumped down with

roughing pump, lid screws were evenly tightened, and the furnace was evacuated via a diffusion pump to less than 10^{-4} torr. Helium gas was then admitted to the system to an overpressure of about one atmosphere. The gas had been dried by passing through a long copper coil immersed in liquid nitrogen. This cold trap was kept open throughout the run to collect any water or outgassed vapours released while heating. Variac voltage was then increased in steps until furnace temperature exceeded the sample melting point. This was signalled by an abrupt increase in reflectivity, R.

After a constant reflectivity and temperature had been obtained, the stirring rod was lowered into the sample crucible and rotated. This removed any solid surface film which may have been present, and made the alloy more homogeneous. Sample height was changed by the external micrometer until R was maximum. Stirring and height optimization were repeated at least once per run.

Measurements at the maximum temperature were made at thermal equilibrium. In addition, while cooling slowly, the reflectivity was recorded to note temperature dependence. Variac voltage was reduced in small steps. The sample thus cooled through the freezing point at an average rate of 12 deg.C per minute. When furnace temperature stabilized at each of the intermediate variac settings, thermocouple signals were

recorded. In addition to these numerical data, a chart recorder (R and 'raw' laser output power versus time) and X-Y recorder (R vs. temperature) constantly recorded changes. The chart recorder was used to note any systematic changes in signal attributable to the laser.

When cooled to below 50 deg.C, the furnace was opened, the sample was again replaced with the aluminum blank, and the measurements were repeated at room temperature to provide a second reference reflectivity. The two reference measurements typically agreed to about 5%. The average of these 'before' and 'after' references was used with the average sample signal to determine normalized reflectivity and measurement uncertainty.

B. BROAD-BAND SPECTRUM MEASUREMENT

Searches for molecular modes, which should appear as sharp features in the far infrared reflection spectrum, were effected using an interferometer system. Compositions corresponding to GaTe and Ga_2Te_3 , compounds known to exist in the solid state, were selected as those most likely to evince molecular-mode properties.

1. Introduction

Fourier Transform Spectroscopy is the most suitable technique for broad-band study in the far infrared. Large-aperture optics and multiplexing - simultaneous detection of all frequencies in the light source - make optimal use of the little energy available from broad-band sources in this spectral region.²⁵ A spectrum covering the entire far infrared is obtained from corresponding interferometer measurements. The interferometer accepts light from a continuous-spectrum source, separates it into two beams, and adjusts their relative phase. This is accomplished by adjusting a mirror position so that the length of path travelled by one of the two beams is increased. The two components are then recombined and passed along to the sample. The intrinsic properties of the sample will modify the intensity of light reflected: this will depend on the

'frequency make-up' of the light i.e. the interferometer mirror position. The intensity modulations are detected and recorded as a function of mirror position. It can be shown that the resulting 'interferogram' is proportional to the Fourier transform of intensity versus optical frequency data, i.e. the desired spectrum.²⁶

Spectrum measurement thus involves several steps. Observations of intensity vs. optical path difference are collected. These are Fourier transformed to yield the sample spectrum. Similar data are obtained for a reference material (something with near-100% reflectivity throughout the spectral region of interest). By dividing the sample and reference spectra, the instrumental effects (e.g. source spectral distribution or filter absorption) can be removed.

2. Apparatus

Fig. 2-4 shows a block diagram of the interferometer apparatus. A modified Beckman RIIC FS-720 Michelson interferometer was used to modulate the radiation from a water-cooled mercury arc lamp. The source intensity was modulated by an oscillator-controlled mechanical chopper to permit lock-in detection. One mirror of the interferometer was stepped by a fixed increment on reception of a signal from a computer. The radiation passed down brass light pipes to

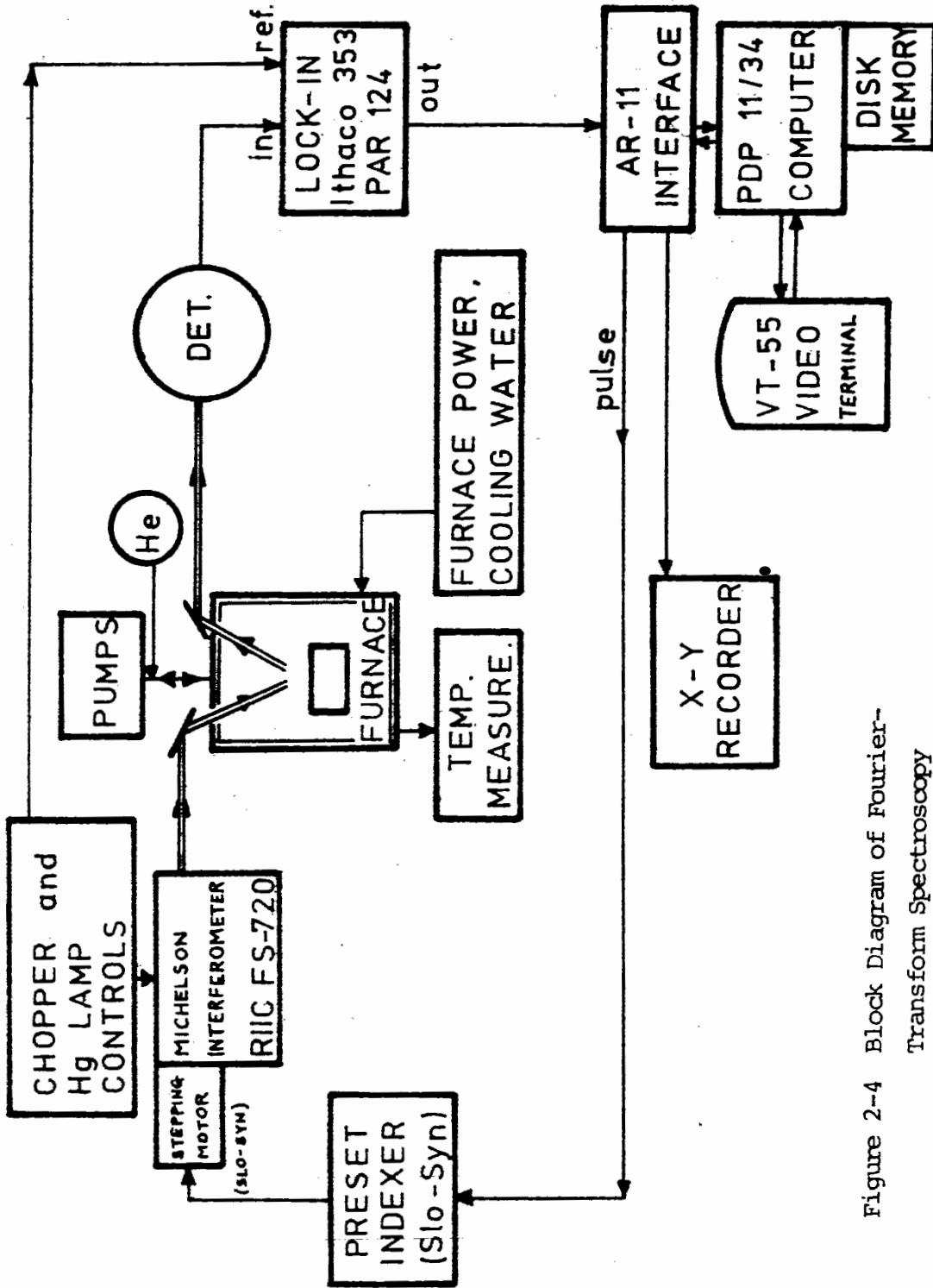


Figure 2-4 Block Diagram of Fourier-Transform Spectroscopy Experiment.

the optical furnace and then to the detector. Between furnace and detector, the light was filtered by various filter combinations to restrict transmission to frequencies smaller than some maximum, as listed in Table II-1. This ensured correct spectral transformation, and prevented overloading of the detector, a He³-cooled Germanium bolometer.²⁷ After electrical filtering of high-frequency noise, the detector signal was passed to a lock-in amplifier, and then to the computer.

3. Computer and Programming

Active control of the experiment, data recording, and display were handled by a minicomputer. The output of the lock-in amplifier was transmitted to an analog-to-digital (A/D) converter, a PDP AR-11. This latter device also performed D/A conversions for transfer of data to an X-Y recorder, and contained an internal clock for timing operations.

The computer itself was a Digital Equipment Corporation PDP 11/34 with 28k-word available memory (16 bit words). Additional storage was available on a double floppy-diskette drive. In addition to the A/D converter, peripherals included a VT-55 video terminal which permitted graph plotting, an X-Y recorder, and a DECWRITER III hard copy terminal.

TABLE II-1

INTERFEROMETER HIGH FREQUENCY CUT-OFF COMBINATIONS

Freq. Range	Mirror Step Size	Filter (thickness)	Beam Splitter Thickness
0 - 700 cm^{-1}	5 μ	---	15G (4 μ)
0 - 250 cm^{-1}	20 μ	Boron Nitride 3 mm	50G (12 μ)
0 - 125 cm^{-1}	40 μ	Quartz + NaCl + LiF 4 mm + 3 mm + 2 mm	100G (25 μ)
0 - 70 cm^{-1}	80 μ	Quartz + NaCl + LiF + KI 4 mm + 3 mm + 2 mm + 2 mm	200G (51 μ)

NOTE: Black polyethylene was used as a cryostat-insert window in all cases.

All filters were cooled to liquid He temperature to absorb room temperature radiation.

The experiment-running program was written in FORTRAN IV by the author, using packaged subroutines²⁸ for operations such as repetitive sampling of the lock-in amplifier's output, timed 'wait', and output of a voltage pulse.

This program, listed in appendix A, accepted run parameters from the operator; these included the desired gate time (period over which the detector signal was to be averaged), deadtime (between-measurement waiting interval, during which the interferometer mirror moved and the amplifier locked-in to the signal), mirror step increment, and number of points to be acquired. The program then caused a voltage pulse to be sent to the mirror indexer, waited the deadtime, sampled the amplifier output for the gate time, plotted this measurement on the video screen, and repeated. Data acquisition could be stopped at any time (without loss of data) by a toggle switch. Periodically during acquisition, a fast-Fourier-transform was performed on the data and plotted on the screen. When the run was complete, the data and/or final spectrum could be plotted and stored as a named file on disk. If desired, real-time transforms or mirror stepping could be excluded from the run operations, to allow either faster acquisition or test of the set-up parameters, respectively. Up to 1120 points could be accepted, yielding, after a thirty-four second transformation, a 1024 point

spectrum.

Simpler programs, not listed here, permitted data files to be averaged for better signal-to-noise ratio and de-emphasis of electrical noise 'glitches', plotted on video screen or X-Y recorder, and divided by 'reference spectrum' files.

4. Procedure

After allowing all electronic apparatus to stabilize for several hours, and having prepared the bolometer detector for operation, the optical furnace and interferometer were evacuated with separate diffusion pumps. A copper mirror in a silica crucible had previously been placed in the furnace. When a vacuum better than 10^{-4} torr had been attained, the furnace was backfilled with dry He. To avoid vibrations which appeared as periodic oscillations in the detector signal, the interferometer pump was replaced by a sorption pump when acquiring data, and the furnace mechanical pump was turned off.

Using the computer, bolometer output was averaged for various time intervals to determine the minimum acceptable gate times. A signal to noise ratio of about 100:1 was typically obtained by using 2 to 3 second averaging times.

The interferometer mirror stepping increment was chosen to conform to previously selected beam splitter and filter combinations, as shown in Table II-1. The step size is restricted to one-half the minimum wavelength transmitted by the filters, in order to avoid 'aliasing', or ambiguous Fourier transformation of the data.

The total distance of interferometer mirror travel is inversely proportional to the spectral resolution obtained. The number of mirror steps was selected accordingly, providing typical resolution of 2 to 10 cm^{-1} .

When the experiment parameters had been chosen, two or more reference spectra were run. Apparatus and data acquisition were computer controlled, requiring only resetting of the interferometer mirror position after each run. Periodically updated spectra, displayed by the video terminal, showed the quality of the data, allowing interesting features to be noted and bad runs to be aborted.

The furnace was next opened to replace the reference with the solid sample, then closed, evacuated, and backfilled with dry He to a pressure of about two atmospheres. After heating the sample past the melting point, it was stirred with the silica stirring rod, and its height was adjusted for specular reflection.

Data were acquired for up to four hours using each melted sample. Intermittently, the melt was stirred to ensure a clean, homogeneous surface. Gradual evaporation of liquid onto the light pipes reduced the radiation leaving the furnace. This caused only a general drop in bolometer signal, and no significant frequency dependent change in the recorded spectra. Because of the length of the interferometer runs, sample evaporation was greater than in the laser runs. The change in sample composition is described further in Section III-C.

Following these runs, two or more Cu reference runs were again recorded.

Reduction of the data included averaging of spectra, numerically dividing spectra, and correcting for the time-dependent light pipe contamination. Averaging was mandatory to obtain good S/N ratios, particularly at the extremes of the frequency range. By dividing sample by reference spectra, the intrinsic instrumental response is removed, leaving the true frequency-dependent sample reflectivity. Furnace contamination was corrected for by averaging reference spectra that had been recorded before and after heating the sample, and by noting and compensating any linear decrease in interferogram intensity in successive sample spectra. The latter operation was seldom required,

because most of the furnace contamination seemed to occur in the first few minutes of sample melting. The absolute reflectivity is estimated to be correct to about $\pm 10\%$.

C. SAMPLE PREPARATION

1. Requirements

For accurate and reproducible measurements of reflectivity, samples had to be well alloyed and reasonably flat (although the requirements for specular reflection at FIR wavelengths are much less severe than for visible work). All samples, once melted, had flat surfaces except for edge meniscus. The similarity of surface shape for the solid and melted sample was confirmed by watching the freezing transition: after the He-backfilled silica tube containing the sample was removed from the melting furnace (at 950 deg.C), the shape and position of the ingot edges remained constant. Based on visual examination of the 'frozen' solids, the meniscus ranged from convex for the pure Gallium-silica boundary, to concave for pure Tellurium in contact with silica. In all alloys, this edge curvature was significant only within about 2 to 3 mm from the crucible sides, affecting only about 20% of surface area. This region was outside the

FIR "beam", and thus did not contribute to the reflectivity measurement.

2. Sample Reactivity

Initial attempts to prepare suitable samples were frustrated by leaks in the optical furnace. Heating above about 500 deg.C caused the sample surfaces exposed to the furnace atmosphere to spatter, become grey or black, and to cover the interior walls with grey-brown greasy dust. This contamination seemed to be accentuated when stainless steel crucibles were used. Several minor changes, such as the use of silica crucibles and an increase in the dry-He pressure in the furnace were only partially successful. After much fruitless effort using a helium mass-spectrometer leak detector to test the furnace exterior, the contamination was traced to leaks in the silver-soldered light pipe joints between the inner surface of the furnace and the surrounding water jacket. These had allowed water vapour to stream over and react with the heated liquid sample. Once the leak was fixed, samples were not visibly degraded by melting in the furnace.

Tellurium has a very high vapour pressure at elevated temperatures. It exists in two solid forms; a crystalline, shiny silver-grey material, and a black, amorphous powder.

The latter form is frequently mixed with the predominant oxide, TeO .²⁹ Attempts to melt solid pieces of Gallium and Tellurium together under good vacuum (about 10^{-5} torr) invariably led to blackening of the container walls with black, sooty substances and metallic 'plating'. The soot was not of a single composition, as evidenced by different rates of dissolution in sulphuric acid. A product of the chemical reaction between the 'soot' and acid was tentively identified as $\text{Te}(\text{SO}_3)_2$ by its purple colour, thus identifying the black material as either amorphous Tellurium or TeO . Although Ga_2O is also grey-black, the vapour pressure of Ga is negligible.³⁰ The metallic plating, which occurred only on the high temperature surfaces (hotter than about 800 deg,C) is believed to have been crystalline Tellurium.

3. Methods

To avoid the excessive vapourization and contamination of Tellurium described above, two sample preparation techniques were tried. The first, used by numerous workers,^{9,10} involved placing solid Ga and Te in a silica tube, evacuating to less than 10^{-4} torr, sealing off using an oxyacetylene torch to form an ampoule, and then heating this ampoule in a larger silica tube in a resistance-heated melting furnace. The larger tube could be easily withdrawn from the furnace cavity, examined, and shaken to mix the liquid contents of the

ampoule. The tubes were then allowed to cool slowly to room temperature, the ampoule was broken, and the alloy ingot was placed in a crucible for subsequent use. Although this method yielded excellent samples, it was lengthy and produced ingots of inconvenient shape for the optical furnace.

For this reason, a simpler procedure was adopted. Weighed fragments of solid Ga and Te were placed in a silica crucible. This crucible was positioned at the bottom of a larger, evacuable silica tube. The latter was pumped down to less than 5×10^{-5} torr, backfilled with dry Helium to an overpressure of about 1/3 atmosphere, and placed in the melting furnace cavity. The Helium gas had been dried by passing it through a liquid-Nitrogen-filled cold trap. Temperature was monitored by a Chromel-Alumel thermocouple placed in the furnace wall near the silica tube. To aid mixing, the larger tube was tapped up and down repeatedly when the sample had melted. The melting furnace used furnace-brick for walls and base, and the silica tube was wrapped by braided asbestos tape. Thermal inertia, therefore, was high, with heating times to reach 900 deg.C being typically 45 minutes. Samples cooled over the same range in about three hours.

The elements were purchased from the Alfa Div. of Ventron Corp., Danvers, Mass. Purities were 99.99% for Ga and 99.9998% for Te. To avoid exposure to poisonous Te fumes or

dust, a face mask and gloves were worn while weighing out the nine gram samples.

Thirteen different alloy compositions, accurate to 0.1%, were prepared for use in three series of runs: 47, 50, 53, 60, 63, and 70 at.% Te (first series); 34, 40, 50, 55, 60, 66, 75, 85 at.% Te (second series); 50, 60 at.% Te (third series).

Very-Ga-rich samples were excluded because of a miscibility gap in the alloy system for at.% Te between 0 and 33%: such alloys simply do not exist. The phase diagram of the alloy system is given in figure 2-5.

Using the second arrangement, little coating of the silica tube walls was observed, though yellow Tellurium vapour was present in the bottom of the tube at high temperatures. Alloys were shiny, silver-grey, uniform in appearance, and usually contained flat or grainy crystals of a few millimeters in diameter. All Te-rich alloys were brittle, easily ground or shattered. They dropped easily as ingots from the cooled silica crucibles. This 'no-wetting' characteristic of silica was advantageous when stirring the melt with the silica stirring rod.

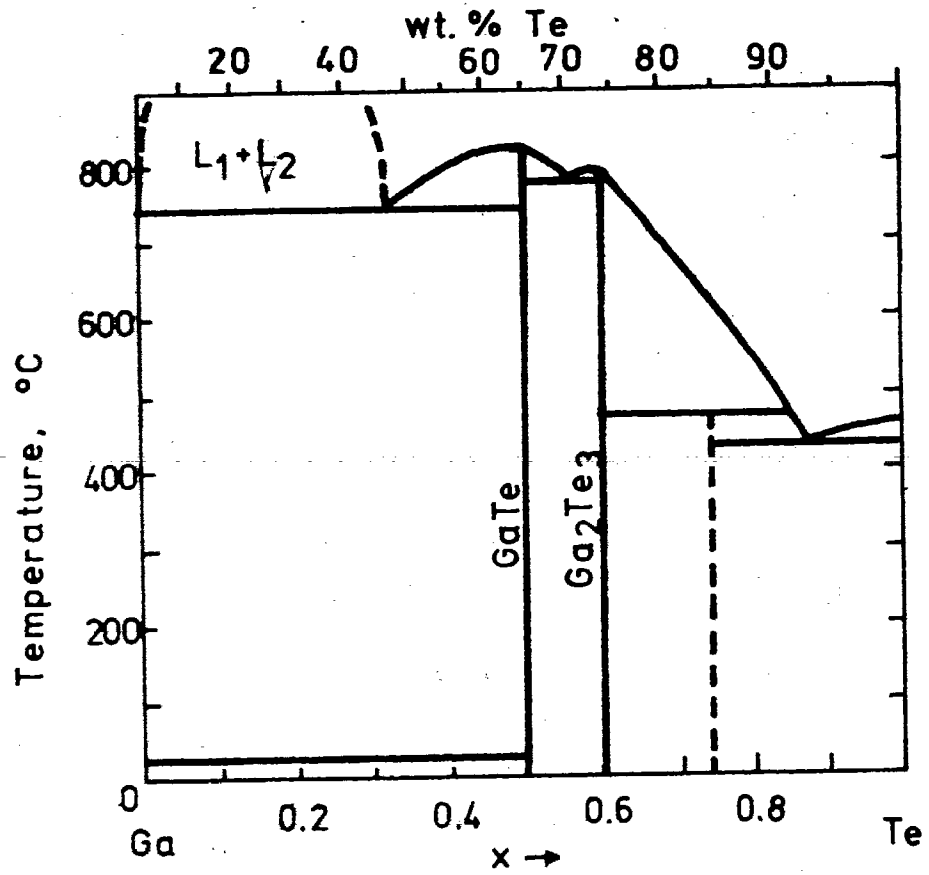


Figure 2-5
Phase Diagram³² of the
Ga-Te Alloy System.

D. In-Situ MELTING

During a run, the prepared ingot in its silica crucible was melted in the optical furnace. Procedure was modified from the initial preparation so that loss of Tellurium was minimized: the cool (about 100 deg.C) interior furnace walls became coated with black Tellurium dust as Tellurium vapour sublimed; this was reduced somewhat by using a higher pressure (about one atmosphere overpressure) of dry Helium gas. The crucible and the light pipes were free of this contamination because of their high temperature. However, over several short laser runs or one long interferometer run, Tellurium accumulated on the bottom few centimeters of the pipes as shiny crystallites. This exposure to Te vapour at high temperature caused deterioration of the bottom edge of the light pipes, necessitating their replacement periodically. The loss in mass of the 8 g crucible plus 9 g ingot as a result of sample melting during a laser run was typically thirty to forty milligrams. Assuming the worst case, with Te evaporation comprising all of the loss, the change in sample composition did not exceed 0.2% per run.

~~The optical furnace could be heated to 900 deg.C within~~
about twenty minutes, and cooled in roughly thirty minutes. Rapid cooling, along with segregation of alloy constituents on freezing,³¹ is believed to account for the variety of crystals

observed on the solid sample surface after cooling. These ranged from fan-like 'window ice' crystals to needles, to the previously mentioned plate or grainy crystallites. The much slower freezing during subsequent runs tended to produce larger flat, mirror-like crystals. The forms are believed to be combinations of GaTe (monoclinic lattice) and Ga_2Te_3 (zincblende lattice).³²



III. INITIAL TESTS AND EXPERIMENTAL PROGRAMME

A. FAR INFRARED LASER

Properties of the FIR laser were catalogued to determine their influence on measurements. Several pertinent effects were noted.

1. Mode Differences

It was initially hoped that repeated reference runs would not be necessary. The furnace output, when divided by reference detector output, (resulting in what will henceforth be called 'compensated output'), was expected to be constant for any one TEM mode of a given wavelength. However, by locking onto different longitudinal modes of the same transverse type (e.g. TEM_{00x}, where x is a large integer), differences in the compensated output of about 10% were observed. This was probably a result of imperfect alignment of the FIR cavity mirrors. Minor differences in angle of exit of the beam from the FIR laser can cause major changes in received power because of incomplete capture of the light reflected from the sample surface. Furthermore, the problem is accentuated at longer wavelengths. (Cf: 'Detection', section II-A-3).

Because of this, experimental procedure involved measuring the reference reflectivity at least once for every laser mode 'locked onto'. As the laser could be kept locked to a single mode for hours, if necessary, this proved to be easily achieved.

2. Laser Stability

Mode jumping was a second troublesome effect. A plot of laser output power vs. FIR cavity length is shown in fig. 3-1. The FIR cavity, when scanned in mirror separation, lases when the cavity length is a half-integral number of wavelengths. However, different transverse modes may have very slightly different 'cavity periods' and so may occasionally overlap.³³ When two modes are both approximately satisfied by a cavity length setting, lasing may change abruptly from one to another as changes in temperature or cavity gas pressure cause the optical path length to vary. Since the 'throughput' for different modes is different, a reflectivity measurement will appear to change abruptly. In practice, this effect occurs only at a wavelength of 119 microns, where, because of the relatively short wavelength, longitudinal modes are closely spaced as a function of FIR cavity mirror separation. Also, by proper mirror alignment and careful optimization of the output power, mode jumping can

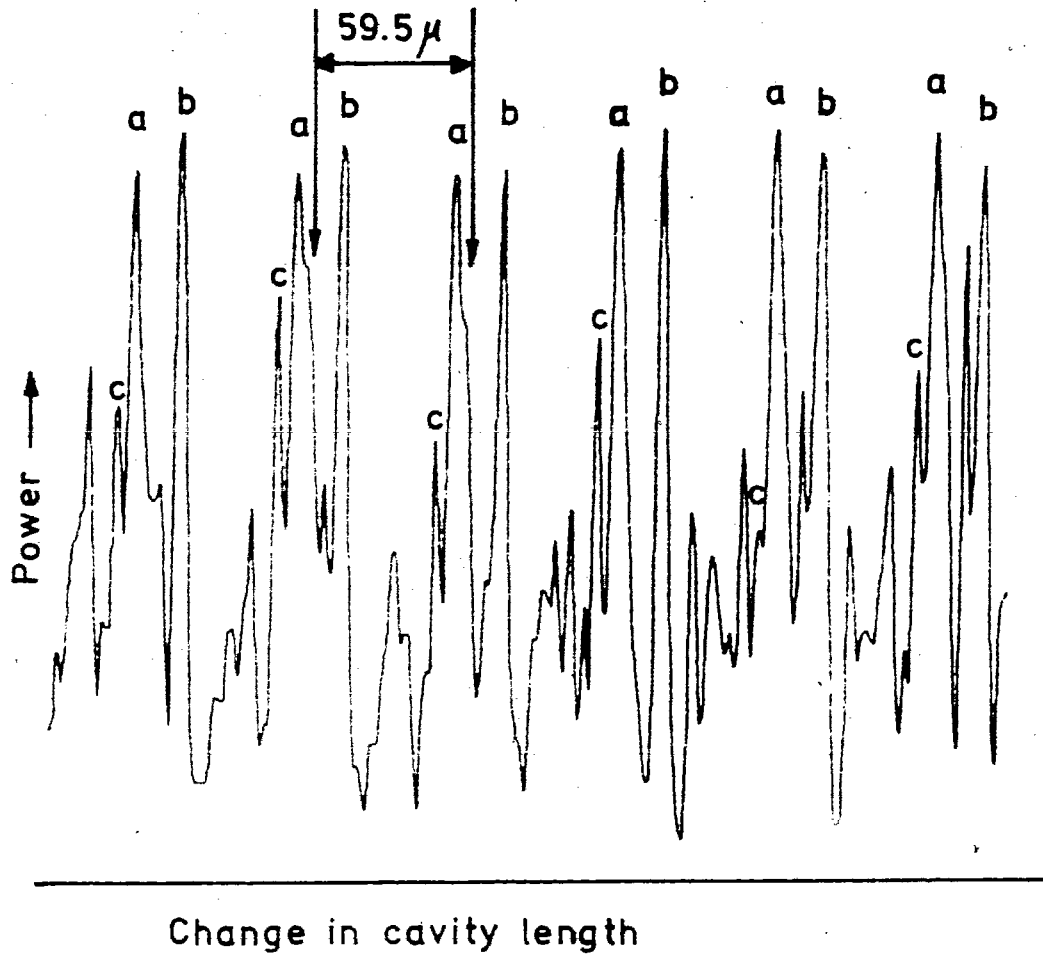


Figure 3-1

Laser Power as a Function of
FIR Cavity Length.

Arrows indicate overlapping
modes. Letters denote modes
of the same transverse type.

always be identified and corrected.

3. Cavity Pressure

A third laser property influencing measurements was the dependence of output power on the pressure of the FIR cavity gas, methanol. While the compensated signal is independent of beam intensity, a reduction in laser power will clearly decrease the signal-to-noise ratio. For six laser lines studied, output power was maximum for a cavity pressure in the range 150-350 millitorr, and varied with pressure in a qualitatively similar way. Fig. 3-2 plots output power as a function of cavity pressure for the 119 micron line.

The cavity gas pressure is controlled to within 5 mT by adjustment of a needle valve between a liquid methanol reservoir and the FIR cavity, which is continuously evacuated by a mechanical pump.

4. Interference Effects

In these experiments, one common characteristic of lasers was unwanted interference of its highly monochromatic radiation. A desirable experimental arrangement - normal-incidence reflection - could not be used because of the appearance of standing waves between the detector surface and

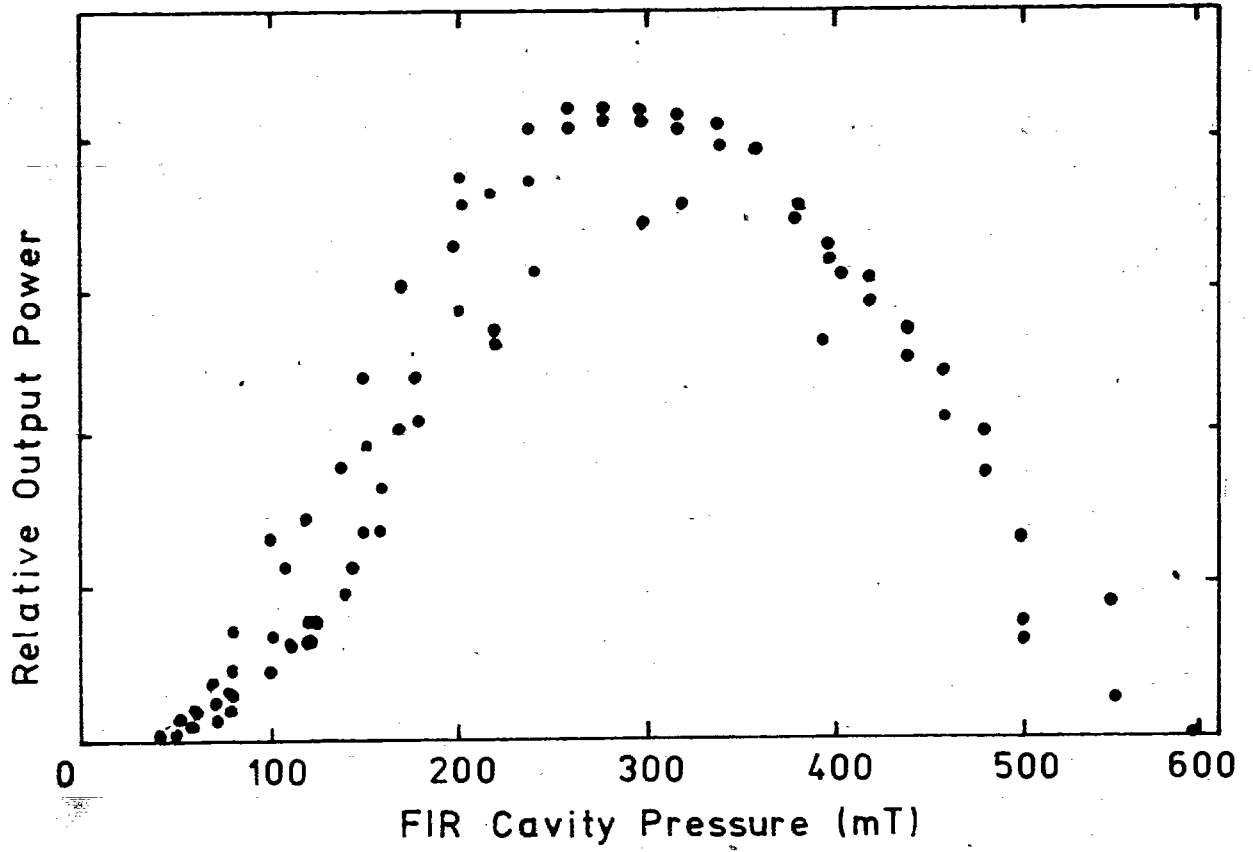


Figure 3-2

Laser Power Vs. FIR

Cavity Pressure.

 $\lambda = 119 \mu$

sample. This made the measured signal very dependent on the sample-detector distance.

By offsetting incident and reflected light paths by 32 degrees, interference disappeared for short-wavelength laser lines. However, for the longest wavelength, 1217 microns (and occasionally at 571 microns), the widely diverging beams apparently reflected from a second surface and recombined. The resulting interference caused intensity modulation of nearly 20% as sample height was varied. In fig. 3-3, radiation output from the furnace is plotted for two wavelengths as a function of sample height. Measurements were performed by adjusting sample height to obtain the maximum peak. Changes in sample height caused by thermal expansion or density change were not sufficiently large to affect reflectivity measurements, at least over ranges of 100 deg.C.

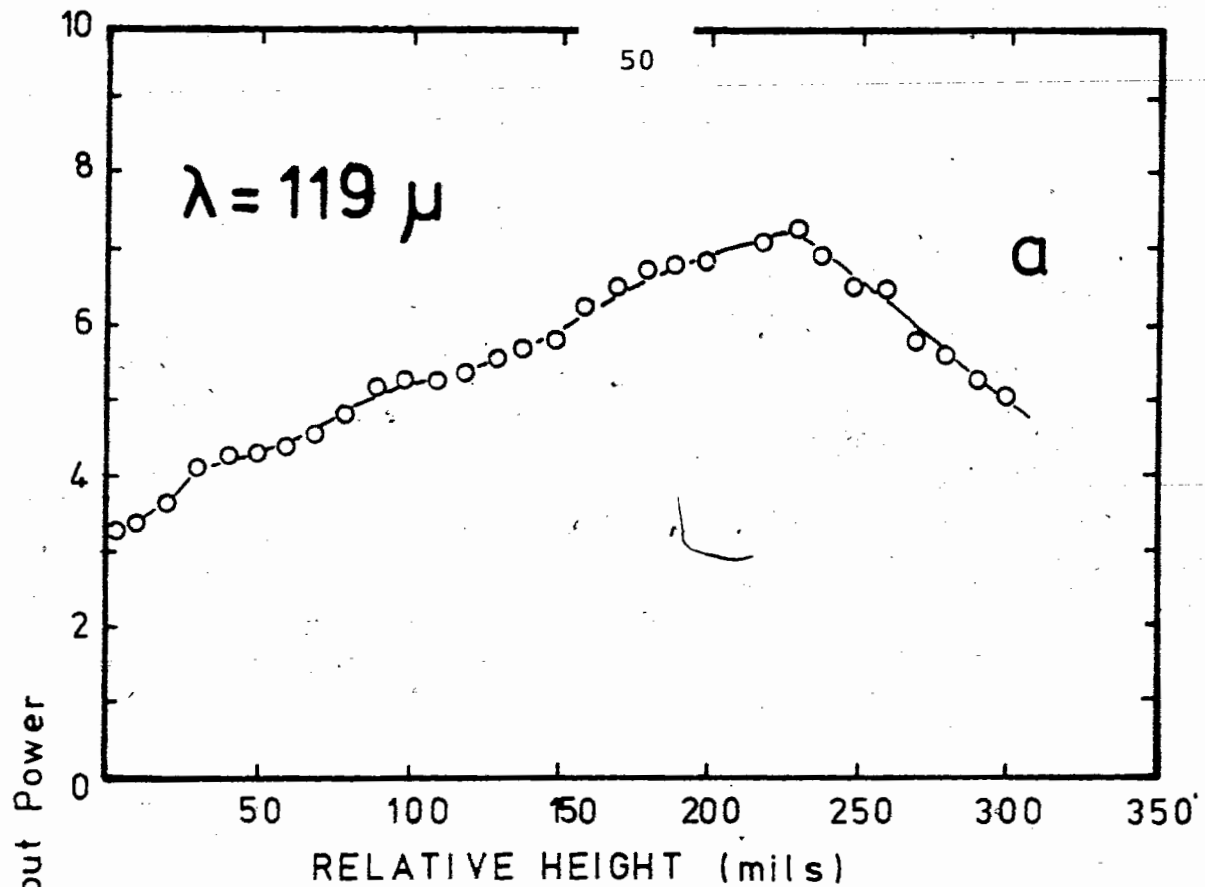
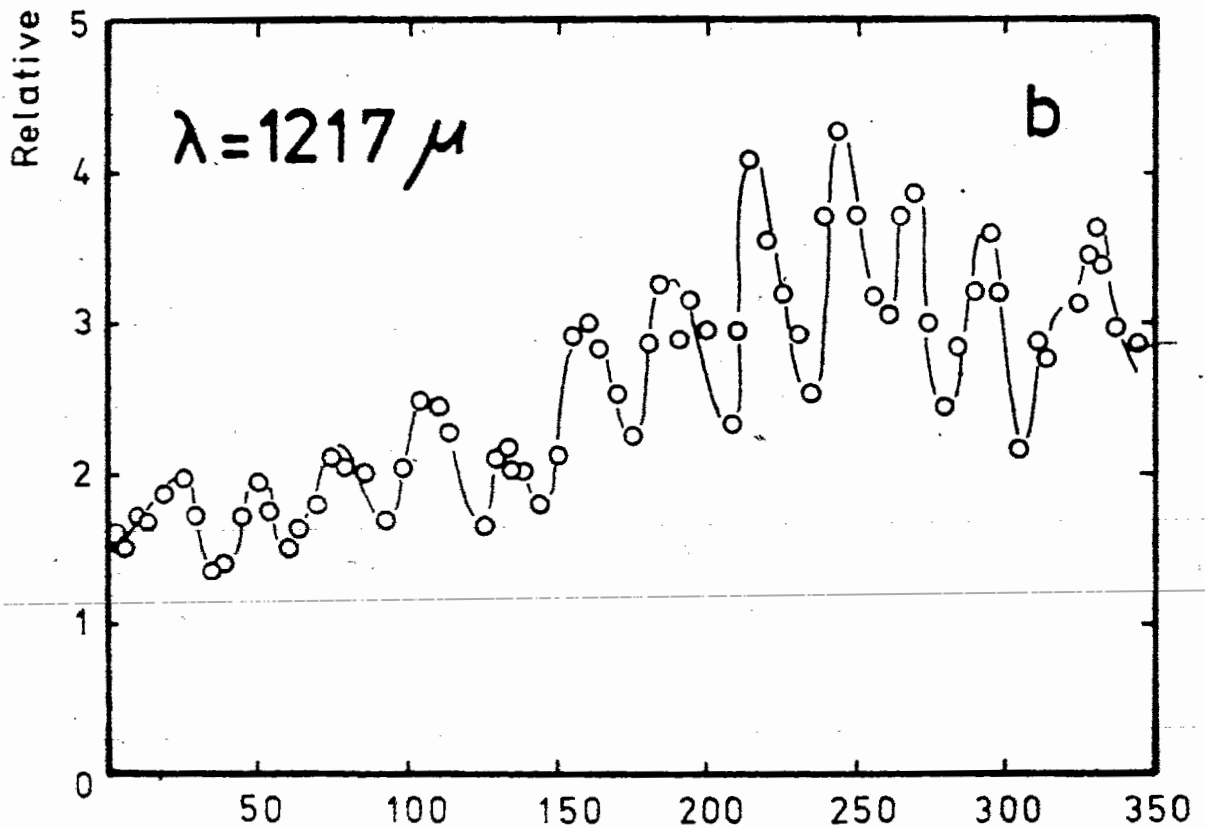


Figure 3-3 Laser Power Leaving Optical Furnace as a Function of Sample Height.



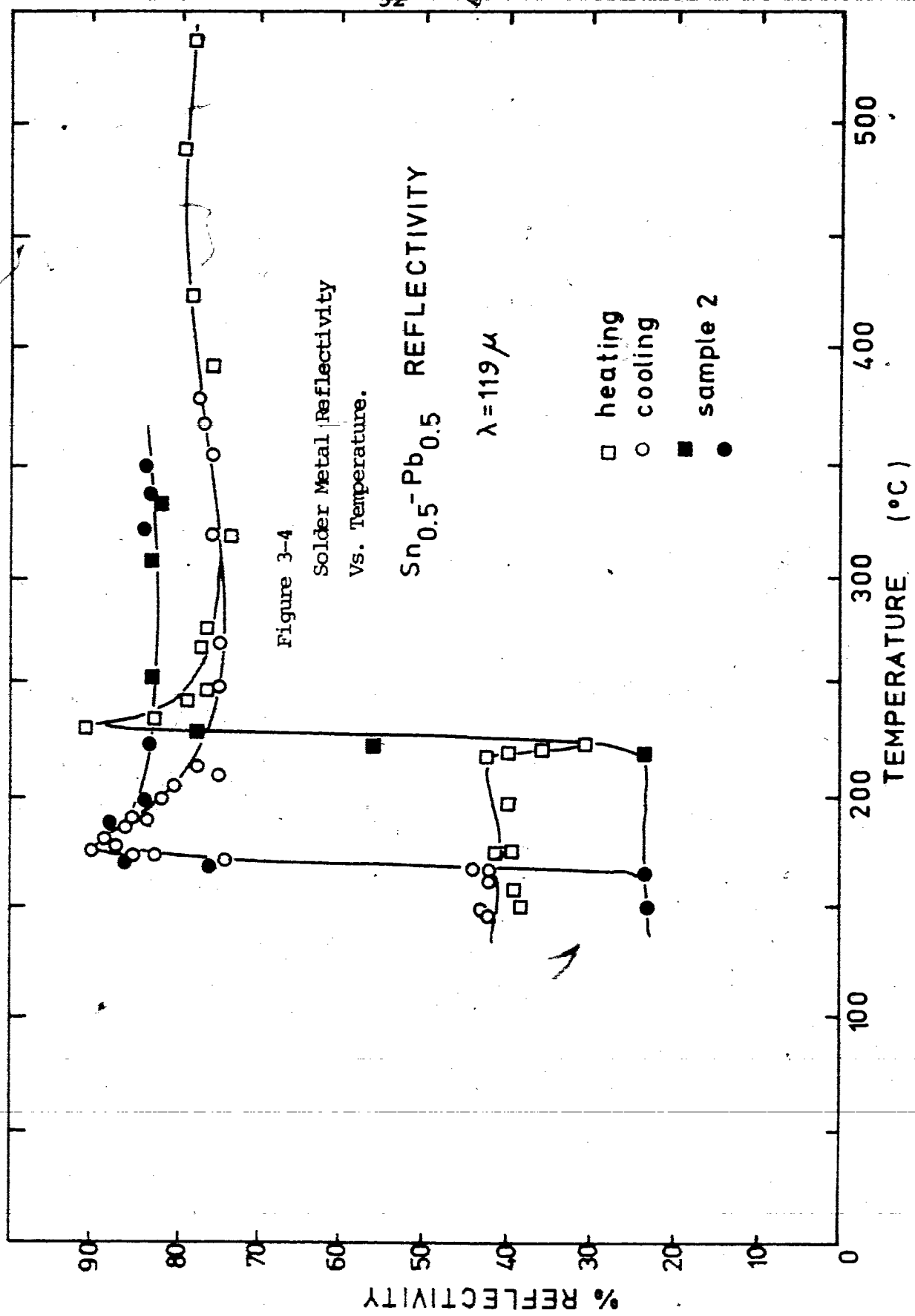
B. PROCEDURAL TESTS

1. Solder Metal

In order to determine the most appropriate procedure and the attainable reproducibility of reflectivity measurements on liquid alloys, several laser experiment runs were made using fluxless solder metal, 50% Pb - 50% Sn, as the sample. Each run entailed melting the sample in the optical furnace as described in section II-D.

Results of two runs are shown in fig. 3-4. On melting, the solder exhibited a significant increase in reflectivity, particularly just above the melting point. Considerable hysteresis in the measured melting temperature was observed; this cannot be attributed to different solidus and liquidus points for the alloy, but is instead ascribed to the low thermal inertia of the measuring thermocouple. This was fastened to the steel crucible holder below the silica crucible, and could be expected to follow changes in heater power more rapidly than the liquid sample. By reducing the cooling rate, hysteresis was avoided and temperature accuracy of ± 10 deg.C was obtained.

Repeated cycling of furnace temperature with any one sample gave reflectivities reproducible to within about 1.5%.



Limitations in accuracy were usually due to imperfect height optimization. The signal maximum was sometimes obscured by laser or detector noise, sensitivity to interference effects, or changes in sample orientation from apparatus jostling.

Comparable uncertainty was introduced in the 'reference reflectivity' measurement: despite careful and standardized procedures for opening and closing the furnace, signal reproducibility using an aluminum sample was typically 4%.

The solid-sample reflectivities were less reproducible, and at the same time were significantly less than the liquid R. This is likely due to some surface contamination (a leak in the furnace existed at the time) and to slight differences in the surface roughness when solid.

2. Ga-Te Observations

The procedure of section II-A-4 was used for all measurements except initial laser runs at 119 microns, for which the melts were not stirred. Visually, unstirred samples appeared to have Gallium-rich surfaces, probably from Te evaporation or floating of Ga to the surface. The density of Ga is roughly 5% less than that of Te.

The first 119 micron runs were also characterized by faster cooling rates. This was later suspected to reduce the accuracy of reflectivity measured at the liquidus point. Furthermore, isotherms at two or three temperatures of the melted alloy were desired. For subsequent runs, therefore, heater power was reduced in small steps.

Using both the laser and interferometer systems, a large drop in reflectivity (about a factor of three) was observed for all alloy samples on freezing. As with the solder metal, the reproducibility of the solid reflectivities was somewhat worse than liquid measurements; based on 6 sets of runs, the ratio $R_{\text{solidus}}/R_{\text{liquidus}}$ had a mean standard deviation of 7%. Some of the decrease on freezing is attributable to light scattering by crystallites on the alloy surface. The contribution of density change - causing a change in sample height and thus making reflection less efficient - was investigated. After a sample had cooled through the freezing point, its height was adjusted to again maximize radiation output from the furnace. In several such trials, the improvement never exceeded a factor of about 1.2. This suggests that a single height adjustment at the peak furnace temperature was sufficient to provide accurate reflectivities over a wide range of temperatures in the liquid.

To avoid errors due to possible systematic change in the apparatus, all laser runs were done randomly in terms of alloy composition. The seven samples of the first series were used at laser wavelengths of 119, 1217, and then 571 microns (84.2, 8.2, and 17.5 cm^{-1} respectively). The same seven samples were used for repeated measurements at 119 microns. Finally, samples of the second series were observed at 119 and 1217 microns. (See Section II-C-3 for sample compositions).

Two sample compositions were used in the interferometer measurements. Based on the published viscosity, enthalpy, and resistivity data shown in figures 1-1 and 1-2, which show anomalies at or very near the intermetallic compositions, the Ga_2Te_3 and GaTe alloys were thought most likely to exhibit unusual reflectivity. This opinion was supported by the previous laser data, which showed dramatic changes in R and its temperature dependence between these compositions.

The 50 and 60 at.% Te alloys of series II and III were found to have constant reflectivities, neglecting furnace contamination, over periods of up to 4 hours. After this time, the furnace interior was quite often blackened by Te dust, reducing the accuracy of further measurements. Light pipes were also encrusted by corrosive, evaporated products.

Initial interferometer runs were performed using a P4-43 pyroelectric detector. This device was found to have an unsatisfactorily high noise level for use with the rather low energy interferometer lamp. In order to obtain reasonable S/N ratios, averaging times were necessarily long, leading to slow data acquisition and poor resolution. Subsequent runs used a He³-cooled bolometer detector. Colder detectors have superior S/N ratios because of the reduction in Johnson noise with temperature.

No blackbody overloading of the detector was observed when using the interferometer system. The detector itself received about 20X less signal than in a typical run without the furnace in the light path, and is designed to respond linearly over a much greater dynamic range.

C. COMPOSITION ANALYSIS

Following the final laser and interferometer runs, the compositions of several solid ingots were determined by X-ray Fluorescence spectroscopy.³⁴

The top surface of each ingot was scraped off to a depth of about 1 mm to yield a powdered or granular sample. To investigate whether a concentration gradient existed through

the ingots (caused by evaporation of one component from the liquid surface), horizontal sections were taken from one ingot. A mechanical mixture of Ga and Te fragments in 50/50 ratio was found to be too structurally dissimilar from the ingot samples to serve as a reference composition in the XRF measurements. Instead, one sample (the 50 at.% Te alloy) was assumed to have retained its original elemental concentrations, and other measurements were scaled accordingly.

Mechanical properties and analysis results are summarized in Table III-1. Using the relative reference scheme, measured sample compositions are seen to be internally consistent: the same order of Te concentration is maintained. Deviations from the initial mixtures are usually below 3 at.% Te, the minimum separation between alloy preparations. Differences between the surface, centre, and bottom compositions of a Ga_2Te_3 ingot were also insignificant, probably because of periodic stirring when melted.

Supporting evidence for the stability of the melted alloys is the previously mentioned mass-loss measurement (section II-D) and the absence of any systematic change in sample spectra in successive interferometer runs.

TABLE III-1 X-RAY FLUORESCENCE COMPOSITION ANALYSIS

Initial Sample Composition (at. % Fe)	Melted Period (hours)	Final Composition (XRF Results, at. % Fe)	Mechanical Properties
40.0	2.5	39.6	Shiny/grey surface, easily cleaved into soft, flat grains.
50.0	4.1	-----	Shiny surface. Soft, 1 mm wide grains are easily scraped off.
55.0	1.5	57.0	Very silvery lustre; brittle, hard consistency.
60.0, top	2.5	64.0	Low strength but brittle; dull silvery surface, but grey/black as a powder.
60.0, middle	2.5	58.9	
60.0, bottom	2.5	63.3	
75.0	1.0	73.9	Hardest, most brittle alloy. Surface scrapes off as grey dust and occasional grains.

IV. RESULTS

A. LASER REFLECTIVITY

Measurements made with the FIR laser revealed relationships between liquid alloy reflectivity and optical frequency, composition, and temperature.

1. Frequency

The use of three wavelengths was sufficient only to provide a rough idea of the dependence of reflectivity on frequency. There are marked differences, though, between these data. Figures 4-1 and 4-2 plot R vs. alloy composition at 17.5 and 8.2 cm^{-1} . The two frequencies yield similar reflectivities, typically in the 60 - 70% range. An anomalous increase in 8.2 cm^{-1} (1217 micron) reflectivity for a narrow range of composition is not seen in the scintier 17.5 cm^{-1} (571 micron) data, though. In contrast, the 84.2 cm^{-1} (119 micron) results, plotted in figure 4-3, exhibit more dramatic behavior, both in range of values (rising to nearly 100% R) and general trend with composition. For most alloy compositions, reflectivity falls with decreasing frequency over the laser range. The interferometer results illustrate the frequency dependence more clearly.

Figure 4-1

Reflectivity at 571μ versus Liquid $\text{Ga}_{1-x}\text{Te}_x$ Alloy Composition. (a) $T = 1200 \text{ deg.K (927 deg.C)}$ (b) $T \sim \text{liquidus}$. In this and following diagrams, the liquidus (completely melted) temperatures for the various alloys are (in deg.C):

$x=0.34, T=740; x=0.40, T=793;$
 $x=0.47, T=815; x=0.50, T=824;$
 $x=0.53, T=812; x=0.57, T=780;$
 $x=0.60, T=790; x=0.63, T=760;$
 $x=0.66, T=730; x=0.70, T=680;$
 $x=0.75, T=612; x=0.85, T=470;$
 $x=1.00, T=453.$

Liquidus temperatures are taken from Hansen and Anderko,³² the published figures most closely followed by the less precise measurements of the present experiments.

$\lambda = 571 \mu$

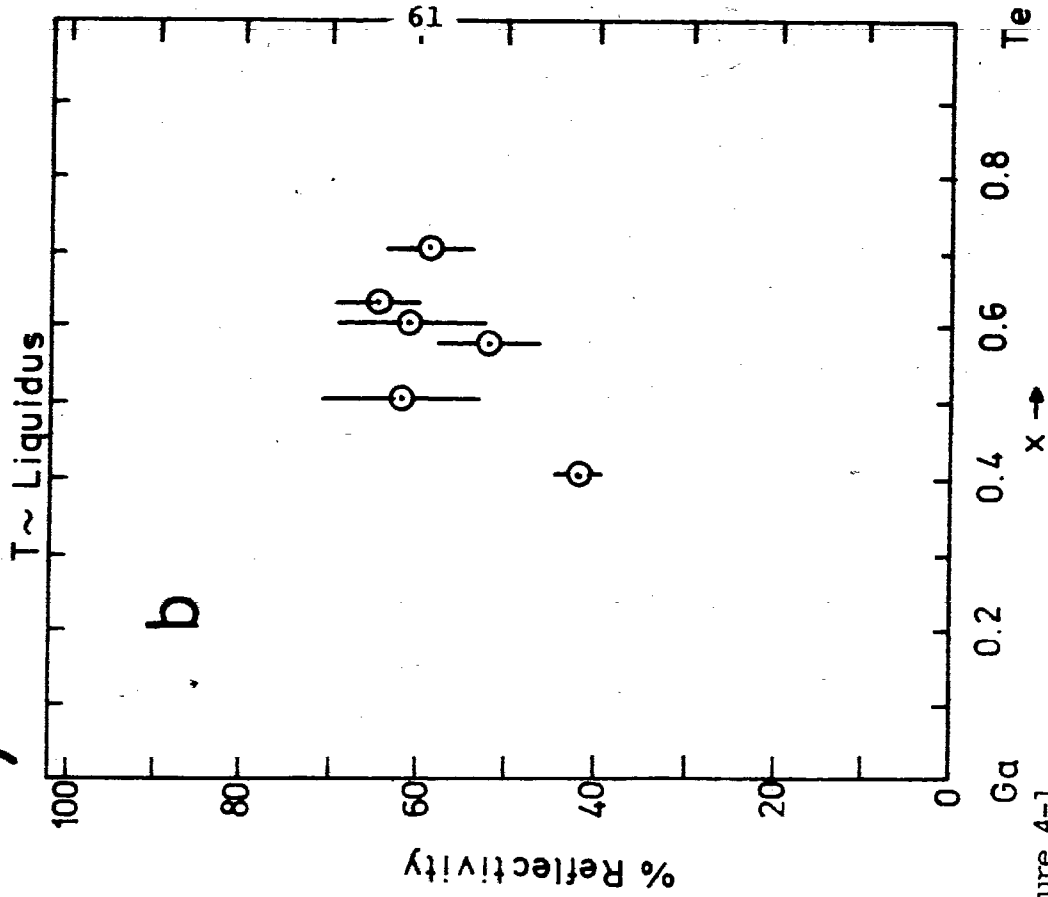
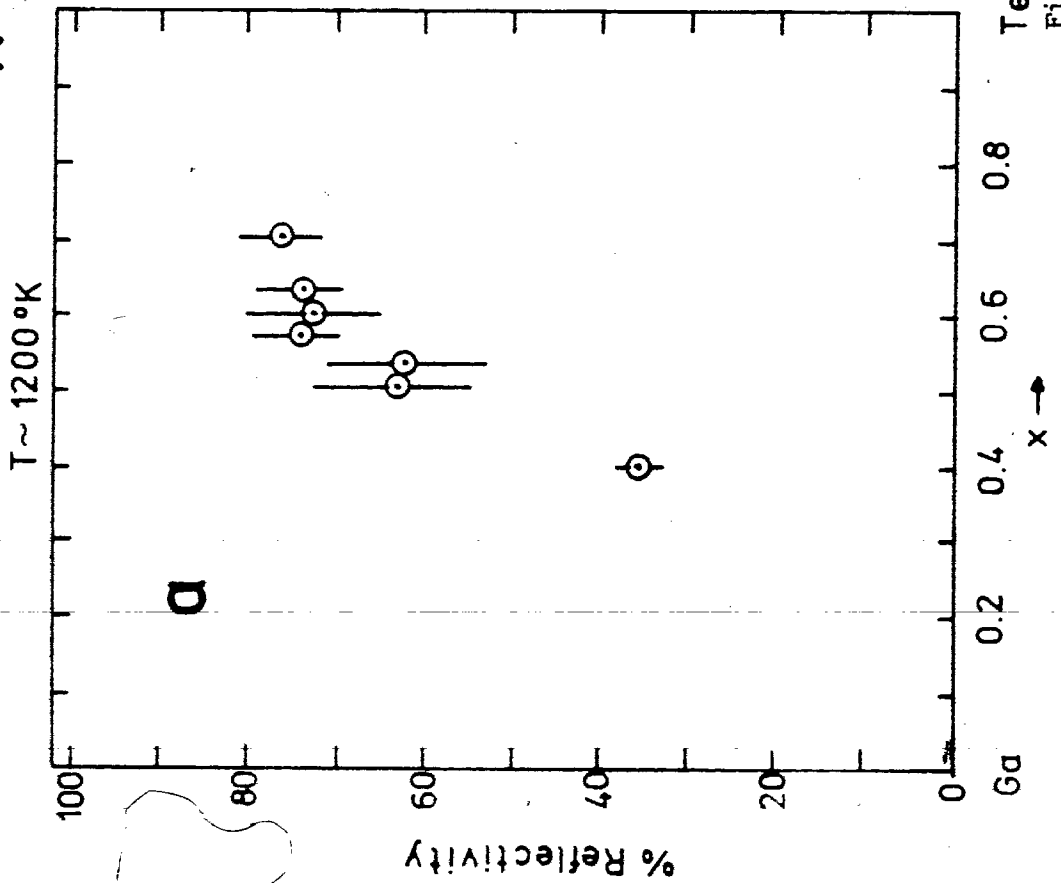


Figure 4-1

$\lambda = 1217 \mu$

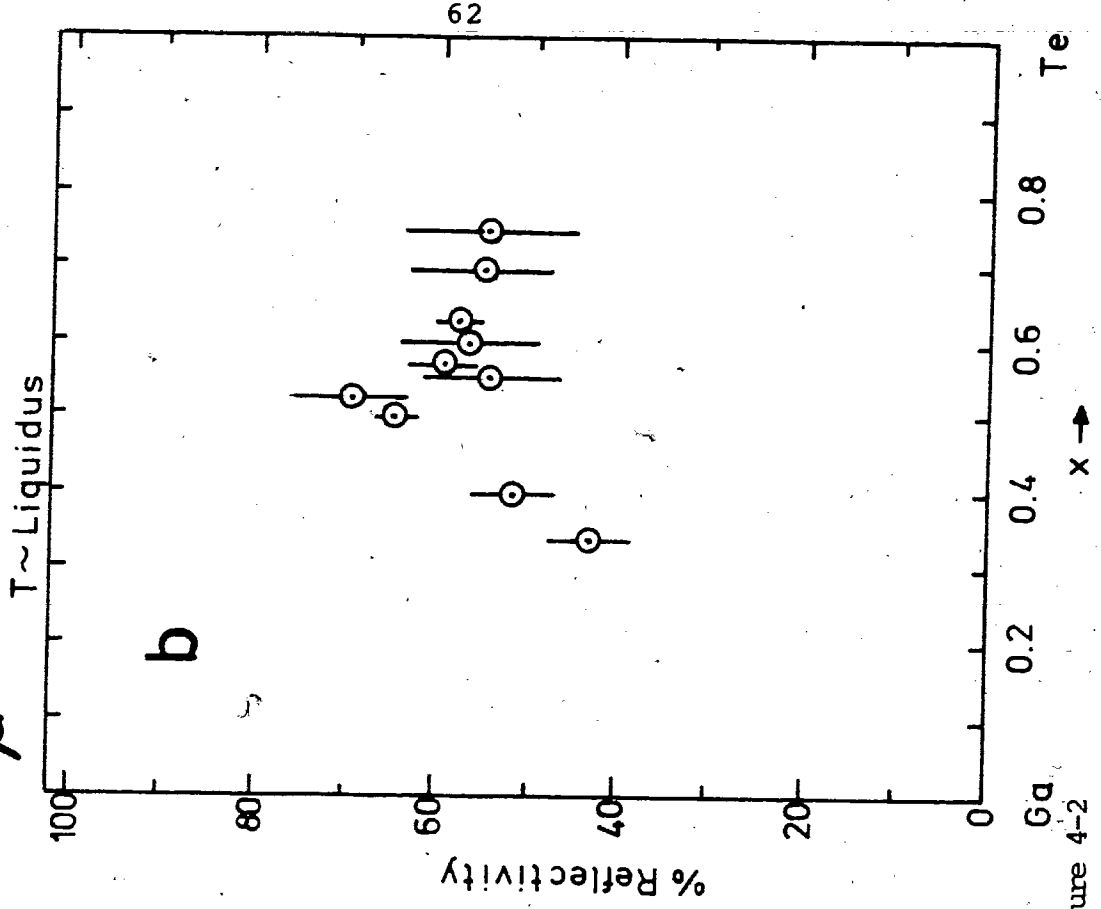
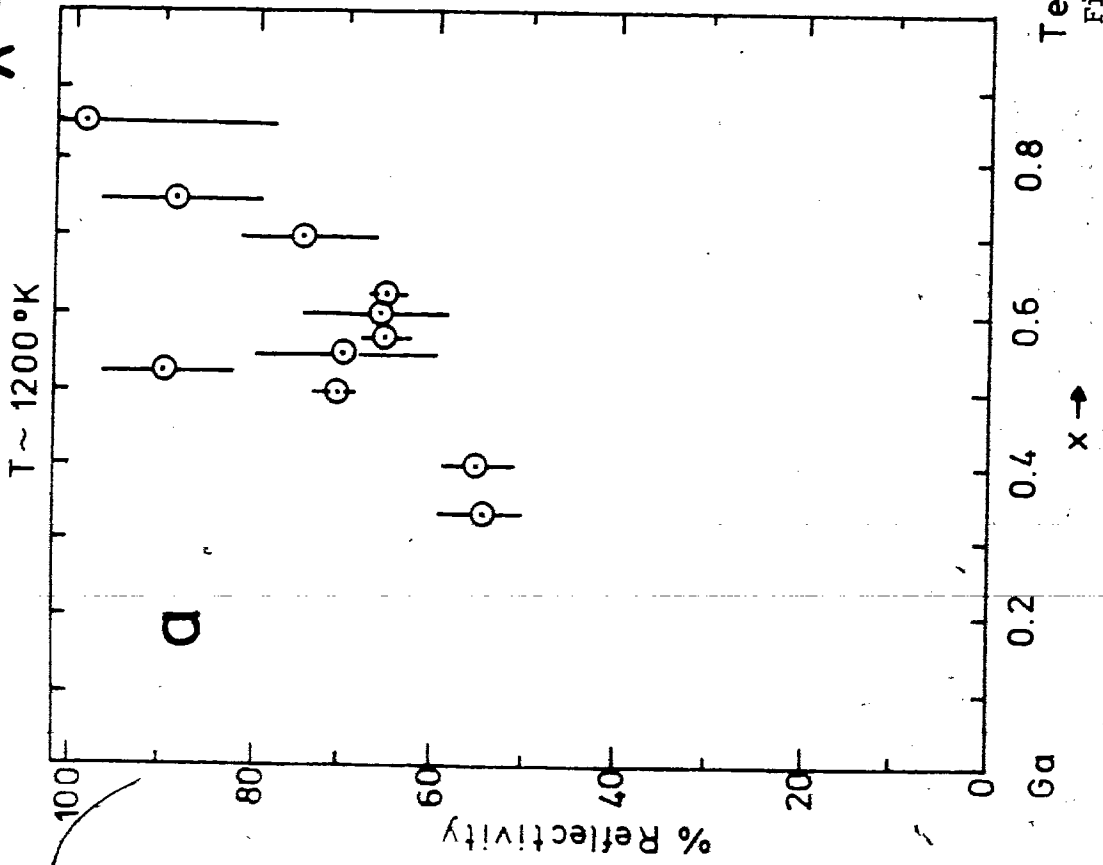
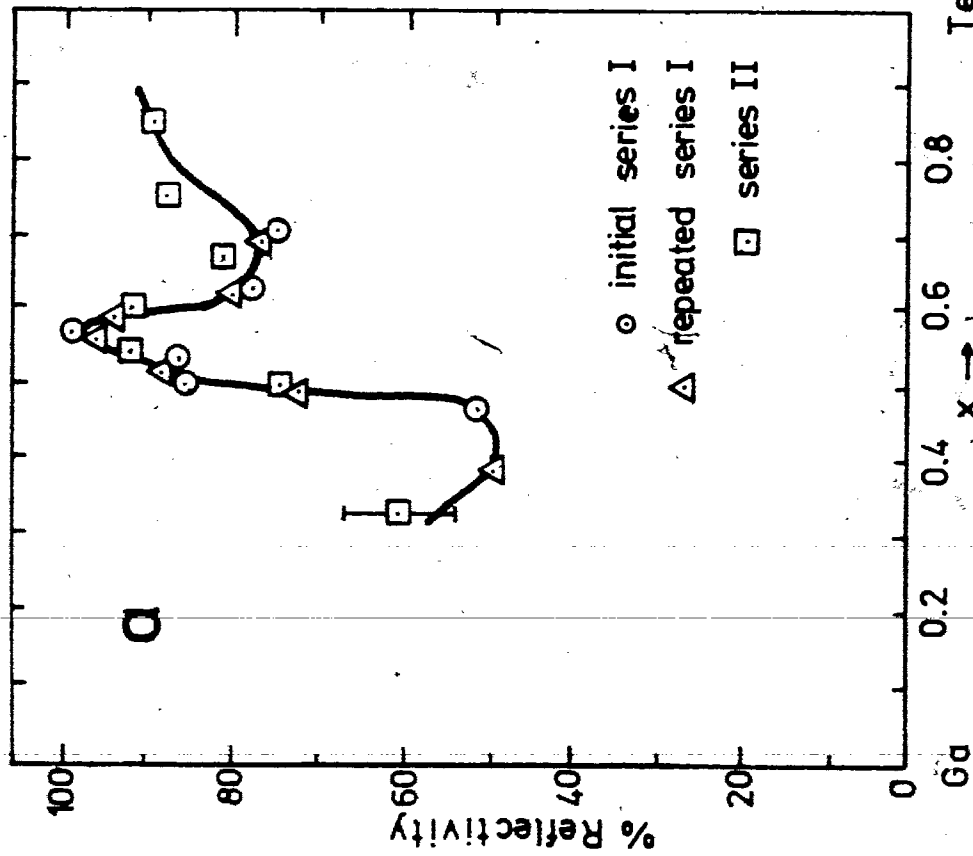


Figure 4-2

$\lambda = 119 \mu$

$T \sim 1200 \text{ }^\circ\text{K}$



$T \sim \text{Liquidus}$

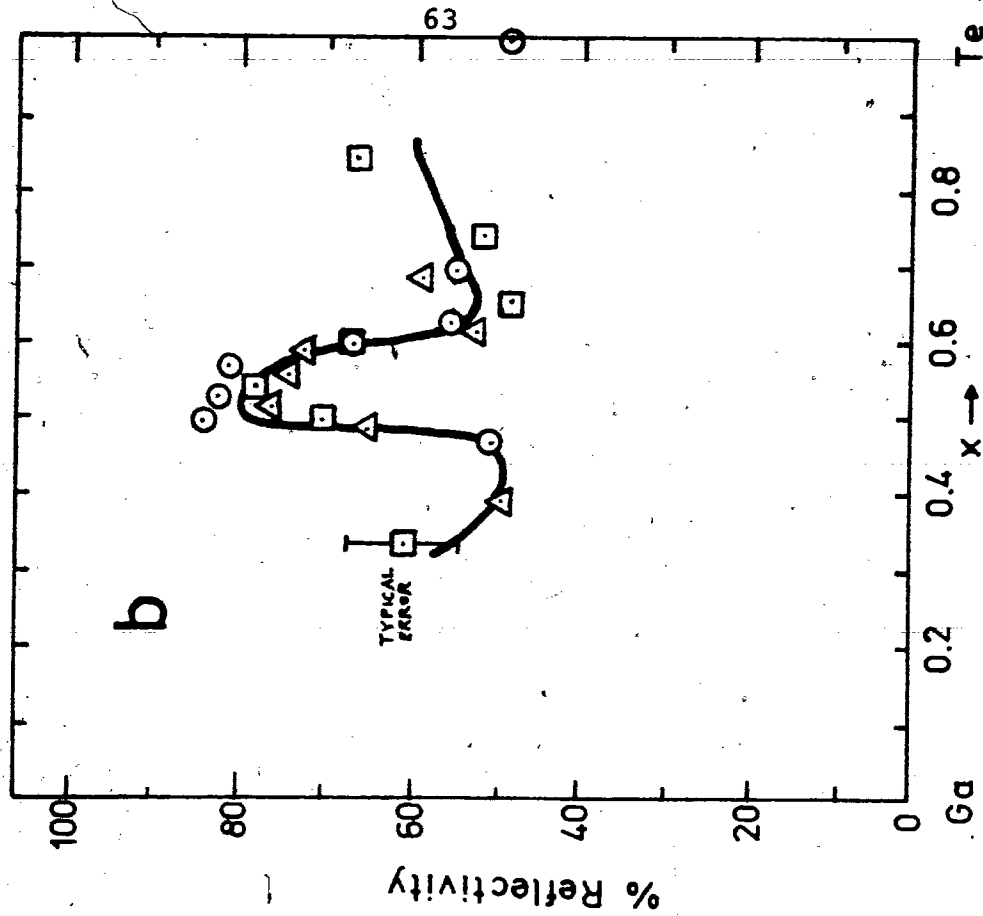


Figure 4-3

2. Composition

Figures 4-1 and 4.2 illustrate a general trend of R with composition. Figure 4-2 plots the mean reflectivity when more than one measurement has been made. At 1200 deg.K (927 deg.C), reflectivity rises almost linearly with Tellurium concentration at 571 and 1217 microns. Some evidence of rapid increase in R over a narrow composition range, $0.45 < x < 0.60$, is present at 1217 microns, but not at 571 microns. The reproducibility at these wavelengths, as indicated by the plotted error bars, is somewhat poorer than at 119 microns. (See Section IV-B for further discussion).

The 119 micron data, plotted in figure 4-3, shows strong composition dependence. At 1200 deg.K and around compositions of $58 \pm 2\%$ Te reflectivity rises to very large values. At lower temperatures, the maximum becomes broader and shifts toward 50% Te. At all temperatures studied, this high reflectivity falls off drastically for $x < 0.50$ or > 0.60 . Except for this anomalously high-R region, the 119 micron results display a composition dependence similar to the longer wavelengths: namely, increasing R with Te composition.

Note that the "Repeated Series I" data is shifted 1% towards Gallium. This was done when plotting, to correct for

the estimated change in sample composition that arose from evaporation of Te during preceding runs. (Each sample was typically used in four runs, with an estimated loss of 0.2% Te per run).

3. Temperature

Dramatic temperature dependence is apparent for 119 micron reflectivity. Examination of figures 4-3a and 4-3b indicates a systematic variation with temperature. Note that while fig. 4-3a is an isothermal plot, fig. 4-3b consists of data taken at a variety of temperatures: the liquidus points of different alloys ranged from about 430 to 830 deg.C (Cf: phase diagram, fig. 2-5). The liquidus-temperature results were included to indicate most sensitively the possible existence of weakly-bound molecular clusters; reflectivity anomalies caused by such molecules would disappear as the clusters dissociated at higher temperatures.

Figure 4-4 plots R at 119 microns vs. x at 3 temperatures: approximately 1200 deg.K, 1150 deg.K, and the liquidus temperatures. Examples of R vs T curves for three alloys (x = 0.4, 0.6, and 0.85) are presented in figure 4-5. All such curves display almost temperature-independent reflectivity below the liquidus point, but an increase in R with T when in the liquid state. For every alloy studied, R

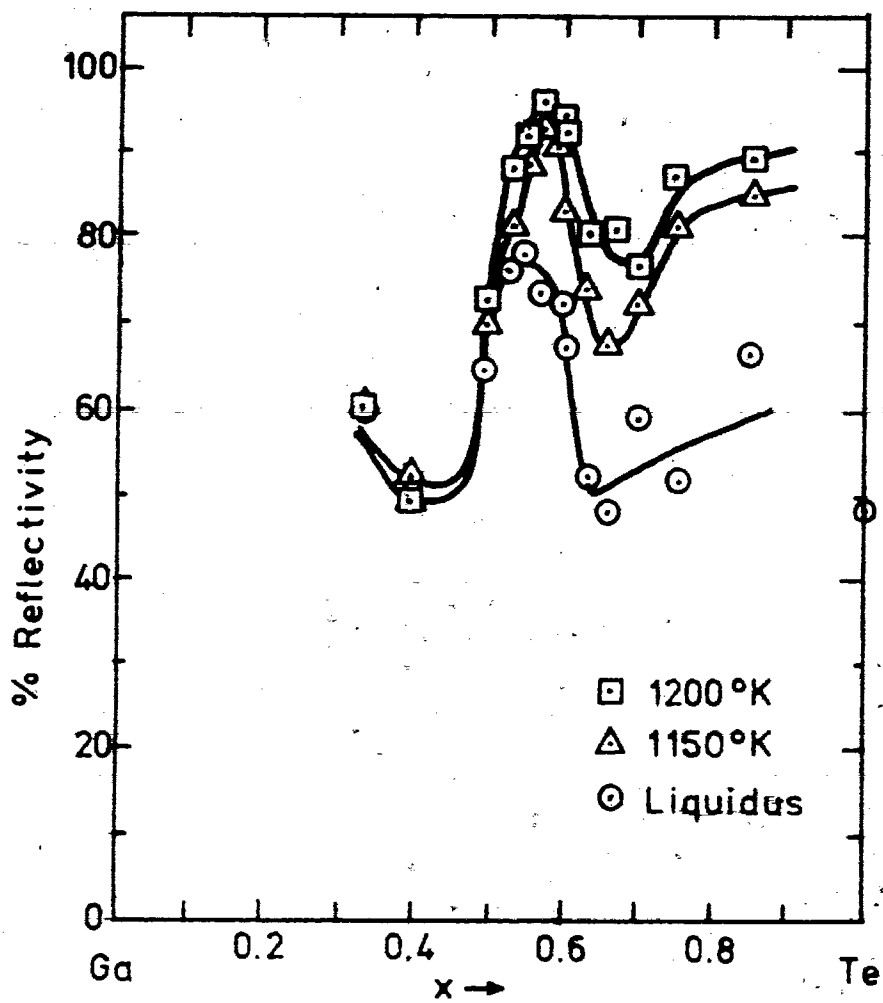


Figure 4-4

119 Micron Reflectivity
Vs. Liquid Alloy Composition
at Three Temperatures.

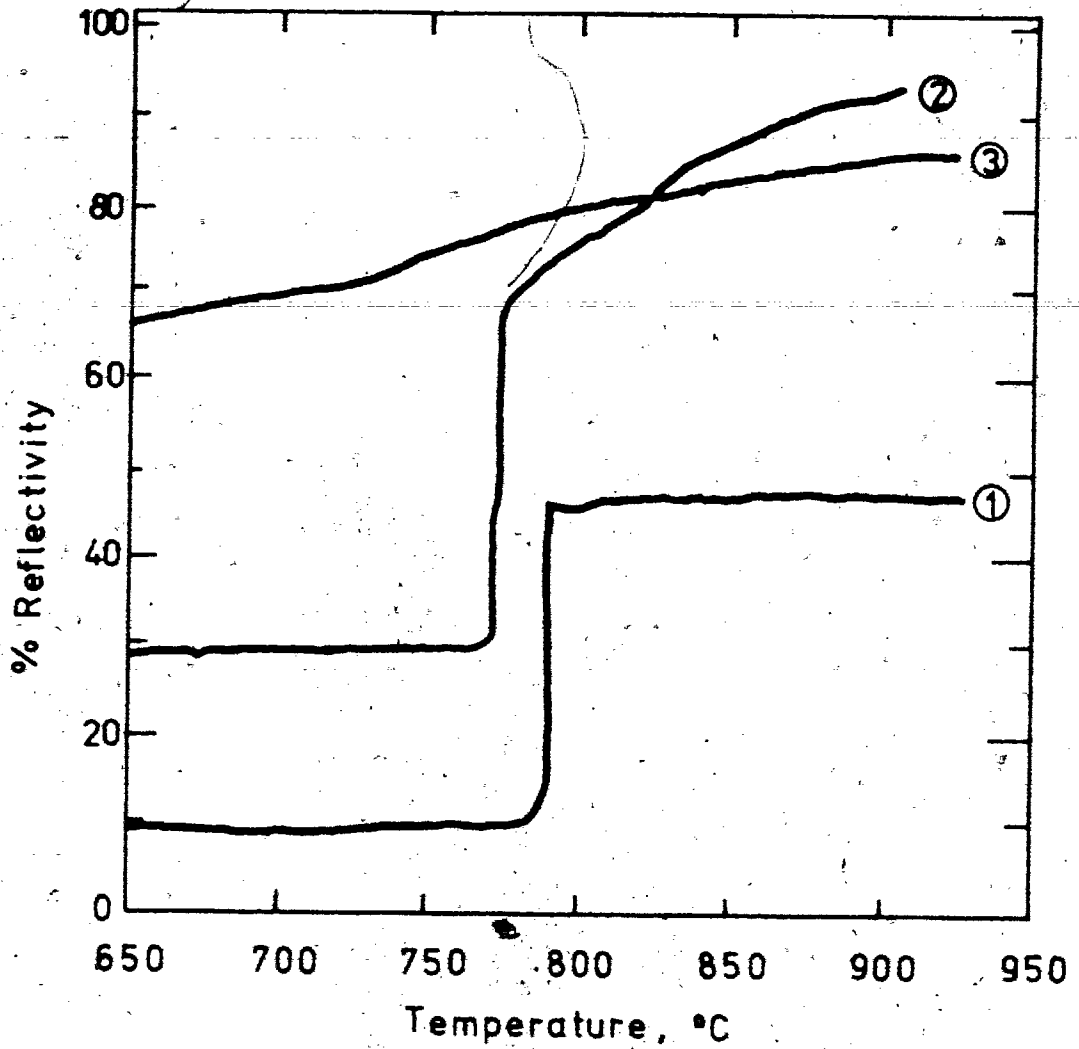


Figure 4-5

119 μ Reflectivity Vs. Temperature

for Three Alloys:

(1) $x = 0.40$ (40 at.% Te)

(2) $x = 0.60$ (60 at.% Te)

(3) $x = 0.85$ (85 at.% Te)

is lower in the solid than in the liquid state. The slopes of the $R(T)$ curves are composition-dependent, being steepest near $x=0.6$.

This variation at 119 microns of R with T is more clearly indicated in figure 4-6, which plots the differential reflectivity, that is, the change in reflectivity between two temperatures, divided by the temperature difference. The maximum temperature in all cases was 1200 deg.K; the minimum was the liquidus point. Published values of liquidus temperature were used: while the experimental melting points agreed most closely with those published in Hansen and Anderko,³² their random error was higher, leading to a less 'smooth' differential reflectivity curve. The figure shows an obvious peak at about $x=0.6$ corresponding to the composition Ga_2Te_3 . The temperature dependence of R falls to zero for $x < 0.4$ and also drops dramatically (but remains finite) for alloys with atomic Te fraction greater than about $x=0.65$. The Tellurium-rich compositions provided less precise data because of rapid Te evaporation and consequent furnace contamination.

Similar plots for 571 and 1217 micron wavelengths (figures 4-7a and 4-7b) show a rather constant shift of R with T , rising somewhat with Te concentration. The experimental uncertainty hides any small effects which may be present. No

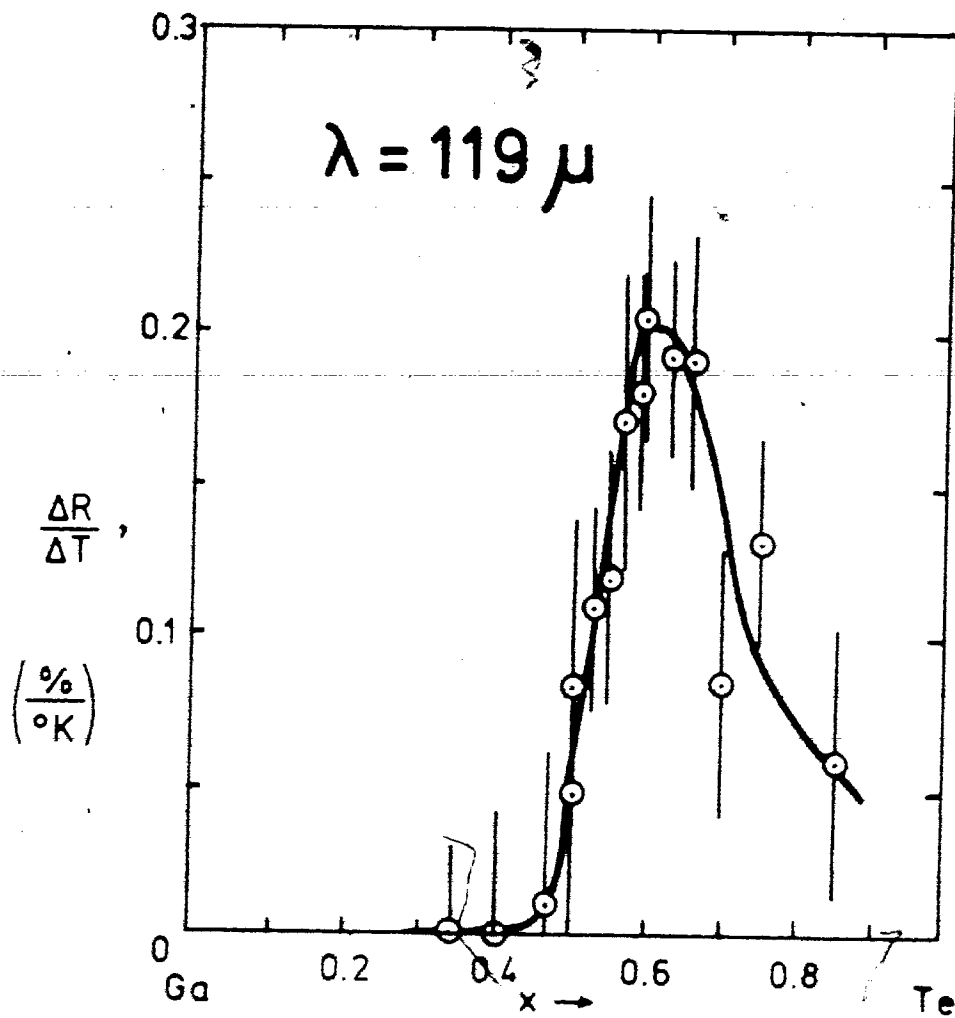


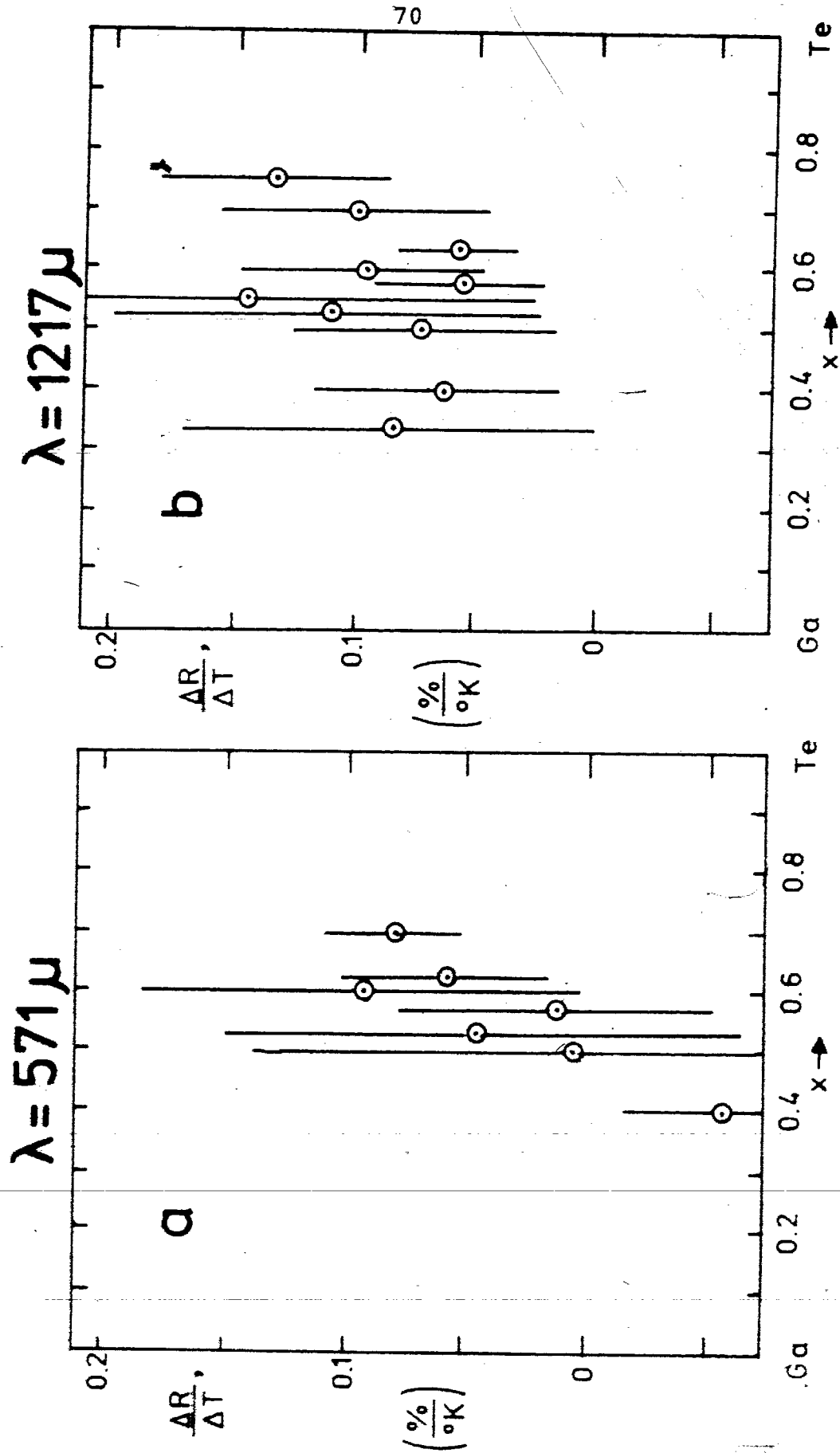
Figure 4-6

 119μ Differential Reflectivity

Vs. Liquid Alloy Composition.

Figure 4-7

Long-Wavelength Differential Reflectivity.

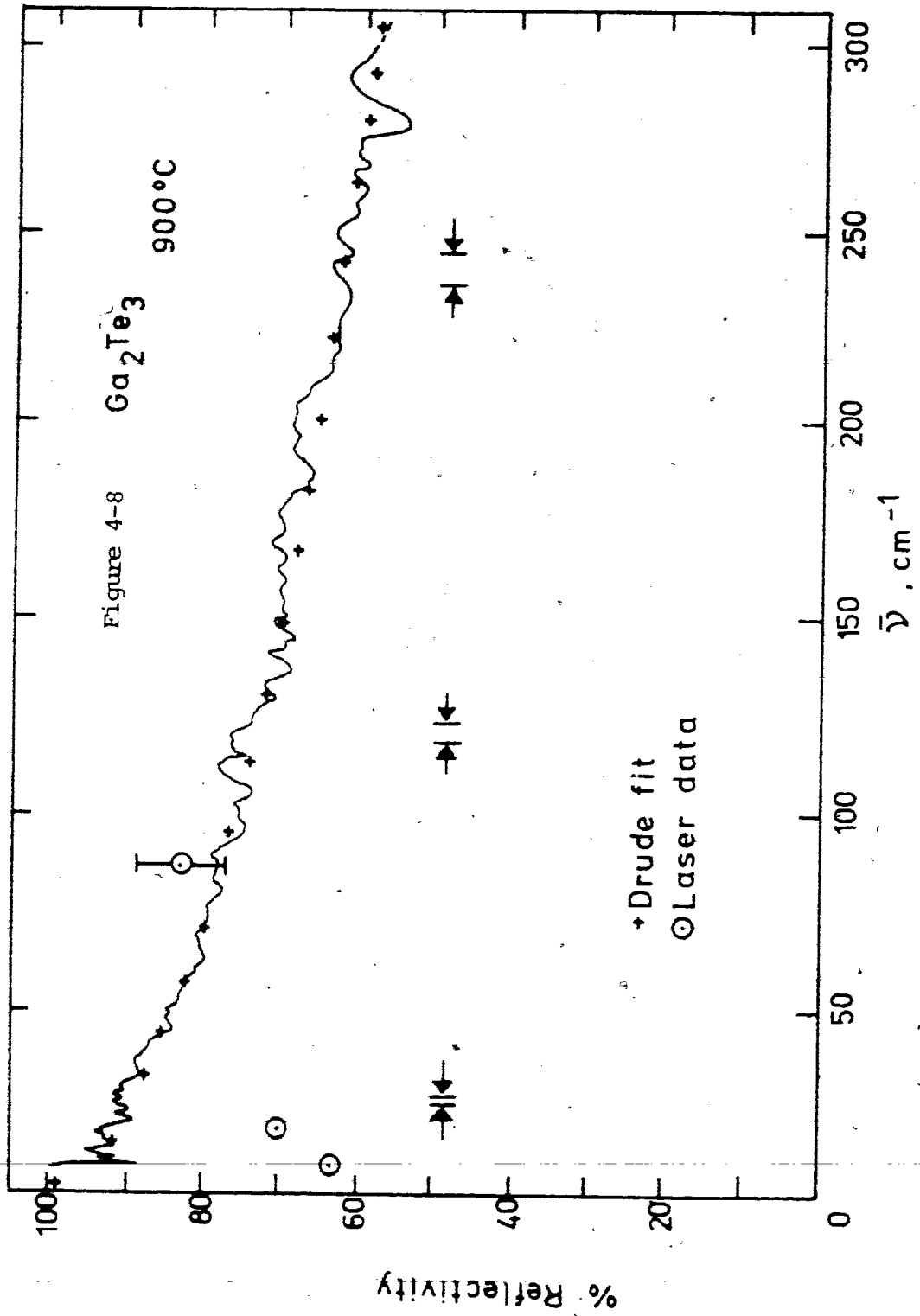


significant peak is obvious. In particular, the differential reflectivity remains high at large Te concentrations, making these results qualitatively different than the 119 micron measurements.

B. INTERFEROMETER REFLECTIVITY

The far infrared frequency spectra of liquid Ga_2Te_3 and GaTe are shown in figures 4-8 and 4-9. Each graph is composed of spectra from two alloy samples and three spectral ranges. The spectra of each frequency range consist of two to four averaged sample and reference runs.

The reflectivity of Ga_2Te_3 shows a gradual rolloff with frequency, and no significant bumps or other spectral features. The irregularities were identified as noise by observing the spectra of separate runs: bumps were different from run to run, and tended to diminish in magnitude as spectra were averaged. The data conform, within the random experimental noise, with the Drude model of metallic reflectivity (see Section V-B). Crude pyroelectric detector measurements, not included in fig. 4-8, indicate that this Drude-like dependence continues at least up to 700 cm^{-1} .



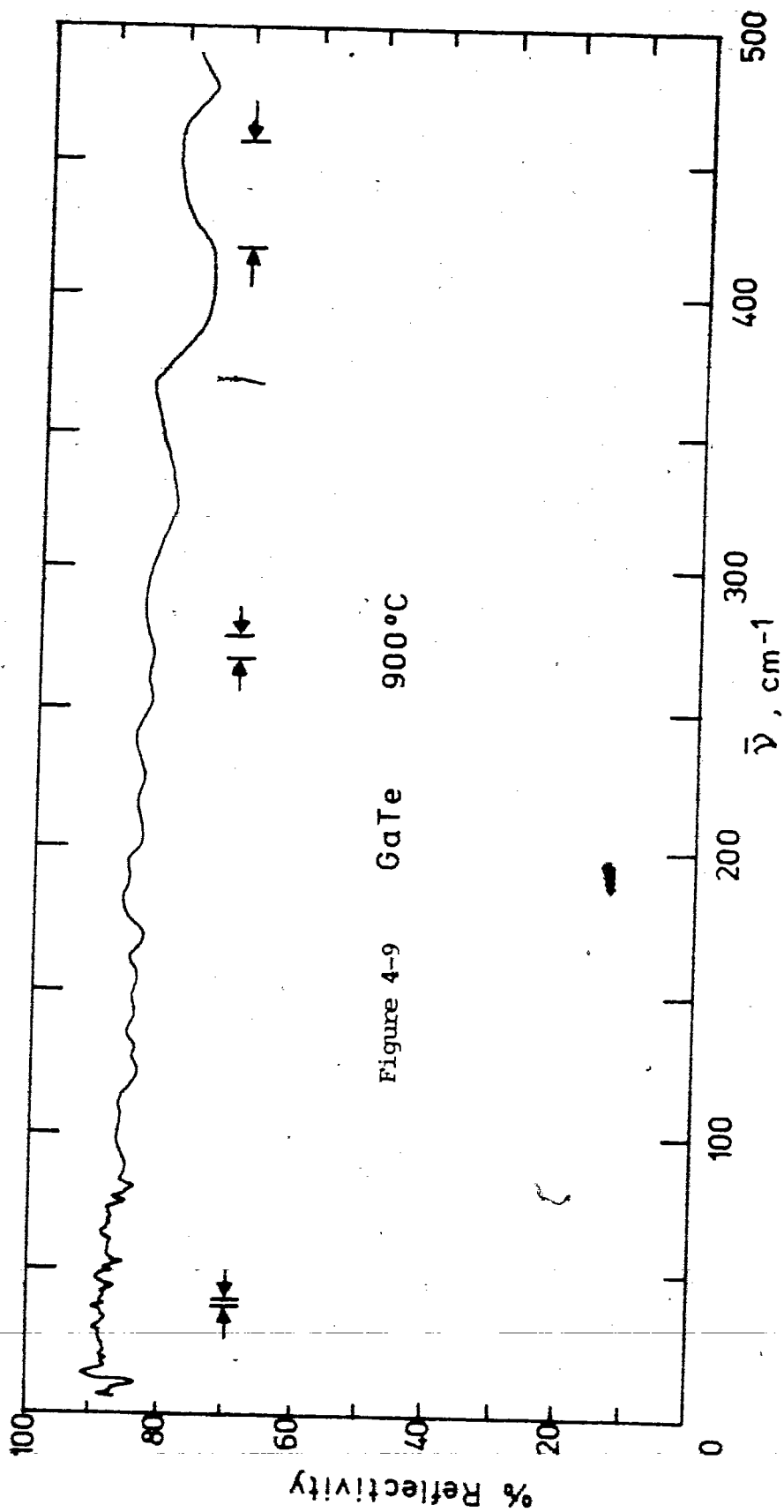
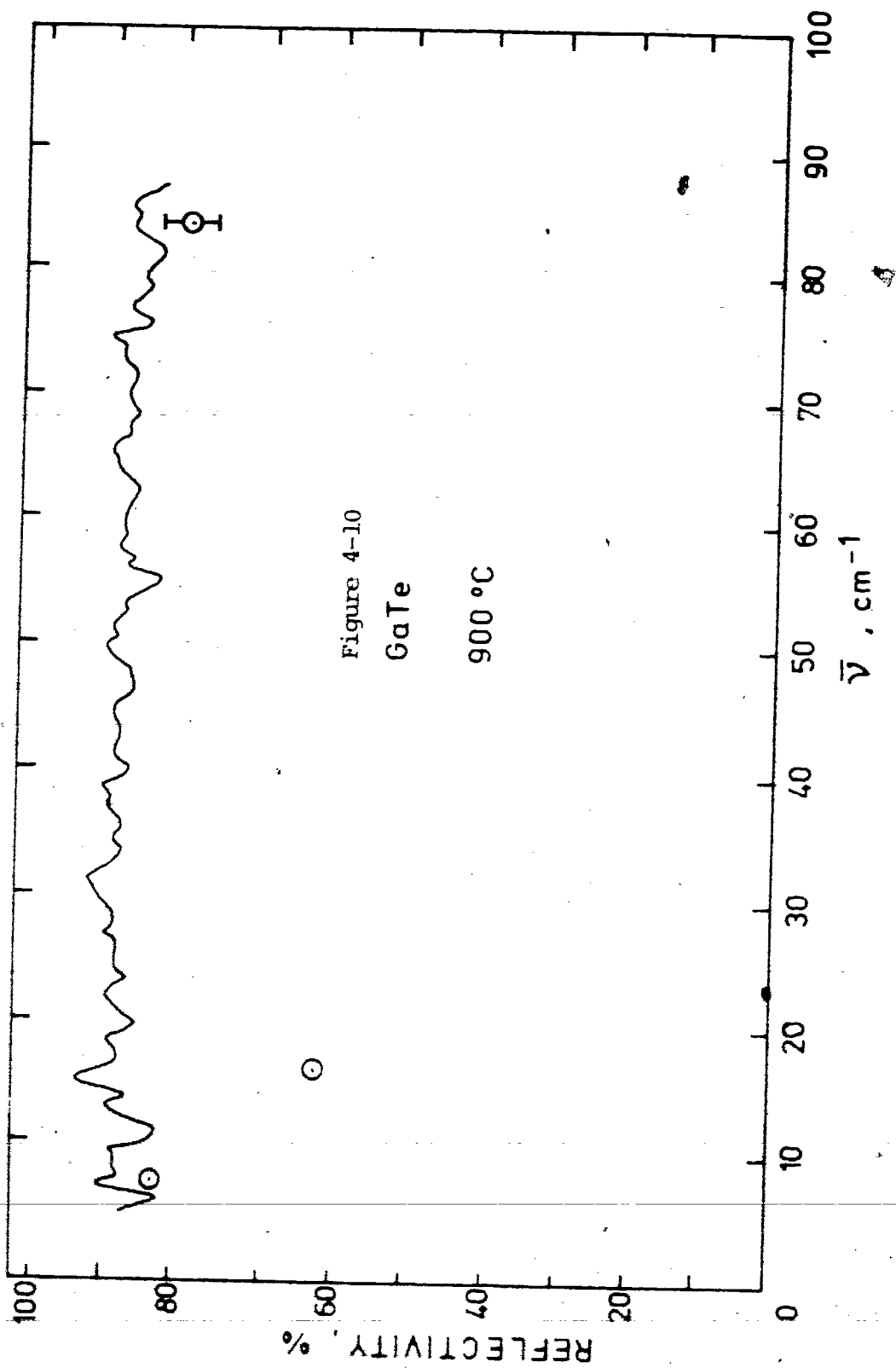


Figure 4-9 GaTe 900°C

Liquid GaTe reflectivity is qualitatively different from that of Ga_2Te_3 . The GaTe spectrum is much flatter, and does not display the monotonic increase in R towards 100% as frequency decreases. A slow decrease in R with frequency, approximating Drude behavior, is evident at higher frequencies, but is lacking below about 175 cm^{-1} . This low frequency region is shown in fig. 4-10. A possible peak around 40 cm^{-1} may be identified, although this is barely above the experimental noise. As with Ga_2Te_3 , the GaTe spectrum shows no features attributable to optically active modes, despite high resolution and moderately good S/N levels.

Laser measurements at 119 microns agree within the estimated error with interferometer results. The interferometer random error is estimated to be roughly the magnitude of the irregularities in the curve, and systematic error in the reflectivity scale may be as much as $\pm 10 \%$. Low frequency laser reflectivities deviate from the broad-band spectra, however: the laser data tend to be 10 to 35% low.



V. MODEL CALCULATIONS

A. Activated Conductivity

The temperature dependence displayed in the differential reflectivity plot, fig. 4-6, can be quantitatively related to conductivity.

At normal incidence, the reflectivity R is related to the dielectric constant ϵ of the alloy by

$$(V-1) \quad R = \left(\frac{\sqrt{\epsilon} - 1}{\sqrt{\epsilon} + 1} \right)^2$$

This relation is a good approximation for the 16 deg. incidence used in these experiments. According to the Drude model,

$$(V-2) \quad \epsilon(\omega) = 1 - \frac{\omega_p^2}{\omega^2 + i\omega/\tau_d}$$

The plasma frequency ω_p and relaxation time τ_d are

related to DC conductivity σ_0 and electron density N by

$$\omega_p^2 = \frac{4\pi N e^2}{m^*}$$

(V-3)

$$\tau_d = \frac{4\pi\sigma_0}{\omega_p^2}$$

where m^* is the effective mass of the charge carriers. Equations (V-1) and (V-2) can be evaluated by computer, using chosen values of ω_p and τ_d , to calculate reflectivity versus frequency. An approximate closed-form expression can be used here, though.

For far infrared frequencies, $\omega\tau_d \ll 1$. Using this condition with (V-1) and (V-2), one obtains the Hagen-Rubens relation, an expression relating reflectivity and Drude conductivity, valid at far infrared and longer wavelengths:

$$R = 1 - \left(\frac{2\omega}{\pi\sigma_0} \right)^{1/2}$$

in air, or

$$(V-4) \quad R = 1 - 2 \left(\frac{10^9}{\sigma_0 \lambda C} \right)^{1/2}$$

in terms of wavelength in MKS units.

By inverting equation (V-4), cooling curve data such as figure 4-5 (R vs. T for liquid alloys) can be converted to $\sigma(T)$ information, extrapolated to zero frequency. The resulting conductivities deviate drastically from those obtained from published resistivity measurements, differing by as much as a factor of 15. Furthermore, this conductivity, σ_{fir} extrapolated from FIR reflectivity, has a concentration dependence which is qualitatively different from that of σ_{dc} . Like the reflectivity itself, σ_{fir} is anomalously large over the range $0.5 < x < 0.6$, and drops back to low values at $x = 0.4$ and $x = 0.7$. Figure 5-1 compares the DC and FIR conductivities as a function of liquid alloy composition. The FIR data based on laser measurements agree within the estimated experimental error with the conductivity inferred from the broad-band spectra. Conductivity varies dramatically with small changes in reflectivity, especially near 100% R.

In contrast, the temperature dependences of σ_{dc} and σ_{fir} at fixed concentration are similar. Plotting the experimental $\ln \sigma_{fir}$ vs. $1/T$, a linear dependence (within the measurement uncertainty) is obtained for alloy compositions $0.55 < x <$

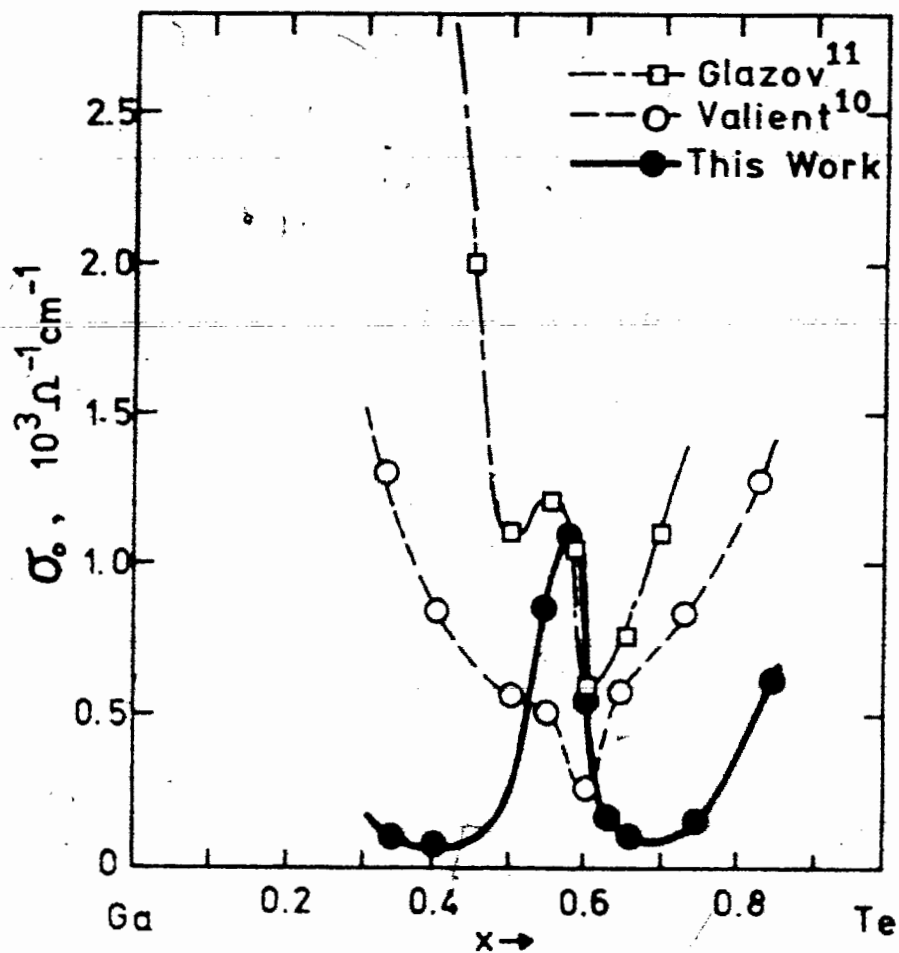


Figure 5-1*

Static Conductivity Vs. Liquid

Ga-Te Alloy Composition: $T = 900^\circ\text{C}$ dashed lines: from DC Resistivity
data;solid line: from 119 μ laser data.

0.66 . For $x < 0.55$, FIR conductivity is nearly independent of temperature; for $x > 0.66$, conductivity rises more than exponentially with T . Some typical curves are shown in figure 5-2. From the slopes of the curves, an activation energy E_0 is obtained:

$$(V-5) \quad \sigma(T) = \sigma_c \exp(-E_0/2kT)$$

A plot of E_0 versus alloy composition conforms fairly well to various published measurements (fig. 5-3).

B. FITS TO BROAD-BAND SPECTRA

1. Drude Reflectivity

The simplest model, and one known to be applicable to pure liquid Ga, is the free electron, or Drude model, described in section V-A. Rather than use the Hagen-Rubens approximation, which becomes invalid at the highest frequencies measured, equation (V-2) for the dielectric constant and equation (V-1) may be evaluated exactly by computer. To fit this model to the broad-band spectra of Ga_2Te_3 and GaTe , the electron concentration N was initially assumed to be, for composition x ,

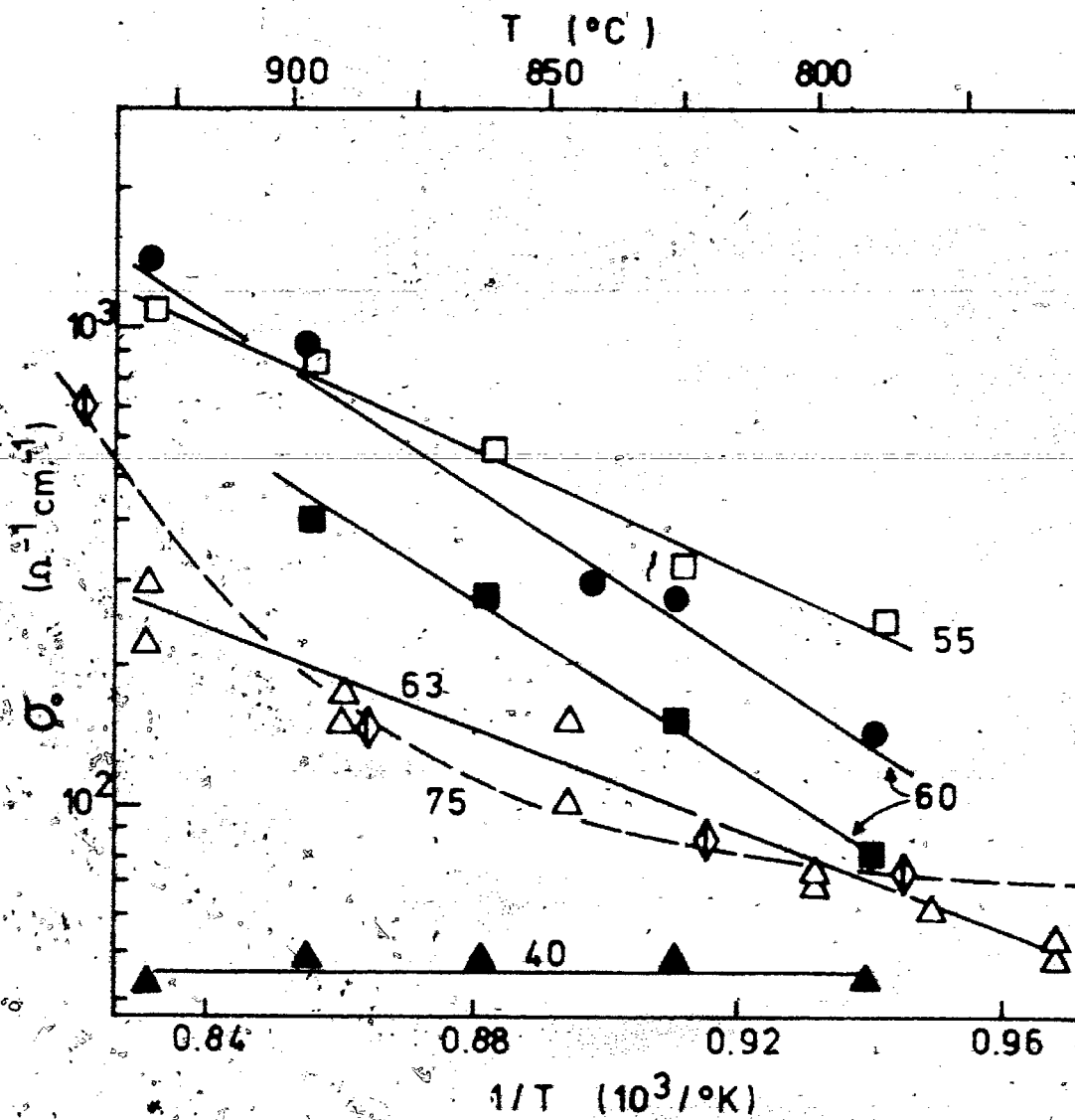


Figure 5-2

FIR Conductivity Vs. $1/T$ for Liquid
Ga-Te Alloys. Numbers indicate composition
in at.% Te. The 63% data are the sum of
two laser runs. Two separate 60% runs are
illustrated.

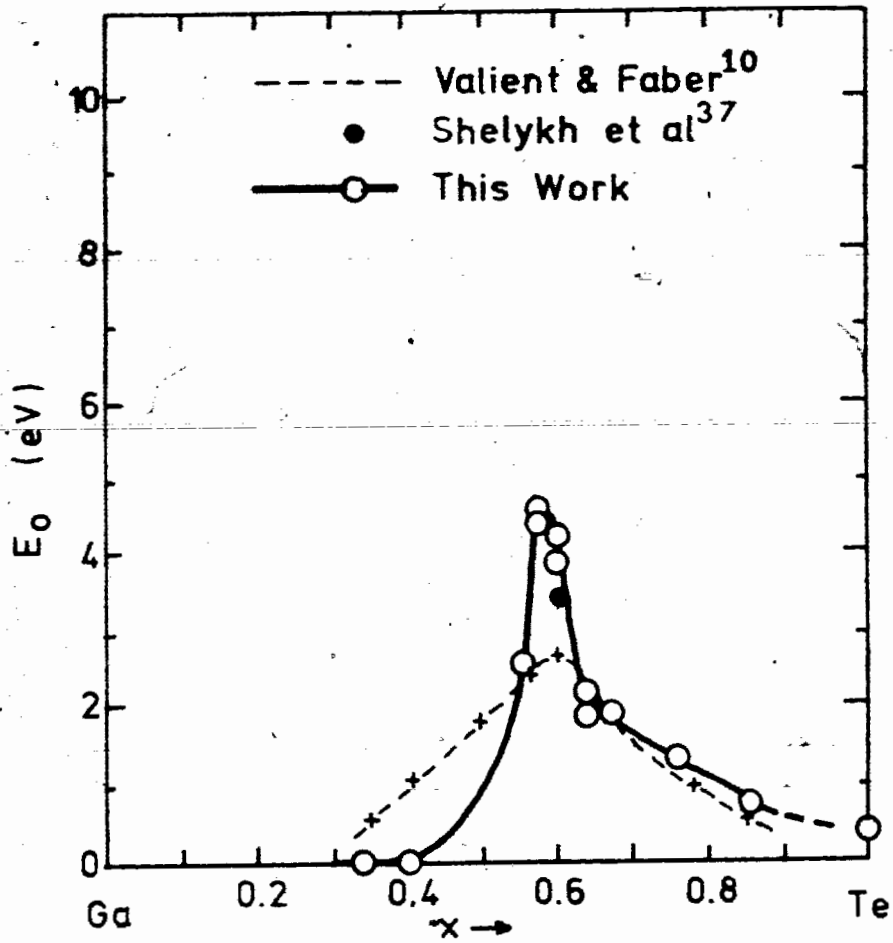


Figure 5-3

Activation Energy for Conductivity
Vs. Ga-Te Alloy Composition.

The solid curve is based on FIR
Laser data; other points result
from DC resistivity measurements.

$$(V-6) \quad N_x = (1-x)N_{\text{Ga}} + xN_{\text{Te}}$$

where, as usual, x denotes the atomic Te fraction. The relaxation time τ_d was then varied to reproduce the shape of the reflectivity curve.

This procedure yielded a reasonably good fit to the spectrum of Ga_2Te_3 , shown in fig. 4-8. The best-fitting Drude curve conformed to the data to within the experimental uncertainty of both the interferometer and 119μ laser measurements. The fitting constants were

$$\omega_p(\text{Ga}_2\text{Te}_3) = 9.3 \times 10^4 \text{ cm}^{-1}$$

$$\tau_d(\text{Ga}_2\text{Te}_3) = 6.3 \times 10^{-18} \text{ sec}$$

$$\sigma_0(\text{Ga}_2\text{Te}_3) = (170 \pm 30) \text{ ohm}^{-1}\text{cm}^{-1}$$

for Ga_2Te_3 at 900 deg.C.

Since equation (V-6) is an interpolation of electron density between the values of N for the separate atoms, it neglects the effect of possible bonding. A more realistic value of N would probably be lower, to account for the dip in DC conductivity at $x = 0.6$. To test this possibility, the plasma frequency was taken to be $2.82 \times 10^4 \text{ cm}^{-1}$ (a figure

obtained in a fit to NIR/Vis data; see section B-2). By setting the relaxation time to be $\tau_d = 7.1 \times 10^{-17}$ sec ($\sigma_0 = 180 \text{ ohm}^{-1}\text{cm}^{-1}$), a Drude fit comparable to that from equation (V-6) was obtained. The random error thus restricts the information obtainable from the Drude fit to the single parameter σ_0 , a function of ω_p and τ_d (cf: equation V-3).

In contrast to the Ga_2Te_3 results, the spectrum of liquid GaTe is certainly not Drude-like at low frequencies. The gradual decrease in reflectivity with rising frequency characteristic of the Drude model is absent in GaTe. As seen in figure 4-10, the low frequency spectrum is almost flat. If only the higher frequency portion ($\bar{\nu} > 175 \text{ cm}^{-1}$) is considered, though, a Drude curve can be fit to within the experimental uncertainty. This gives

$$\omega_p(\text{GaTe}) = 9.7 \times 10^4 \quad \text{cm}^{-1}$$

$$\tau_d(\text{GaTe}) = 2.7 \times 10^{-17} \text{ sec}$$

$$\sigma_0(\text{GaTe}) = (800 \pm 150) \text{ ohm}^{-1}\text{cm}^{-1}$$

for GaTe at 900 deg.C.

Neglect of the low frequency reflectivity lacks physical justification, however, because the free electrons responsible for the higher-frequency reflectivity would also raise the low frequency R to near unity.

2. Quantum Oscillator

In the work of Trotter et al., visible and near-IR reflectivity data for a wide range of liquid Ga-Te alloys were fitted using the 'quantum oscillator' model. This is the quantum mechanical analog of the Lorentz model and is a simple description of a material with a band gap.³⁴ It assumes the alloy to have a sharp valence band and a conduction band of width $\hbar\Gamma$, separated by $\hbar\omega_0$. The resulting dielectric constant is given by

$$(V-7) \quad \epsilon(\omega) = \epsilon_{\infty} + \frac{\omega_p^2}{\omega_0^2 - \omega^2 - i\omega\Gamma}$$

where ϵ_{∞} represents the contribution of lower-lying bands. This expression reduces to the Drude formula when the band gap $\hbar\omega_0 \rightarrow 0$, so the model is able to deal with alloy properties ranging from metallic to semiconducting. Using (V-7) and equation (V-1) to calculate reflectivity, rough fits to the NIR data were obtained⁹ by varying the plasma frequency ω_p , the band gap ω_0 , and the conduction band width Γ . For example for Ga₂Te₃, their fitting parameters were $\hbar\omega_p = 3.5$ eV, $\hbar\omega_0 = 0.9$ eV, and $\hbar\Gamma = 2.1$ eV. When extrapolated to the far infrared, however, these fits yield a

nearly constant reflectivity far below the observed values. This is not surprising, since the simplistic model does not include the contribution of free electron absorption, which dominates reflectivity in this region. The quantum oscillator model accounts only for the interband transitions responsible for visible reflectivity, and so is inappropriate to describe the FIR results.

3. Mechanical Oscillator

Unlike Section 2, in which a dielectric constant calculated for a particular band model was used, the effect of a mechanical oscillator (e.g. vibrating molecule) can be considered. Furthermore, the Drude expression (introduced to describe free electron effects from excess Ga atoms, for example) should be included. The dielectric constant then becomes

$$(V-8) \quad \epsilon(\omega) = 1 - \frac{\omega_p^2}{\omega^2 + i\omega/\tau_d} + \frac{S\omega_m^2}{\omega_m^2 - \omega^2 - i\omega\Gamma_m}$$

where ω_m = resonant-mode frequency, Γ_m is the oscillator line width, and S = oscillator strength. Even assuming the low frequency laser results to be valid, this expression is unable to fit them; the high free-electron reflectivity swamps any contribution due to resonant modes.

D. DISSOCIATION MODEL FOR ENTHALPY OF MIXING

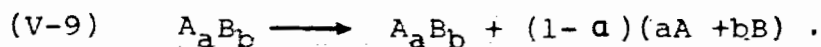
This section does not deal directly with the data obtained in the present experiments, but yields previously unreported information concerning the Ga-Te system.

The enthalpy of mixing provides information about the binding energy of a molecule: for any reaction involving the formation of a compound, a negative enthalpy implies the release of energy. In an alloy system, an infinite gradation of mixtures is possible, with corresponding enthalpies of formation. The way in which the enthalpy varies with alloy composition is determined by the numbers of atoms available for compound formation. For example, the existence of an intermetallic compound in a binary system would tend to cause atoms to associate in the stoichiometric proportions, leaving an excess of one constituent (this is essentially the pseudobinary alloy model).

A more realistic model for hot liquids permits the intermetallic compound to have a finite lifetime; that is, not all atoms, even at the stoichiometric composition, are associated into molecules. In this event, the enthalpy of mixing will obviously be changed, since the reaction numbers will be reduced. Several such models have been used for more complex thermodynamic calculations, but that of McAlister and

Crozier⁷ is one of the simplest.

Assuming a fraction α of the atoms to be associated into molecules A_aB_b , the dissociation expression is



Chemical equilibrium requires

$$(V-10) \quad \frac{(\phi'_B)^b (\phi'_A)^a}{\phi'_{A_aB_b}} = \text{constant} \equiv K$$

where ϕ'_n = volume fraction of species n in the pseudobinary system, i.e. $\phi'_n = V_n/V'_{\text{tot}}$, where V_n = molar volume of species n .

According to the model, which relates the concentrations of species in the dissociated and completely associated pseudobinary systems, the total molar volume for a system with a molecular compound A_2B_3 is

$$(V-11) \quad V'_{\text{tot}} = \frac{x(V_B - V_A) + V_A}{1 - 2\alpha(1-x)}$$

where x = concentration of species B.

From this, an expression relating the equilibrium constant, associated fraction of molecules, and alloy composition is obtained:

$$(V-12) \quad K = \frac{V_B^3 V_A^2}{(2V_A + 3V_B)} \left[\frac{1 - 2a(1-x)}{x(V_B - V_A) + V_A} \right]^4$$

Finally, the composition dependence of the enthalpy of mixing is taken to be

$$(V-13) \quad \Delta H = \begin{cases} \frac{5ax}{3} N \Delta h, & x < 3/5 \\ \frac{5a(1-x)}{2} N \Delta h, & x > 3/5 \end{cases}$$

where Δh = molar enthalpy of formation, per atom, of the compound molecules. Note that the model considers only one intermetallic composition (A_2B_3 in this case); for the Ga-Te system, the effects of a GaTe compound are not included.

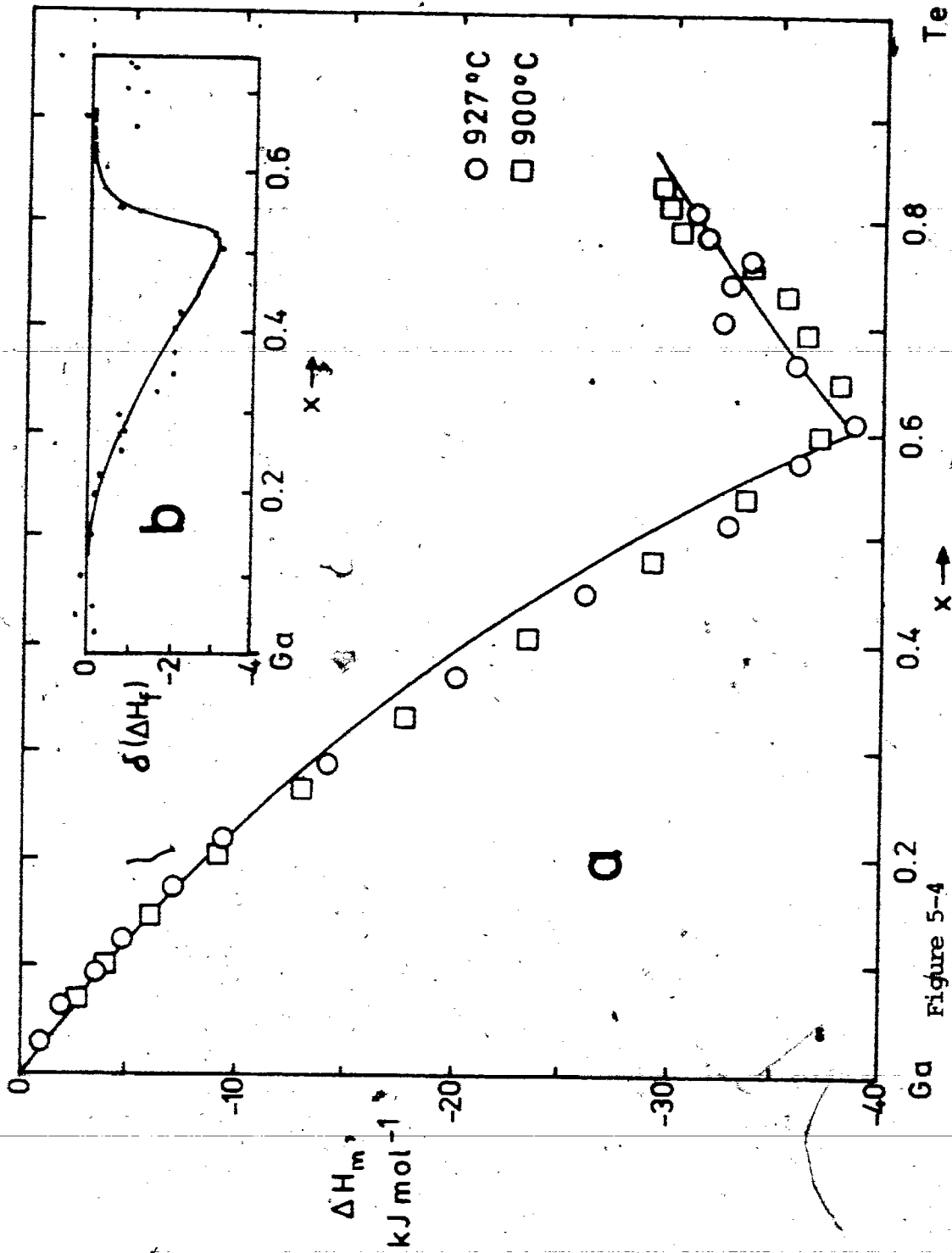
These relations were used to fit the model to experimental measurements of enthalpy of mixing made by Castanet and Bergman¹². The data were obtained by dropping

small known quantities of solid Te into liquid Ga at 1200 and 1238 deg.K (927 and 965 deg.C) contained in a calorimeter.

The model has two adjustable parameters: $N\Delta h$ and α . The associated fraction at some alloy composition x is adjusted; this fixes the equilibrium constant K for all other compositions, and, for the correct α , reproduces the shape of experimental curve.

The resulting fit, shown in fig. 5-4a, is quite good. The fitting parameters yield the enthalpy of formation of Ga_2Te_3 , $N\Delta h = 86 \text{ kJ/mole}$, and the fraction of molecules associated at $x = 0.6$: $\alpha = 0.45 \pm 0.03$. Furthermore, a systematic deviation between model and experiment occurs near $x = 0.5$; the discrepancy, plotted in the inset of fig. 5-4 versus alloy composition, is similar in shape to that of the entire curve. This suggests that GaTe is present along with Ga_2Te_3 as a dissociating compound, though in smaller amounts. This inference is in accord with Glazov's viscosity and conductivity data, which also show relatively weak anomalies around the composition of GaTe.

The fitted enthalpy of formation implies very weak bonding for Ga_2Te_3 molecules: $86 \text{ kJ/mole-molecule} = 17.2 \text{ kJ/mole-atom}$, while $RT = 9.98 \text{ kJ/mole}$ at 1200 deg.K., i.e. heat of formation for Ga_2Te_3 is approximately 1.7 kT per atom.



Te

 $x \rightarrow$

Figure 5-4

Enthalpy₂ of Mixing of Ga-Te: (a) Points: data of Castanet & Bergman ; solid line: dissociative pseudobinary model; (b) Deviations of model from experimental data.

VI. DISCUSSION

A. CHARACTERIZATION

Referring to the temperature variation of the laser results shown in figures 4-6 and 5-3, three regions of composition are apparent:

- (a) Ga-rich, $x < 0.4$: reflectivity independent of T.
- (b) $0.5 < x < 0.7$: very large T dependence, peaked near $x=0.6$. The large values fall rapidly at the boundaries of this region.
- (c) Te-rich, $x > 0.7$: smaller but non-zero T dependence.

The reflectivities tend to be low in regions (a) and (c), but are enhanced over most ($0.5 < x < 0.6$) of region (b).

Such properties have previously been used to characterize liquid semiconductors; for example, region (a) is M-type and regions (b) and (c) are S-type (metallic and semiconducting, respectively, deduced solely from the temperature dependence or freedom from it of the data) in Cutler's partitioning.

Allgaier would place all the alloys in his category B (intermediate conductivity, $100 < \sigma_0 < 5000 \text{ ohm}^{-1}\text{cm}^{-1}$) according to the conductivities inferred from reflectivity data. Models corresponding to such classifications are discussed in Section C below.

Applicable theories must address the following observations.

1. Temperature Dependence

Thermally activated conductivity, the basis of the calculations of Section V-A, has previously been reported in liquid Ga-Te alloys by Valient & Faber,¹⁰ who measured resistivities; it has also been observed in other liquid semiconductors³ and amorphous solid semiconductors³⁶.

The activation energy deduced from the reflectivity temperature dependence (fig. 5-3) agrees well with resistivity measurements for compositions $x > 0.63$. At the Ga_2Te_3 composition, however, the activation energy of the present experiments ($E_0 \sim 4 \text{ eV}$) is somewhat higher than previously published data ($E_0 \sim 2.5 \text{ eV}$ [Valient, & Faber] or 3.4 eV [Shelykh & Zhuze³⁷]). This large value for E_0 seems too large to be interpreted as a band gap (the high conductivity is incompatible with such a wide gap). In

contrast, the crude 'quantum oscillator' fits made by Trotter et al.⁹ to their visible reflectivity data indicated that the band gap varies only slowly with alloy composition, peaking at about 0.9 eV for Ga_2Te_3 .

2. Frequency Dependence

The good conformity of the Ga_2Te_3 spectrum to the Drude model implies that conduction is mainly by free carriers. However, the DC conductivity σ_{DC} is somewhat lower than the value inferred from the FIR conductivity, as illustrated in fig. 5-1. The FIR composition dependence is almost the inverse of the DC data: σ_{fir} is small except near $x=0.6$, while σ_{DC} reaches a minimum there.

This departure from the Drude model is apparent in the reflectivity spectrum of GaTe. The low-frequency flattening of the spectrum may actually be a mild peak, making it qualitatively like those of some amorphous solids. At least two such materials - As_2Se_3 and $\text{Tl}_2\text{SeAs}_2\text{Te}_3$ - have some of the optical characteristics of liquid Ga_2Te_3 : (a) FIR conductivity is about 10 times larger than the DC value; and (b) the DC and FIR conductivities are thermally activated, with similar activation energies.³⁸ Low frequency conductivity ($\nu < 10^{10}$ Hz.) has also been measured in disordered solids: such materials display a power-law

increase in $\sigma(\omega)$ with frequency in this region. σ reaches a plateau at microwave or FIR frequencies, and then decreases again. The conductivities of liquid GaTe and Ga_2Te_3 show the latter behaviour over the FIR frequencies studied. The visible reflectivities of liquid Ga-Te, measured by Trotter et al., also resemble those of amorphous solids. However, glasses have conductivities some 2 to 5 orders of magnitude lower than liquid semiconductors.

The present GaTe spectrum is qualitatively different from that of the solid single crystal, which has several infrared-active modes and reflectivity only half that of the liquid.³⁹ The lack of features in the liquid spectrum confirms that a well-defined crystal lattice is absent in this state.

B. COMPARISON WITH THE Mg-Bi SYSTEM¹⁵

Liquid Mg-Bi alloys are the only binary liquid semiconductors other than Ga-Te for which the FIR properties have been studied. The two systems are rather different:

Mg-Bi is a metal-metal system, while Ga-Te is a metal-chalcogen, the most common type of liquid semiconductor. Other quantities also differ, in particular the thermopower, which changes sign at the intermetallic composition Mg_3Bi_2

but which remains positive for most Ga-Te compositions, and the ionicity of the bonds, greater in Mg-Bi than in Ga-Te. However, their far infrared reflectivities display several common features:

(1) Reflectivity is enhanced within a few percent of the intermetallic composition - around Mg_3Bi_2 and between GaTe and Ga_2Te_3 .

(2) R drops precipitously to moderate values (40 to 60%) away from the intermetallic compositions, but rises somewhat near the pure components.

(3) Extrapolated σ_{fir} is quantitatively different from σ_{dc} obtained from resistivity measurements; for Mg-Bi, σ_{fir} at Mg_3Bi_2 is enhanced 100 X over σ_{dc} ; for Ga-Te, deviations are as much as factors of 10 to 15.

(4) At the major intermetallic compositions, broad-band spectra are Drude-like, at least over the range 10 to 250 cm^{-1} . The GaTe composition, however, departs from this behaviour at low frequencies.

(5) Optically active modes in the far infrared are absent.

The similarities, most notably (3), suggest that liquid semiconductors as a class may exhibit such far infrared properties. Property (4) has been observed in the near-infrared for Bi-Te and Cd-Sb alloys.⁴⁰

C. EXPLANATIONS FOR Ga-Te

1. Pseudogap

Mott et al.⁵ suggest that the linear $\ln \sigma$ vs. $1/T$ dependence observed in several binary liquid semiconductors may actually represent only a strongly temperature dependent conductivity. As temperature increases, disorder in the liquid also rises, leading to the accentuation of 'tails' at the edges of conduction and valence bands. These tails eventually overlap to form the pseudogap, a minimum in the electron density of states. Higher temperatures raise disorder and increase the probability of the promotion of carriers to the pseudogap, causing the pseudogap to 'fill in'. If the Fermi energy E_f is in the middle of the pseudogap, conductivity of the melt is expected to rise with temperature, as the gap fills in and the density of states approaches a free-electron-like shape. The particular $\sigma(T)$ and composition dependences are determined by the characteristics of the pseudogap and bandstructure of the liquid alloy. For example,

Sutton⁴¹ has fitted visible reflectivity data for various amorphous Mg-Bi alloys by postulating a particular model for density of states: parabolic valence and conduction bands with exponential tailing into the gap. When conduction is via diffusion of electrons (i.e. mean free path \approx interatomic distance, denoted by Allgaier as conductivity region B), the density of states is related to the optical conductivity by the Kubo-Greenwood formula

$$\sigma(\omega) = \frac{2\pi e^2 \hbar^2 \Omega}{m^2 \omega} \int \{f(E) - f(E+\hbar\omega)\} |D|^2 N(E) N(E+\hbar\omega) dE$$

where $N(E)$ is the electron density of states, $|D|^2$ is an average probability for transitions of energy $\hbar\omega$, and $f(E)$ is the Fermi function. His results indicate that the pseudogap is deepest at the intermetallic composition, and 'fills in' for surrounding alloy compositions. However, the fits are not good at low frequencies, the region of interest here.

Based on NMR measurements, W.W. Warren¹⁴ infers molecular associations of Ga_2Te_3 and probably GaTe for $0.5 < x < 0.7$, along with the presence of excess Ga or Te atoms. He interprets an enhancement of the magnetic relaxation rate as evidence of localization of electron states in a pseudogap, the depth of which decreases with increasing temperature, as predicted by Mott.

In the pseudogap model, the existence of localized states leads to conductivity via thermally-activated hopping. Mott calculates the very-low-frequency conductivity to be

$$(VI-1) \quad \sigma(\omega) = A \omega^s$$

where $A = \text{constant}$ and s is approximately 0.8.

The present data do not obey this relation, since, according to Mott, (1) Equation (VI-1) holds only for frequencies $\nu < 10^{10}$ Hz.; (2) true hopping conduction may not exist in liquids, in which localized states rapidly appear and disappear with changing microstructure; (3) The presence of highly conducting Ga or Te states would swamp the small hopping contribution. Near liquidus in Ga_2Te_3 , however, conductivity is quite low, and might make such hopping dependence observable. The FIR laser results show a constant activation energy from liquidus to at least 140 deg.C above it, though; no additional T-dependence is seen.

Mott has given an argument (without explicit calculations) that a pseudogap in the density of states should yield a spectrum consistent to that of GaTe: Drude-like at high frequencies, but flattening and falling to smaller values

with decreasing frequency.⁴² As mentioned above, however, fits by Sutton by this model of density of states failed to reproduce a peak in optical conductivity in the far infrared, known to exist from reflectivity measurements¹⁵ and implied by radio frequency measurements on amorphous Mg-Bi.⁵⁴ By permitting the Fermi energy to shift by as little as <0.1 eV in a rigid band model (rather than have the density of states vary dramatically with composition), Sutton⁴¹ and Ferrier & Herrell⁴³ appear to obtain the required conductivity peak. A pseudogap density of states seems, therefore, consistent with the reflectivity data only when the Fermi energy is not pinned to the centre of the gap.

2. Molecular Clusters

An alternative proposal shifts the scale of explanation from atomic to submacroscopic. Ga-Te alloys may be thought of as heterogeneous mixtures of molecular clusters in a sea of free atoms or ions. This 'soup' of components is implied by the good fit of the dissociative pseudobinary alloy model (Section V-C). Viscosity¹¹ measurements are a second convincing indicator of clusters.

The effect of molecular bonds should be discernible in the reflectivity spectrum. For example, the approximate vibrational-rotational frequencies of the GaTe molecule, calculated in Appendix B, are

$$\bar{\nu}_R = 204 + 7.2n_R \text{ cm}^{-1}$$

$$\bar{\nu}_P = 190 - 7.2n_P \text{ cm}^{-1}$$

$$\bar{\nu}_Q = 197 \text{ cm}^{-1}.$$

where $\bar{\nu}_R$, $\bar{\nu}_P$, and $\bar{\nu}_Q$ are the lowest frequency absorption bands for this diatomic molecule, and n_R and $n_P = 0, 1, 2, 3, \dots$

Reflectivity maxima at these wavenumbers would have been resolvable in the interferometer experiments. Their absence suggests that, if GaTe molecules exist, their concentration or lifetimes are sufficiently small to weaken or broaden the lines to beyond detectability. Warren estimates the lifetime for a Ga_2Te_3 'molecule' near the melting point, 10^{-11} sec, to be about five times smaller than the time for molecular rotation, indicating that molecular rotational-vibrational modes should not be expected. This argument also holds for GaTe, for which evidence suggests weaker molecular association. It is possible that the gentle hump at about 40 cm^{-1} is the highly broadened remnant of the molecular vib-rot band. Such a peak in amorphous solid spectra has been attributed to washed-out vibrational modes.³⁸

The temperature and composition dependence of R may be attributed to heterogeneity. Consider pure liquid Te. As mentioned in Section V-A, Te-rich compositions [i.e. region (c)] showed more-than-exponential temperature dependence of $\sigma(T)$ (cf: fig. 5-2). An increase in band gap with increasing temperature would cause such an effect, but is not physically reasonable. On the other hand, this could be explained as the combination of two mechanisms:

(1) Pure liquid Te is known to be a narrow-gap semiconductor, with activation energy⁴⁴ $E_0 \sim 0.4$ eV. This introduces T-dependence by thermal activation across the band gap, just as in solid semiconductors.

(2) Te is not a homogeneous material: it is believed to exist as a fluctuating covalently-bonded lattice in the liquid state, with the number of covalent Te-Te bonds decreasing with higher temperature.⁴⁵ Rising temperature thus leads to increased bond breakage and makes available more conduction electrons (from the dangling bonds). The conductivity rises accordingly. A model incorporating these features has been presented by Johnson⁴⁶ for pure Te, in which a metallic conductivity $\sigma_M = A/T$ due to free electrons ($A = \text{constant}$), semiconductor conductivity $\sigma_{SC} = \sigma_C \exp(-E_0/2kT)$ due to Te bonds, and a Boltzmann weighting factor $f = \exp(-W/kT)$

representing the probability of finding bonded Te atoms, are combined:

$$(VI-2) \quad \sigma_o = (1-f)\sigma_{SC} + f\sigma_M.$$

W is the Te-Te bond energy. Johnson obtained good agreement with experiment (note, however, that several fitting parameters [A, E_o , σ_c , and W] are involved). For Ga-Te, the number of Te bonds will decrease with Te concentration. According to the pseudobinary alloy model, the number of Te-Te bonds should be proportional to $(x-0.6)$ if all atoms are associated as Ga_2Te_3 at $x=0.6$, and could exist in higher concentrations for all x if the molecules can dissociate.

A similar explanation, that is, temperature dependent cluster geometry, with covalent Te-Te bonds replaced in part or entirely by molecular bonds of Ga_2Te_3 , may account for a portion of the observed T-dependence of region (b). According to this, the temperature independence of reflectivity for compositions $x < 0.4$ implies that the concentration of Te-Te bonds and molecular clusters is very small there. Hence, the Ga-rich liquid alloys of region (a) probably consist of a random mixture of free Ga and Te atoms.

The different conductivities σ_{fir} and σ_{dc} could indicate different bulk and surface qualities. Liquid mercury

is believed to have such surface anomalies.⁴⁷

In the absence of any supporting evidence, however, such an explanation is completely ad hoc.

Alternatively, the differing σ_{dc} and extrapolated FIR conductivities may be reconciled by the following Inhomogeneous model, due mainly to Cohen & Jortner,⁴⁸ and to Hodgkinson.⁴⁹

The inhomogeneity of a liquid consisting of semiconducting molecular clusters threaded by a random, metallic melt reduces electron mobility. Scattering is likely to be less for Te-rich compositions, because of the partial ordering of Te in a covalent network. The mixture of microscopic metallic and semiconducting regions increases scattering by forming a local band gap in the electronic density of states which excludes electrons near the Fermi energy. When this gap is deep enough (density of states at E_f below a 'percolation threshold'), extended conduction paths disappear; DC conductivity plummets. Electron transport is then by Mott hopping between regions or by promotion of electrons across the mobility gap in the semiconducting regions. The AC conductivity could exceed the DC value: DC conduction requires continuous paths through the melt, while AC conduction can proceed even with isolated conducting

islands in a poorly conducting matrix. The temperature variation of σ would be dominated by the semiconducting clusters, but enhanced by the metallic regions; hence, the anomalously large 'activation energy' at Ga_2Te_3 .

This explanation can be applied to several classes of disordered material. Quantitative models have been developed for metal-grain suspensions in a dielectric matrix. One such model, Effective Medium theory, predicts frequency dependence qualitatively like that observed for GaTe in the FIR: a Drude-like drop-off in R at higher frequencies, but reaching a peak at a low frequency which is dependent on alloy composition.⁵⁰ Such a peak must also occur in Ga_2Te_3 (somewhere below 10 cm^{-1} , the lowest frequency observed) because the DC conductivity is smaller than the FIR value.

3. Conventional Semiconductor

M. Cutler³ describes liquid Ga-Te mainly in terms of conventional semiconductor theory, with densities of electron states determined by the concentrations of Te-Te and Ga-Te bonds; it is further assumed that the band structure remains unchanged over a wide range of composition. He cites the parallel increase of magnetic susceptibility and conductivity on melting for Ga_2Te_3 as evidence that considerable covalent bonding persists in the molten compound. The large

activation energy and peaks in viscosity and resistivity at GaTe and Ga₂Te₃ are ascribed to chemical reaction as well as electronic effects. As concluded by other investigators, the evidence seems to support pseudobinary-alloy separation of species, with the excess Te covalently bonded. Because of the dissimilarity in thermopower for Ga-Te (positive except in the miscibility gap, rather than reversing sign at the stoichiometric composition), the system cannot be described in terms of the detailed theory developed for Tl-Te, the most completely characterized binary liquid alloy. Cutler's qualitative descriptions, however, are supported in the main by the FIR reflectivity results. Trotter et al. base explanations of their visible reflectivity results on the existence of bands assumed to be formed from Ga-Te and Te-Te bonding and anti-bonding states. The lack of prominent features in the spectra makes interpretation ambiguous, though. As discussed in Section V-2, their deduced band parameters are not supported by the present data.

The present FIR reflectivity measurements can thus confirm earlier descriptions of the liquid Ga-Te system, but are insensitive to the differences between the prevailing liquid semiconductor models. The models are not all mutually exclusive. Pseudobinary separation of species or molecular

formation in the liquid melt is not specifically dealt with in the Mott model: the pseudogap simply explains electronic transport properties in terms of density of states. The pseudobinary alloy model describes the compositional variation of those properties. These complementary descriptions account for the present FIR data.

The Inhomogeneous model (Section 2) relates optical properties to microstructure of disordered materials in general. Effective medium theory, its most quantitative expression, has not been applied in detail, owing to the complicated mixture of species suspected to exist in liquid Ga-Te.

Most importantly, the reflectivity data provide new information on high-frequency AC conductivity between the earlier DC measurements and visible/near-infrared experiments, and relate the properties of a particular liquid semiconductor to other disordered materials. Presumably, semiconducting glasses, metal-grain suspensions, and liquid semiconductors evince similar frequency-dependence of conductivity because of similarities in their structures; that is, short range order with discontinuities in the conduction paths.

D. LONG WAVELENGTH LASER DATA

Laser measurements at 571 and 1217 μ were anomalous. The reflectivity was frequently below that expected from simple model calculations, previous work on other systems, and interferometer measurements; no clear trend was apparent in the differential reflectivity; and interference effects were observed as a function of sample height.

The results at these wavelengths are believed to be spurious: even neglecting the trustworthy broad-band spectra, the observed low reflectivities cannot be ascribed to absorption by resonant modes (the free electrons that account for the observed DC conductivity would maintain high reflectivity).

Instead, the anomalies should be attributed to the effects of beam divergence. The 2 mm laser exit window strongly diffracted the long wavelength laser lines; assuming the angular distribution of radiation from the laser to follow a $(\text{sinc})^2$ dependence (this approximates the actual zero-order Bessel function dependence), the intensity was

$$(VI-2) \quad I(\theta) = \frac{\sin^2(\xi)}{(\xi)^2}$$

where $\xi = \pi d \sin \theta / 1.22 \lambda$, and d = laser exit hole diameter.

The angles, with respect to the light pipe axis, contained in the first order diffraction envelope (the Airy disc) were thus

$$\theta_{\max} = \left\{ \begin{array}{l} 4 \text{ deg at } 119 \mu \\ 20 \text{ deg at } 571 \mu \\ 48 \text{ deg at } 1217 \mu. \end{array} \right.$$

Rays reflecting down the entrance light pipe at more than 16 deg. could strike the sample surface normally and reflect back up the pipe, as shown in figure 6-1. Subsequent reflection at the entrance window would reverse the ray and allow interference with another incoming ray. Other interference paths may have been present, but this geometry explains the lack of interference at 119μ and the observation of interference maxima at $\lambda/2$ multiples of sample height at 1217μ . The observed intensity of the interference modulation supports the hypothesis that only a single reflection from the polyethylene window occurred.

The interference is one reason for the systematically low long wavelength reflectivity. Because the backward-reflected beam undergoes at least one extra reflection from the sample surface, its intensity will be reduced in proportion to the sample reflectivity, R . This interfering beam therefore varies by an extra factor R compared to the straight-through beam. As a result, the interference modulation (which depends

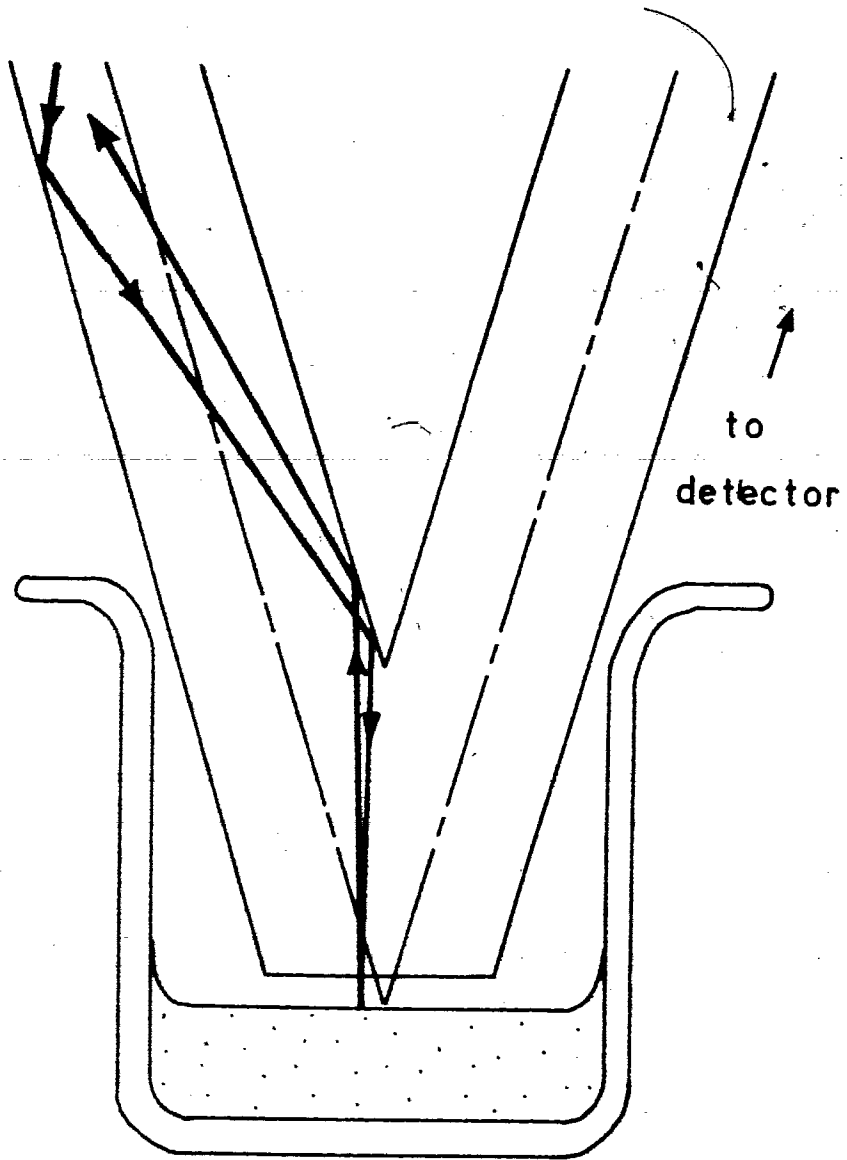


Figure 6-1
Interference Path for
Laser Radiation with
 $\lambda > 500 \text{ cm}^{-1}$.

on the sum of the back-reflected and straight-through beam amplitudes) will not be proportional to the reflectivity of the sample. By adjusting the sample height to obtain the interference maximum, instead of using the average of the interference extremes, a systematic error in the measured reflectivity is thereby introduced. A simple calculation based on the measured interference modulation shows that this effect can cause as much as a 9% lowering of the measured reflectivity below the true value at 1217μ , and somewhat less at 571μ . (Lack of interference effects made 119μ measurements free of this error). The interference thus partially accounts for the observed measurement errors.

The remaining discrepancies in the long wavelength laser data are most likely due to minor misalignments of the light pipes and detector light cone between sample and reference runs. Using equation (VI-2), and noting that the detector light cone accepts only rays at angles smaller than 6 deg. with respect to its axis, the change in signal for a minor angular misalignment can be computed:

TABLE VI-1

EFFECT OF LIGHT PIPE MISALIGNMENT ON MEASURED SIGNAL

Wavelength	Fraction of light channeled in correct align.	Fraction of light channeled after 3 deg. misalign.	Reduction in intensity due misalignment
119 μ	1.000	0.993	0.7 %
571 μ	0.587	0.539	8.2 %
1217 μ	0.301	0.294	2.3 %

As shown in the right hand column, a 3 degree change in light pipe orientation is sufficient to cause signal changes of fair magnitude. Such misalignments could have occurred by slight movement of the furnace pipes when handling the sample. (The furnace light pipes were either replaced or aligned by eye before each initial reference run). Furthermore, several small misalignments at the various light pipe joints could have an equivalent effect. Such an effect should cause a large RANDOM error in measurement. If light pipes were bumped after the reference runs, however (e.g. when inserting the sample into the furnace, or when stirring the melt), misalignments would consistently lead to low reflectivity measurements. A subsequent reference measurement, when averaged with the initial correctly aligned reading, would not completely correct for this error. Examination of the chart

records verified these statements: the 'after heating' reference runs averaged 1%, 11%, and 6% lower than the 'before' references for $\lambda = 119, 571, \text{ and } 1217 \mu$, respectively.

The long wavelength anomalies are thus attributable to interference effects and a random alignment error exacerbated by large beam divergence.

The problems could be removed by

- 1) Increasing laser exit hole diameter (to reduce divergence at the expense of beam intensity).
- 2) Replacing the exit hole with a partially reflecting exit mirror at the full aperture of 1 cm. (This would tend to couple-out higher order modes, but the wavelength-measuring Fabry-Perot interferometer could be placed in the laser exit area to act as a tunable band-pass filter).
- 3) Modifying detector light cone dimensions to increase acceptance angle.
- 4) Improving mechanical rigidity to reduce misalignment.

E. SUMMARY AND CONCLUSIONS

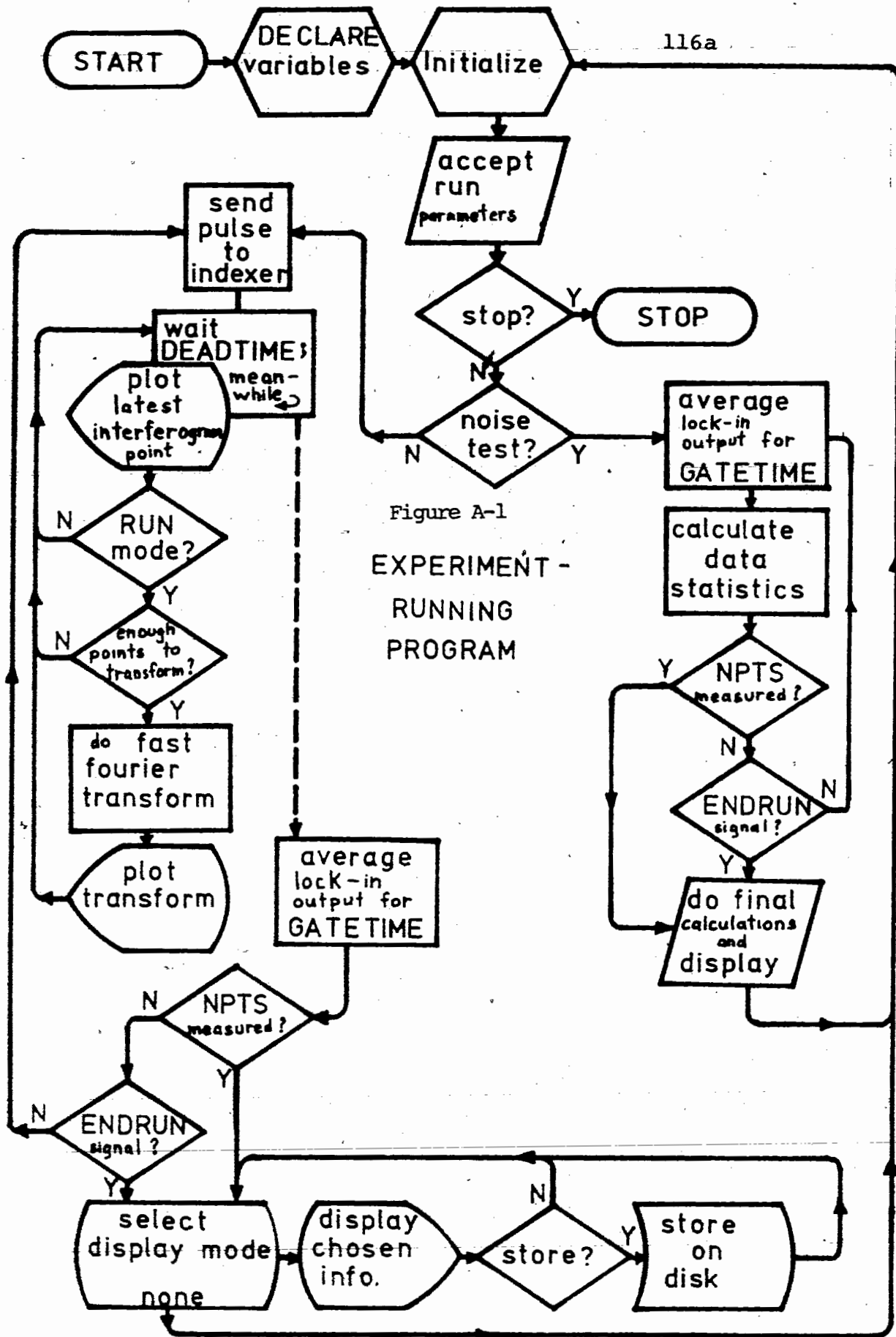
The FIR properties of liquid Ga-Te show several similarities to those of other liquid and amorphous-solid semiconductors. The temperature and frequency dependences of FIR reflectivity appear to be general features of electronic conduction in disordered materials. The appropriate model has not been isolated, but the Mott Pseudogap and Inhomogeneous models are consistent with the data. (The theoretical description of liquid semiconductors is itself in a disordered state).

The variation of reflectivity with the third parameter, composition, indicates how this disorder is related to alloy make-up. The most likely model for liquid $\text{Ga}_{1-x}\text{Te}_x$ appears to be a pseudobinary alloy, consisting of Ga + Ga_2Te_3 (and probably GaTe) for $x < 0.6$, and Ga_2Te_3 + Te for $x > 0.6$. If partial dissociation takes place, as implied by NMR measurements by Warren and the enthalpy fit of Section V-C, all four species may be present, to some extent, for all x . The enhanced reflectivity and its temperature dependence between GaTe and Ga_2Te_3 compositions are interpreted as the strongest evidence of an 'organized' species (i.e. molecular clusters) of semiconducting nature.

F. SUGGESTIONS FOR FURTHER WORK

It is clearly desirable to investigate the FIR reflectivity of other liquid binary alloys to determine whether they show properties analogous to Ga-Te and Mg-Bi. The alloy systems chemically closest to Ga-Te are In-Te, In-Se, Ga-Se, and Ga-S. The three chalcogens Te, Se, and S each have rather dissimilar and complex physical properties, however, and are considered semiconductors themselves. Simpler metal-metal systems analogous to Mg-Bi, such as Cd-Sb or Cs-Au, should probably be studied first.

In addition, the transition from DC to AC conduction should be investigated in the low frequency range ($\nu < 10^{10}$ Hz.) to verify whether the conductivity of liquid semiconductors is similar to that of amorphous-solid semiconductors. The latter exhibit power-law dependences of σ on ν , the exponents of which are predicted by various theories.^{5,51}



APPENDIX AEXPERIMENT-RUNNING PROGRAM

```

C      WRITTEN IN FORTRAN IV, WITH 'FORTRAN EXTENSIONS'
C      (FOR A PDP-11/34,RT-11 OPERATING SYSTEM, WITH AR-11
C      LAB PERIPHERAL)
C
C
C      DIMENSION IPULSE(2)
C      LOGICAL*1 ID(10)
C      COMMON Y(4098),DATA(1120)
C      DATA A,B/'A','B'/
C      INAME=0
C      IRUN=0
C      CREATE "PULSE ARRAY":
C
C      IPULSE(1) = 1000
C      IPULSE(2) = 0
C      CALL CLRD(IPULSE,2,ISPCE,1.0)
C      INITIALIZE :
C
125    CALL PLOT55(2,512,)
C      L=0
C      LL=0
C      CONST=6.
C      IGFLG=A
C      DO 130 I=1,1120
C      DATA(I) = 0.
130    CONTINUE
C
C      IRUN=IRUN+1
C      IF (IRUN.EQ.1) GO TO 150
C      IF (MODE.EQ.'C') GO TO 150
C      IBACK = NPTS*STEP
C      TYPE 140,IBACK
140    FORMAT(' ## ## ## BACK UP',I6,' STEPS')
C
150    CALL PARAM(MODE,NPTS,IGATIM,DEADTM,STEP)
C      IF (MODE.EQ.'D') GO TO 1999
C      IF (MODE.EQ.'C') GO TO 1099
C      CLEAR ALPHANUMERICS FROM VIDEO SCREEN:
C
435    CALL PLOT55(9,0,0)
C      CALL PLOT55(10,,)
C
C      DO 1000 N=1,NPTS
C      IF(N.EQ.1) GO TO 970

```

```

C      SEND A PULSE TO THE INDEXER TO INCREMENT THE
C      INTERFEROMETER MIRROR POSITION:
C
C      CALL FSH(IPULSE,ISPCE,2,1,1)
C      WAIT A "DEAD TIME" FOR THE APPARATUS TO SETTLE,
C      AND FOR AMPLIFIER TO LOCK-IN TO THE NEW SIGNAL:
C
C      IFLG=0
C      CALL SETR(5,0,DEADTM,IFLG)
C      WHILE WAITING, PLOT DATA:
C
C      K = N-1
C      CALL PLOT55(9,8*L,0)
C      TYPE 940,DATA(K)
940    FORMAT(1X,F5.0)
C      CALL PLOT55(9,30,1)
C      TYPE 942,K
942    FORMAT(1X,I4,' MEASUREMENTS ')
C      CALL GRAPH1(K,IPLT)
C      L=L+1
C      IF(L.LT.10) GO TO 960
C      L=0
C      REDUCE DEAD TIME BY 10% :
C
C      IF(DEADTM.LT.20.) GO TO 950
C      DEADTM = 0.90*DEADTM
950    IF(K.GT.512) GO TO 960
C      IF(MODE.EQ.'B') GO TO 960
C      LL = FLOAT(NPTS)/CONST
C      IF(K.LT.LL) GO TO 960
C      IF(LL.GT.NPTS) GO TO 960
C      CONST = 0.75*CONST
C      CALCULATE FOURIER TRANSFORM OF DATA SO FAR, AND
C      PLOT IT:
C
C      CALL FFT(K,STEP,SMAX,SMIN,MM,RES)
C      CALL GRAPH2(K,STEP,B,SMIN,SMAX,RES,MM)
960    CALL LWAIT(IFLG,0)
C
C      MAKE A MEASUREMENT:
C
C      CALL GATE(DATA(N),IGATIM)
970    IPLT = IFIX(0.2295*DATA(N))
C      CHECK FOR EXTERNAL SIGNAL FROM EXPERIMENTER
C      (A SWITCH CLOSURE) TO STOP FURTHER DATA COLLECTION:
C
C      ENDRUN = CVSWG(IADC(1,3))
C      IF(ENDRUN.GT.50.0) GO TO 1200
1000  CONTINUE
C      GO TO 1300
C      SIGNAL STATISTICS:
C

```

```

1099 SUM = 0.
      SUMSQ = 0.
C     MAKE MEASUREMENTS WITHOUT INDEXING THE INTERFEROMETER:
C
      DO 1100 I=1,NPTS
      CALL GATE(DATA(I),IGATIM)
      SUM = SUM + DATA(I)
      SUMSQ = SUMSQ + DATA(I)*DATA(I)
      TYPE 1110,I,DATA(I)
1110  FORMAT(1X,I4,' --- ',F5.0)
      STOPIT = CVSWG(IADC(1,3))
      IF(STOPIT.GT.50.0) GO TO 1115
1100  CONTINUE
      GO TO 1118
1115  NPTS = I
      TYPE 1117
1117  FORMAT(' ### SIGNAL RECOGNIZED; RESET SWITCH.')
1118  AVG = SUM/FLOAT(NPTS)
      SD = SQRT((SUMSQ - (SUM*SUM/FLOAT(NPTS)))/FLOAT(NPTS - 1))
      TYPE 1120
1120  FORMAT('/ ##### NOISE TEST RESULTS #####'//)
      TYPE 1130,NPTS,AVG,SD
1130  FORMAT(' NO. OF MEASUREMENTS: ',I4, '/' MEAN SIGNAL: ',F5.0,
X     '/' STANDARD DEVIATION: ',F5.0//)
      GO TO 125
C
1200  NPTS = N
      TYPE 1205
1205  FORMAT('/ ## ENDRUN SIGNAL RECOGNIZED; RESET SWITCH'//)
1300  IF(MODE.EQ.'B') GO TO 1335
      CALL FFT(NPTS,STEP,SMAX,SMIN,MM,RES)
C
C     DISPLAY DATA:
C
1302  CALL PLOT55(2,512,)
      TYPE 1305
1305  FORMAT(' SELECT PLOTTING MODE: '/' A. INTERFEROGRAM | '/'
X     ' | VIDEO DISPLAY'/' B. TRANSFORM | '
Y     '/' C. INTERFEROGRAM | '/' | X-Y RECORDER'
Z     '/' D. TRANSFORM | '/' E. NO MORE')
      ACCEPT 1310,IGFLG
1310  FORMAT(A1)
      IF(IGFLG.EQ.'E') GO TO 125
      CALL GRAPH2(NPTS,STEP,IGFLG,SMIN,SMAX,RES,MM)
C
1335  TYPE 1340
1340  FORMAT(' DO YOU WANT TO STORE THIS ON DISK?')
      ACCEPT 1345,ANS2
1345  FORMAT(A1)
      IF(ANS2.EQ.'Y') GO TO 1350
      IF(MODE.EQ.'B') GO TO 125
      GO TO 1302

```

```

1350 CALL STORIT(NPTS,MM,IGFLG,ID,INAME,STEP)
      IF(MODE.EQ.'B') GO TO 125
      GO TO 1302
C
1999 CALL PLOT55(2,0,2+4+8+32+64)
      STOP 'SHUT DOWN'
      END

      SUBROUTINE PARAM(MODE,NPTS,IGATIM,DEADTM,STEP)
C
C ASK EXPERIMENTER FOR PARAMETERS:
C
      TYPE 135
135  FORMAT(//' SELECT MODE: '// ' A. RUN'/' B. SYMMETRY CHECK'
X    /' C. NOISE TEST'/' D. SHUT DOWN EXPERIMENT'/)
      ACCEPT 140,MODE
140  FORMAT(A1)
      IF(MODE.EQ.'D') GO TO 999
      TYPE 145
145  FORMAT(//' NO. OF POINTS?')
      ACCEPT 150,NPTS
150  FORMAT(I4)
      IF(NPTS.EQ.0) NPTS=1120
      TYPE 155
155  FORMAT(//' GATE TIME (INTEGER MULTIPLE OF 1/2 SECOND)?')
      ACCEPT 160,IGATIM
160  FORMAT(I4)
      IF(IGATIM.EQ.0) IGATIM=2
      IF(MODE.EQ.'C') GO TO 999
      TYPE 415
415  FORMAT(//' DEAD TIME (UP TO 2.55 SEC.)?')
      ACCEPT 420,DEADTM
420  FORMAT(F4.2)
      IF(DEADTM.EQ.0.0) DEADTM=0.50
      DEADTM = 100*DEADTM
      TYPE 425
425  FORMAT(//' STEP SIZE?')
      ACCEPT 430,STEP
430  FORMAT(F5.0)
      IF(STEP.EQ.0.0) STEP=2.
C
999  RETURN
      END

      SUBROUTINE GRAPH1(N,IPLT)
C INTERFEROGRAM-PLOTTING ROUTINE:
C
      CALL PLOT55(2,1+2+8,)
      CALL PLOT55(1,0,)
      CALL PLOT55(3,N,IPLT)
      RETURN
      END

```



```

SUBROUTINE GATE(AVRG,ITIMES)
C   MEASUREMENT ROUTINE
C   THE LOCK-IN AMPLIFIER'S VOLTAGE IS SAMPLED 100 TIMES A
C   SECOND, IN BURSTS OF 1/2 SEC. THE DATA ARE STORED IN AN
C   ARRAY, CONVERTED, AND THEN AVERAGED. THE NUMBER OF
C   BURSTS (ITIMES) IS EQUIVALENT TO A GATE TIME.
C

```

```

DIMENSION IDAT(50)
SUM = 0.
M = 0
DO 700 I=1,ITIMES
IFLG=0
ISFLG=0
CALL RTS(IDAT,50,,,,,3,2,IFLG,IDUM)
CALL SETR(5,9,1.,ISFLG)
CALL LWAIT(IFLG,0)
CALL SETR(-1,,,)
DO 700 J=1,50
SUM = SUM + CVSWG(IDAT(J))
M = M + 1
700 CONTINUE
AVRG = SUM/FLOAT(M)
RETURN
END

```

```

SUBROUTINE GRAPH2(NPTS,STEP,IGFLG,SMIN,SMAX,RES,MM)
DIMENSION PLOT(1025),IYPLT(1025),IXDISP(1),IYDISP(1)
COMMON Y(4098),DATA(1120)
EQUIVALENCE (Y(2048),PLOT(1)),(Y(3073),IYPLT(1))
C   SCALE DATA TO BE PLOTTED:
C

```

```

IF(IGFLG.EQ.'A') GO TO 820
IF(IGFLG.EQ.'B') GO TO 840
IF(IGFLG.EQ.'C') GO TO 860
DO 815 J=1,MM
815 PLOT(J) = (Y(J)-SMIN)/(SMAX-SMIN)*1023.
CONTINUE
NN = MM
GO TO 870
820 DO 825 J=1,NPTS
PLOT(J) = 0.2295*DATA(J)
825 CONTINUE
NN = NPTS
GO TO 870
840 DO 845 J=1,MM
845 PLOT(J) = (Y(J)-SMIN)/(SMAX-SMIN)*235.
CONTINUE
NN = MM
GO TO 870

```

```

860 DO 865 J=1,NPTS
      PLOT(J) = DATA(J)
865 CONTINUE
      NN = NPTS
870 XGAIN = 512./FLOAT(NN)
      IF(XGAIN.LT.1.0) XGAIN=1.0
C     PLOT DATA:
C
      IF(IGFLG.EQ.'C') GO TO 900
      IF(IGFLG.EQ.'D') GO TO 900
C
      CALL PLOT55(9,0,0)
      CALL PLOT55(10,,)
      CALL PLOT55(2,1+4+32+64,)
      CALL PLOT55(1,1,)
      CALL PLOT55(4,1,0)
      CALL PLOT55(5,0,1)
      CALL PLOT55(7,0,0)
      IGAIN = IFIX(XGAIN+0.5)
      LEN = (NN-1)*IGAIN
      DO 880 I=1,NN-1
        YDISP = PLOT(I)
        INTERP = PLOT(I+1) - PLOT(I)
        IF(INTERP.EQ.0) INTERP=1
        DO 880 L=1,IGAIN
          YDISP = YDISP + FLOAT(INTERP)/XGAIN
          IYPLT((I-1)*IGAIN + L) = IFIX(YDISP)
880 CONTINUE
C
      CALL PLOT55(3,-LEN,IYPLT)
C
      CALL PLOT55(9,20,8)
      TYPE 890,NPTS,NN-1
890 FORMAT(1X,I4,' PNTS. USED - ',I4,' PT. TRANSFORM')
      IF(IGFLG.EQ.'A') GO TO 930
      RANGE = 1000./STEP
      CALL PLOT55(9,17,23)
      TYPE 892,RES,RANGE
892 FORMAT(' RESOLUTION = ',F7.3,8X,' RANGE = ',F5.0)
      CALL PLOT55(9,0,0)
      GO TO 930
C
900 CALL CLRD(IXDISP,1,ISP,1.0)
      CALL CLRD(IYDISP,1,ISP,1.0)
      IXGAIN = IFIX(XGAIN)
C     SET-UP PROCEDURE -
C     MOVE PEN TO CENTRE POINT OF DATA:
C
901 IXDISP(1) = IFIX(0.5*FLOAT(NN*IXGAIN))
      IYDISP(1) = 1
      CALL FXY(IXDISP,IYDISP,1,1,1)
      PAUSE ' MIDDLE POINT - ADJUST X-ZERO FOR PAPER CENTRE'

```

```

C      MOVE PEN TO FIRST POINT:
C
      IXDISP(1) = 1
      IYDISP(1) = IFIX(PLOT(1))
      CALL FXY(IXDISP,IYDISP,1,1,1)
      TYPE 902
902   X  FORMAT(' 1ST POINT - ADJUST X-GAIN FOR LEFT EDGE'/
      ' TO REPEAT SET-UP, TYPE Y; OTHERWISE, DROP PEN')
      ACCEPT 904,ANSR
904   FORMAT(A1)
      IF(ANSR.EQ.'Y') GO TO 901
      DO 920 I=1,NN-1
      YDISP = PLOT(I)
      YINTRP = PLOT(I+1) - PLOT(I)
      ILOOP = IFIX(ABS(YINTRP)/(XGAIN)+0.5)
      IF(ILOOP.LT.2) ILOOP=2
      DO 920 L=1,IXGAIN
      IXDISP(1) = (I-1)*IXGAIN + L
      DO 920 M=1,ILOOP
      IF(YINTRP.EQ.0.0) GO TO 910
      YDISP = YDISP + YINTRP/FLOAT(IXGAIN*ILOOP)
      IYDISP(1) = IFIX(YDISP)
910   CALL FXY(IXDISP,IYDISP,1,1,1)
C      WAIT BETWEEN PLOTTING INCREMENTS:
C
      DO 920 J=1,20
      ABORT = CVSWG(IADC(1,3))
      IF(ABORT.GT.50.0) GO TO 925
920   CONTINUE
925   PAUSE ' COVER PEN AND PRESS ''RETURN''.'
C      RESET ANALOG OUTPUT VOLTAGE TO -5 V. FOR THE
C      INDEXING ROUTINE:
C
      IYDISP(1) = 1
      CALL FXY(IXDISP,IYDISP,1,1,1)
C
930   RETURN
      END

SUBROUTINE STORIT(N,MM,IGFLG,ID,INAME,STEP)
C      FILE STORAGE ROUTINE: ACCEPTS A FLOATING-POINT ARRAY FOR
C      DISK STORAGE AND RETURNS THE CHOSEN FILENAME FOR POSSIBLE
C      DEFAULT USE.
C
      COMMON Y(4098),DATA(1120)
      LOGICAL*1 EXPTID(15),ID(10),PRFX(4),NUL
      DATA NUL/0/
      DATA PRFX/'D','X','1',':'/
C      GET A 10 CHARACTER FILENAME:
C
      IF(INAME.EQ.0) GO TO 1606
      TYPE 1602,ID

```

```

1602  FORMAT(' THE PREVIOUSLY USED NAME WAS ',10A1)
1606  TYPE 1608
1608  FORMAT(' DESIRED FILENAME? (E.G. ABCDEF.XYZ)')
      ACCEPT 1610, ID
1610  FORMAT(10A1)
C     BUILD FILENAME THAT IS READABLE BY THE OPERATING SYSTEM:
C
1640  DO 1650 J=1,4
      EXPTID(J) = PRFX(J)
1650  CONTINUE
      DO 1660 J=5,14
      EXPTID(J) = ID(J-4)
1660  CONTINUE
      EXPTID(15) = NUL
C     MAKE A LOGICAL CONNECTION TO THE DISK DEVICE, STORE THE
C     FILE, AND THEN BREAK THE CONNECTION:
C
      OPEN(UNIT=2,TYPE='NEW',NAME=EXPTID,ACCESS='SEQUENTIAL')
      IF(IGFLG.EQ.'B') GO TO 1670
      IF(IGFLG.EQ.'D') GO TO 1670
      WRITE(2,1665) N,STEP
1665  FORMAT(I4,/F5.0)
      LINES = N/10+1
      DO 1668 J=1,LINES
      WRITE(2,1667,ERR=1690) (DATA(K),K=10*J-9,10*J)
1667  FORMAT(10(F6.0,1X))
1668  CONTINUE
      GO TO 1690
1670  WRITE(2,1665) MM,STEP
      LINES = MM/10+1
      DO 1685 J=1,LINES
      WRITE(2,1680,ERR=1690) (Y(K),K=10*J-9,10*J)
1680  FORMAT(10(F6.0,1X))
1685  CONTINUE
1690  CLOSE(UNIT=2,DISPOSE='SAVE')
      TYPE 1695,EXPTID
1695  FORMAT(// ' ‡ ‡ ‡ STORED ON DISK AS FILE ',15A1)
      INAME = 1
      RETURN
      END

```

* The FFT subroutine is a minor modification of a Fortran II *
 version written by T. Templeton:

```

      SUBROUTINE FFT(NP,STEP,SMAX,SMIN,MM,RES)
C     ASYMMETRICAL,TRIANGULAR-APODIZING, FAST FOURIER TRANSFORM
C
      COMMON Y(4098),DATA(1120)
      DO 1799 I=1,4098
1799  Y(I) = 0.
      XN = NP
      J2 = NP

```

```

C      READ DATA SET
C      NP= NO. OF POINTS, J1= NO. OF POINTS IN LONGER SIDE OF
C      INTERFEROGRAM, N= NO. OF POINTS ON SHORTER SIDE.
C
      J1 = 0
      N = 0
      DO 1805 J=1, NP
      J1 = J1+1
      Y(J) = DATA(J)
      IF (Y(J)-Y(4098)) 1805,1800,1800
1800  Y(4098) = Y(J)
      N = J
      J1 = 0
1805  CONTINUE
C      COMPUTE AVERAGE VALUE AND STANDARD DEVIATION OF
C      INTERFEROGRAM, USING LAST TEN POINTS, AND SUBTRACT
C      THIS ZERO OFFSET:
C
      JJ = NP-9
      DO 1810 K=JJ, NP
1810  Y(4096) = Y(4096) + Y(K)/10.
      DO 1815 K=1, NP
1815  Y(K) = Y(K) - Y(4096)
      SUM = 0.
      DO 1820 K=JJ, NP
1820  SUM = SUM + Y(K)*Y(K)/10.
      SDEV = SQRT(SUM)*100./Y(4096)
      RES = 2000./STEP/FLOAT(J1)
      TYPE 1822, RES, SDEV
1822  FORMAT(' RESOLUTION = ', F7.3, '/', ' PCNT SDEV = ', F6.3)
C      STORE MINIMUM AND MAXIMUM:
C
      Y(4098) = Y(4098) - Y(4096)
      Y(4097) = Y(4098)
      DO 1825 K=1, J2
      IF (Y(K)-Y(4097)) 1824,1825,1825
1824  Y(4097) = Y(K)
1825  CONTINUE
C      DETERMINE MP, THE SMALLEST POWER OF 2 LARGER THAN
C      THE NO. OF DATA POINTS ON THE LONGER SIDE OF THE
C      INTERFEROGRAM:
C
1845  MP=2
1850  IF (MP+1-J1) 1855,1860,1860
1855  MP = MP*2
      GO TO 1850
C      EXTEND INTERFEROGRAM TO 2*MP POINTS:
C      APODIZE, CENTRE
C      APODIZE FOR LONG TRANSFORM, PUT IN REAL PART OF ARRAY;
C      APODIZE FOR SHORT TRANSFORM, PUT IN IMAGINARY PART;
C
1860  MM = 2*MP

```

```

MX = MP-N
J1 = MP-N+1
J2 = MP+N-1
XA = J2-J1
DO 2000 I=1,MM
K = MM-I+1
KR = 2*K-1
KI = KR+1
J = K-MX
IF (K-MP-NP) 1610,1610,1900
1610 IF (K-J1) 1900,1620,1620
1620 X1 = FLOAT(K-MP)/XN
X1 = ABS(X1)
X1 = 1.-X1
X2 = 1.
X3 = 0.
IF (K-J2) 1650,1650,1880
1650 X2=1.-FLOAT(J2-K)/XA
X3 = FLOAT(MP-K)*2./XA
X3 = ABS(X3)
X3 = 1.-X3
1880 Y(KR) = Y(J)*X1*X2
Y(KI) = Y(J)*X1*X3
GO TO 2000
1900 Y(KR) = 0.
Y(KI) = 0.
2000 CONTINUE
C COMPUTE FOURIER TRANSFORM BY ERENNER ALGORITHM:
C
N = 4*MP
IR = 1
J = 1
DO 45 I=1,N,2
IF (I-J) 41,42,42
41 TEMPR = Y(J)
TEMPI = Y(J+1)
Y(J) = Y(I)
Y(J+1) = Y(I+1)
Y(I) = TEMPR
Y(I+1) = TEMPI
42 K = N/2
43 IF (J-K) 45,45,44
44 J = J-K
K = K/2
IF (K-2) 45,43,43
45 J = J+K
KR = 2
46 IF (KR-N) 47,50,50
47 II = 2*KR
XN = 6.283185/FLOAT(IR*KR)
XM = SIN(XN/2.)
X3 = -2.*XM*XM

```

```

X4 = SIN(XN)
X1 = 1.
X2 = 0.
DO 49 K=1,KR,2
DO 48 I=K,N,II
J = I+KR
TEMPR = X1*Y(J)-X2*Y(J+1)
TEMPI = X1*Y(J+1)+X2*Y(J)
Y(J) = Y(I)-TEMPR
Y(J+1) = Y(I+1)-TEMPI
Y(I) = Y(I)+TEMPR
48 Y(I+1) = Y(I+1)+TEMPI
TEMPR = X1
X1 = X1*X3-X2*X4+X1
49 X2 = X2*X3+TEMPR*X4+X2
KR = II
GO TO 46
50 CONTINUE
C UNSCRAMBLE DATA:
C
DO 2400 I=2,MP
K = MM-I+2
IR = 2*I-1
II = 2*I
KR = 2*K-1
KI = 2*K
Y(1) = (Y(IR)+Y(KR))/2.
Y(2) = (Y(II)-Y(KI))/2.
Y(4097) = (Y(II)+Y(KI))/2.
Y(4098) = (Y(IR)-Y(KR))/2.
Y(4098) = -Y(4098)
C PHASE CORRECT:
C
Y(1) = Y(1)*Y(4097)+Y(2)*Y(4098)
Y(4097) = SQRT(Y(4097)*Y(4097)+Y(4098)*Y(4098))
IF(Y(4097)) 2400,2300,2400
2300 Y(4097) = 0.0001
2400 Y(I) = Y(1)/Y(4097)
Y(1) = 0.
C DETERMINE MAXIMUM AND MINIMUM VALUES FOR LATER SCALING
C AND PLOTTING:
C
MM = MP+1
Y(MM) = Y(MP)
SMAX = -1.E+10
SMIN = 1.E+10
ISVAL = .12*MP
DO 24 L=ISVAL,MM
IF(Y(L)-SMIN) 21,21,22
21 SMIN = Y(L)
22 IF(SMAX-Y(L)) 23,23,24
23 SMAX = Y(L)

```

```
24 CONTINUE
    DO 25 I=1, ISVAL-1
    IF (Y(I).GT.SMAX) Y(I)=SMAX
    IF (Y(I).LT.SMIN) Y(I)=SMIN
25 CONTINUE
C
RETURN
END
```


APPENDIX BPREDICTED VIBRATIONAL-ROTATIONAL MODES FOR THE GaTe MOLECULE

As shown in standard texts⁵², the allowed vibrational energies of a diatomic molecule are given by

$$(A2-1) \quad E = hc\bar{\nu}_{\text{vib}} \left(v + \frac{1}{2} \right) = \frac{h}{2\pi} \left(v + \frac{1}{2} \right) \sqrt{\frac{f}{\mu}}$$

where μ = reduced mass

f = force constant

$v = 1, 2, 3, \dots$

According to Gordy⁵³, an empirical formula for the force constant is

$$(A2-2) \quad f = 1.67 \left(\frac{X_a X_b}{d^2} \right)^{3/4} + 0.3 \text{ millidynes/\AA}$$

where X_a, X_b = electronegativities of atoms in the molecule

d = equilibrium atomic separation.

The allowed rotational energies of the molecule are

$$(A2-3) \quad E = \frac{h^2 J(J+1)}{2I} \quad (J = 0, 1, 2, \dots)$$

where I = moment of inertia = μd^2 .

The molecular energy is the sum of the vibrational and rotational terms. A transition from energy state E_1 to E_2 ($E_1 < E_2$) causes absorption (and thus a reflectivity maximum) at wavenumber $\bar{\nu}_{12} = E_2 - E_1 / hc$.

So, vibrational-rotational reflectivity maxima can occur at wavenumbers

$$\bar{\nu}_P = \bar{\nu}_{\text{vib}} - \frac{h}{cI} J_1 \quad (\text{for } \Delta J = J_2 - J_1 = -1)$$

$$(A2-4) \quad \bar{\nu}_Q = \bar{\nu}_{\text{vib}} \quad (\text{for } \Delta J = 0)$$

$$\bar{\nu}_R = \bar{\nu}_{\text{vib}} + \frac{h}{cI} (1 + J_1) \quad (\text{for } \Delta J = +1)$$

For GaTe, these wavenumbers are

$$(A2-5) \quad \bar{\nu}_P = 190, 182, 175, 168, \dots \text{ cm}^{-1}$$

$$\bar{\nu}_Q = 197 \text{ cm}^{-1}$$

$$\bar{\nu}_R = 204, 212, 219, 226, \dots \text{ cm}^{-1}.$$

Because of the estimation of the force constant and atomic separation, these values are only approximate.

REFERENCES

1. J. Tauc, ed., "Amorphous and Liquid Semiconductors", Plenum Press, London, 1974.
2. R.S. Allgaier, Phys. Rev. 185, 227 (1969).
3. M. Cutler, "Liquid Semiconductors", Academic Press, N.Y., 1977.
4. J.E. Enderby, Can. J. Chem. 55, 1961 (1977).
5. N.F. Mott and E.A. Davis, "Electronic Processes in Non-Crystalline Materials", Clarendon Press, Oxford, 1971, chapters 1-3.
6. J.E. Enderby and C.J. Simmons, Phil. Mag. 20, 125 (1969).
7. S.P. McAlister and E.D. Crozier, J. Phys. C: Solid State Physics 7, 3509 (1974).
8. S.P. McAlister and E.D. Crozier, Inst. Phys. Conf. #30, 1977.
9. D.M. Trotter, U. Even & J.C. Thompson, Phys. Rev. B17, 4004 (1978).
10. J.C. Valient and T.E. Faber, Phil. Mag. 29, 571 (1974).
11. V.M. Glazov, S.N. Chizhevskaya, & N.N. Glagoleva, "Liquid Semiconductors", Plenum Press, N.Y., 1969, pp. 282-288.
12. R. Castanet and C. Bergman, J. Chem. Thermodynamics, 9, 1127 (1977).
13. M. Fischer and H.J. Guntherodt, Inst. Phys. Conf. #30, 1977.
14. W.W. Warren, J. Non-Cryst. Sol. 8-10, 241 (1972).
15. E.D. Crozier, R.W. Ward & B.P. Clayman, Inst. Phys. Conf. #30, 1977.
16. C.K.N. Patel, Proc. IEEE 32, 713 (1964).
17. L.E.S. Mathias and J.T. Parker, Appl. Phys. Lett. 3, 16 (1963).
18. H.R. Fetterman, H.R. Schlossberg and J. Waldman, Laser Focus 8 (9), 42 (1972).

19. B.L. Bean and S. Perkowitz, J. Opt. Soc. Amer. 67, 911 (1977).
20. O.A. Simpson, B.L. Bean, & S. Perkowitz, J. Opt. Soc. Amer. 69, 1723 (1979).
21. T.Y. Chang, IEEE Trans. Microwave Theory and Tech. MTT-22, 983 (1974).
22. H.P. Roser and G.V. Schultz, Infrared Phys. 17, 531 (1977).
23. "Pyroelectric Product Guide", Molelectron Corp., Sunnyvale Calif., 1977.
24. D.E. Williamson, J. Opt. Soc. Amer. 42, 712 (1952).
25. H.A. Gebbie, Appl. Opt. 8, 501 (1969).
26. R.J. Bell, "Introductory Fourier Transform Spectroscopy", Academic Press, N.Y., 1972, chapter 3.
27. H.D. Drew and A.J. Sievers, Appl. Opt. 8, 2067 (1969).
28. "PDP Fortran/RT-11 Extensions Manual", Digital Equipment Corp., Maynard, Mass., Oct. 1977.
29. K.W. Bagnall, "The Chemistry of Selenium, Tellurium, and Polonium", Elsevier Publishing Co., N.Y., 1966, chapter 4.
30. I.A. Sheka, I.S. Chaus, & T.T. Mityureva, "The Chemistry of Gallium", Elsevier Publishing Co., N.Y., 1966, pp. 215-219.
31. W. Hume-Rothery, R.E. Smallman, & C.W. Haworth, "The Structure of Metals and Alloys", Metals and Metallurgy Trust of IMIM, London, 1969.
32. M. Hansen and K. Anderko, "Constitution of Binary Alloys" McGraw-Hill Book Co., N.Y., 1958, pp. 758-759.
33. G.W. Chantry, "Submillimetre Spectroscopy", Academic Press, N.Y., 1971, chapter 6.4.
34. The author is grateful to Dr. J. M. D'Auria, S.F.U. Chemistry Department, for making these measurements.
35. F. Wooten, "Optical Properties of Solids", Academic Press, N.Y., 1972, chap.3.

36. D.L. Mitchell, S.G. Bishop, & P.C. Taylor, *J. Non-Cryst. Sol.* 8-10, 231 (1972).
37. A.I. Shelykh & V.P. Zhuze, *Sov. Phys. Solid State* 7, 942 (1965).
38. D.L. Mitchell, P.C. Taylor, & S.G. Bishop, *Solid State Commun.* 9, 1833 (1971).
39. J.C. Irwin, B.P. Clayman, & D.B. Mead, *Phys. Rev.* B19, 2099 (1979).
40. J. Tauc & A. Abraham, *Helvet. Phys. Acta.* 41, 1225 (1968).
41. C.M. Sutton, *Solid State Commun.* 16, 327 (1975).
42. N.F. Mott, *Phil. Mag.* 13, 1011 (1966).
43. R.P. Ferrier & D.J. Herrell, *Phil. Mag.* 19, 853 (1969).
44. J.N. Hodgson, *Phil. Mag.* 8, 735 (1963).
45. B. Cabane & J. Friedel, *J. de Physique* 32, 73 (1971).
46. V.A. Johnson, *Phys. Rev.* 98, 1567 (1955).
47. A.N. Bloch & S.A. Rice, *Phys. Rev.* 185, 933 (1969).
48. M.H. Cohen & J. Jortner, *Phys. Rev. Lett.* 30, 699 (1973).
49. R.J. Hodgkinson, *J. Phys. C: Solid State Phys.* 9, 1467 (1976), and in "Amorphous & Liquid Semiconductors", ed. J. Stuke & W. Brenig, Taylor and Francis, Ltd., London, 1974.
50. N.E. Russell, E.M. Yam & D.B. Tanner in "Electrical Transport and Optical Properties of Inhomogeneous Media", ed. J.C. Garland & D.B. Tanner, *Am. Inst. Phys. Conf. #40*, N.Y., 1978.
51. U. Strom, J.R. Hendrickson, R.J. Wagner, and P.C. Taylor, *Solid State Commun.* 15, 1871 (1974).
52. H.A. Szymanski, "IR: Theory & Practice of Infrared Spectroscopy", Plenum Press, N.Y., 1964, chap.4.2.
53. W. Gordy, *J. Chem. Phys.* 14, 304 (1946).
54. M.J. Sik & R.P. Ferrier, *Phil. Mag.* 29, 877 (1974).